

# Midterm Report

## Design Synthesis Exercise

Group 15 - Manned Martian Aircraft

May 24, 2023

Javier Alonso Garcia	5228530	Adrian Beňo	5338514
Freek Braspenning	5291526	Joachim Bron	5259754
Pedro Coimbra Dos Santos	4682335	Sebastian Harris	5277418
Timo de Kemp	5310474	Patrick Kostelac	5238676
Thomas van de Pavoordt	5312329	Dominik Stiller	5253969

# Midterm Report

## Design Synthesis Exercise

by

Group 15 - Manned Martian Aircraft

May 24, 2023

Javier Alonso Garcia	5228530	Adrian Beňo	5338514
Freek Braspenning	5291526	Joachim Bron	5259754
Pedro Coimbra Dos Santos	4682335	Sebastian Harris	5277418
Timo de Kemp	5310474	Patrick Kostelac	5238676
Thomas van de Pavoordt	5312329	Dominik Stiller	5253969

Version Control			
Version	Date	Author(s)	Description
1.0	24-05-2023	All	First draft

Project duration: April 24, 2023 – June 30, 2023

Thesis committee: Dr. A. Sciacchitano, TU Delft, tutor  
Dr. S. J. Paardekooper, TU Delft, coach  
Dr. ir. J. A. Pascoe, TU Delft, coach

*Cover image credit: Pam van Schie (accessed April 2023 and adapted)*

# Executive Overview

Humans have been exploring Earth for centuries, and as technology advanced, this curiosity extended beyond our planet. The most promising target for making humanity interplanetary is our neighbor Mars. For astronauts going to Mars and exploring the planet in the next decade, rapid transportation between different locations on the surface of Mars is crucial. The mission statement is the following:

*MS: Transport two astronauts with payload quickly over a long range on Mars.*

After both conversations with the customer and the use of Requirement Discovery Trees, the driving requirements were developed and subsequently frozen. To recall, Table E.1, summarizes what requirements were determined to be driving following this process.

**Table E.1: Driving requirements**

Identifier	Description
REQ-ASTR-SAFE-01	The system shall not produce more than <TBD>positive gs in any direction.
REQ-SAG-REUS-03	The system's assembly process shall be repeatable.
REQ-GOPS-ACT-ASS-01	The system shall be able to be assembled by 2 astronauts.
REQ-AERO-LFT-02	The aerodynamic system shall have a maximum lift coefficient of <TBD>.
REQ-AERO-LFT-04	The aerodynamic system shall have a stall angle of <TBD>degrees.
REQ-STG-PAY-02	The system shall be able to hold 100 kg of payload.
REQ-PWR-ELEC-01	There shall be <TBD>Watts of power available to power all essential systems.
REQ-ETHC-02	The system shall not pollute the Martian environment.
REQ-CLMB-01	The climb rate at take-off altitude shall be at least <TBD>m/s.
<b>Key requirements</b>	
REQ-SAG-LF-03	The system shall obtain power from sources available on Mars.
REQ-LCD-LVEH-SIZE-01	The system shall have a volume of less than <TBD>[m <sup>3</sup> ].
REQ-LFSP-AIR-01	The system shall provide breathable air to the astronauts.
REQ-CRUS-05	The nominal cruise speed shall be 111 m/s.

Five concepts were selected to be developed following these requirements and the development of a Design Option Tree. In sub-teams of two, each team was tasked with developing the best design possible, after which these would be traded off. To recall, the concepts selected were: fixed-wing aircraft, of which a flying wing and a biplane were considered, a tiltrotor aircraft, a multicopter, and an airship.

## E.1. Fixed-Wing Aircraft

The preliminary sizing of the fixed-wing aircraft was performed for two design concepts: a flying wing aircraft (whose main parts are a large wing and fuselage with no horizontal tail), and a biplane aircraft (which consists of two wings stacked on top of each other connected to a fuselage containing a horizontal stabilizer). The sizing of both concepts was performed in various steps and in an iterative fashion. First, based on the requirements, the wing area wing planform, and fuselage dimensions were found. The drag was then estimated, from which the needed thrust was estimated and used to size the engines. Weights were concurrently calculated using class I weight estimations and iterated after more information was found on the sizing of the different subsystems. This was then followed up with a preliminary sizing of the structural aspects, as well as a stability analysis (qualitative for the flying wing using elevons and quantitative for the biplane using horizontal stabilizer).

For both concepts, the S1223 airfoil was chosen, which has a max lift coefficient  $C_{L_{max}} \approx 2.3$ . Based on some assumed (conservative) parameters, the wing area for the flying wing and biplane was found to be 227 m<sup>2</sup>. The fuselage consists of a crew space, a cargo space, and additional space connecting the former two, as well as parabolic front and aft fairings. It has a length of 10 m and a diameter of 2.5 m, for both concepts. Both concepts use two Mg-CO<sub>2</sub> turbojet with a total mass of 220 kg. Regarding performance, the flying wing and biplane were both found to have a maximum airspeed of 154 m s<sup>-1</sup> and can reach a

maximum altitude of approximately 16 km. Both of these concepts make use of horizontal take-off and landing and thus need a long landing distance. The propulsion system was sized for a minimum distance for TO/landing of 2 km for both. The flying wing and biplane have an operative empty mass of 2000 kg & 1430 kg, and a fuel mass of 625 kg & 920 kg, respectively, for a payload mass of 350 kg. Finally, the flying wing has a range of 1780 km while the biplane has a range of 2160 km. A top view of the flying wing and biplane is shown in Figure E.1 and Figure E.2, respectively. The flying wing has an aspect ratio of 20, a taper ratio of 0.2, and a quarter chord sweep of 20 degrees. The biplane has an aspect ratio of 12, a taper ratio of 1, and no quarter chord sweep.

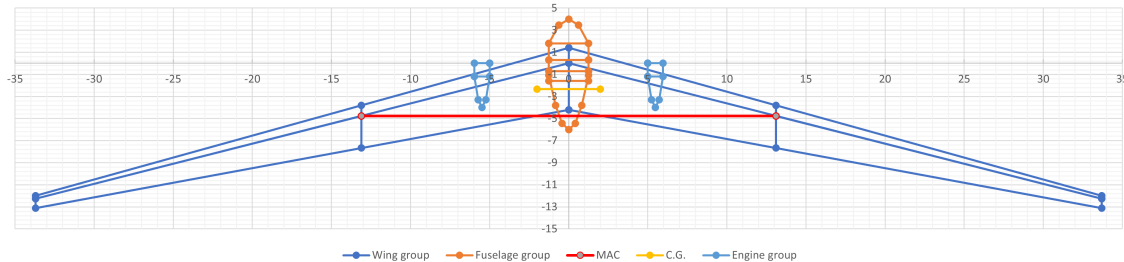


**Figure E.1:** Top view of the flying wing concept

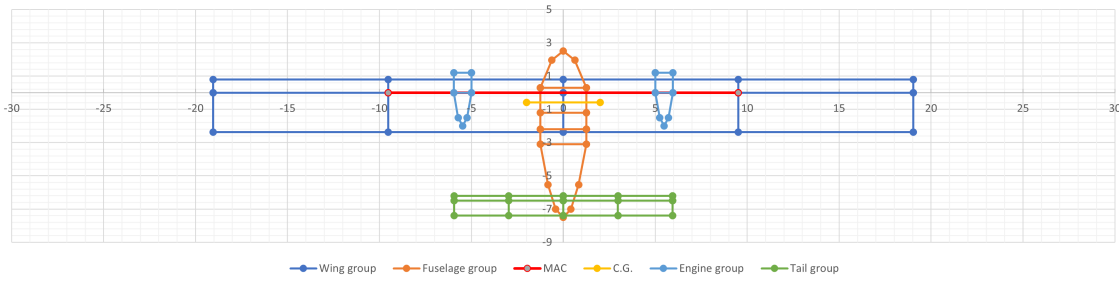


**Figure E.2:** Top view of the biplane concept

## E.2. Tiltrotor Aircraft

The preliminary sizing of the tiltrotor aircraft was performed with a series of calculations and estimations. Firstly, from the determined design take-off mass of 3000kg, density of  $0.01\text{kg/m}^3$ , and maximum tip speed of Mach 0.92, the rotors were sized. These were placed in a configuration of six blades per rotor, with two sets of counter-rotating rotors at the tip of each wing. Through iteration of the so-called *Combined Momentum and Blade Element Method*, the length of the rotor blade was determined to be 10.4m. The mass of each blade was estimated by assuming it was 91% empty, leading to a mass of 265kg for each rotor.

The second main part of a tiltrotor aircraft is the wing, used to produce lift in cruise and thus allow for extended range. This wing was sized to produce the equivalent of 3000kg of lift in cruise conditions. This lead to a total required wing area of  $112.7\text{m}^2$ . With this sizing performed, it is now possible to estimate the drag of the total aircraft following procedures present in the book *Synthesis of Subsonic Airplane Design* by Torenbeek.

Once the drag during the cruise was determined, it was possible to design the preliminary power subsystem. During take-off in a vertical configuration, the required power goes up to 226.1kW, while the consumed energy is only 18.8kWh. In cruise, however, the power is brought down to 82.1kW, with a minimum energy consumption of 205.4kWh. This combination of both high loads and extended consumption leads to a total battery mass, including margins for degradation and safety, of 878kg. Furthermore, it was chosen to add a lining of solar panels on the wing section of the aircraft, as the large surface area will provide up to 11.1kW, assuming half the wing surface is used.

Given these parameters, an initial estimation of the mass of the aircraft could be performed. Although

these methods are based on existing aircraft on Earth, the values still allowed for a "ballpark" estimate of the mass of the total aircraft. This leads to a mass for the wing system of 165.6 kg, a tail mass of 103.6 kg, a body mass of 263.6 kg and a solar panel mass of 99.2 kg. Along with the mass of the rotors, this leads to a total mass of the aircraft of 2921.8 kg, thus allowing for iteration.

Regarding the performance of the design, the rate of climb was calculated in both a cruise situation and in a vertical take-off situation, leading to a value of 62.5 m/s and 2.3 m/s respectively. The payload-range diagram was also drawn by varying the payload mass and calculating the range for each of these values, leading to Figure E.3. The blue horizontal line indicates the maximum mass available has been attained, as the design can not have a mass of more than 3000 kg.

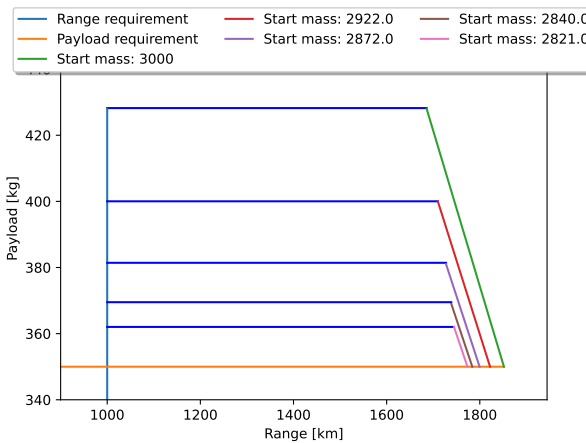


**Figure E.3:** Payload Range Diagram of the Tiltrotor

### E.3. Multicopter

The multicopter design concept is a rotorcraft with fixed rotors and no additional lifting surfaces. The multicopter design uses four coaxial rotors (eight rotors), each consisting of six individual blades bringing the total to 48 blades. The blades are 7 m long and during the critical condition (take-off), they spin with an angular velocity of 250 rpm. The blade airfoil is based on Ingenuity, a flight proven concept. Based on the theory from Kaya and Kutay [1] the rotors are capable of producing 11800 N of lift during take-off, which is enough to achieve Vertical Take-Off and Landing (VTOL) capabilities. Under the same conditions 3500 Nm of torque is produced. The engines were sized according to the torque experienced under take-off, an engine of 115 hp is needed to provide 3500 Nm of torque. The in-situ resource requirement means that standard Earth engines can not be used. Additionally, the power required is too high for energy-efficient batteries which is why the magnesium carbon dioxide engine is used. To estimate the engine mass, a statistical analysis was performed on current helicopter engines' masses of similar power. Also accounting for the Technology Readiness Level, the engine mass was found to be between 41 kg-81 kg. The specific fuel consumption is based on the specific fuel consumption of current 115 hp engines and the fact that the magnesium carbon dioxide reaction is weaker compared to the current engines. This means that the mass of the fuel will be 1.76 times higher than on Earth. This brings the total mass of the fuel needed for three hours, 1000 km flight to be  $M_{fuel} = 437 \text{ kg}$ .

The mass estimation approach is based on a mix of custom physical calculations and empirical relations for helicopters from Prouty [2]. For the physical relations, a structural analysis was performed on the blades, where the stresses due to the lift and the centrifugal force were calculated for different geometries. The geometry was chosen by taking the minimum mass for which the loads can be sustained. The same analysis was performed on the spars connecting the blades to the main body. The mass of the rest of the components was derived from the empirical relations. Because the relations are based on Earth helicopters from the 1990s, safety factors were added.

The design stability was analytically analyzed, showing that the design has both static and dynamic sta-

bility in the lateral and longitudinal directions. The multicopter does not require any control surfaces, as vertical movement, pitch, and roll can be achieved by throttling individual pairs of rotors. The horizontal movement can be achieved by either pitching or rolling and thus vectoring the lift component to produce thrust, or by tilting the rotors themselves in a desired direction. Yaw can only be achieved by tilting the rotors. The multicopter has VTOL capabilities making the take-off and landing easy and increasing the overall Mars coverage. The ideal cruise speed is 111 m/s as at higher speeds, the tip Mach number would exceed its limits. The design cruise height is as low as possible as that allows for the lowest angular velocity and thus the highest cruise speed. However, the design is capable of flying at 5000 m but at a reduced cruise speed.

## E.4. Airship

Although the airship proves advantageous in theory, considering it can create lift in a passive way without the need for wings or rotors, it proved less capable in practice. Since the skin of the volume encapsulating the hydrogen increases with weight as the volume increases, it would quickly decrease the amount of "effective" mass that could be carried. This, in combination with the fact that the airship requires a massive volume, almost as large as the Hindenburg-zeppelin, also creates a fairly large amount of drag, despite the low-density atmosphere. This would leave so little mass left for payload, fuel, and other subsystems that the airship was deemed unable to achieve the given requirements.

It was thereafter decided to find the optimal combination of cruise speed and attainable range for the airship for which the mass requirement is still fulfilled. The spirit of this idea was that each given design option should optimize to its best potential to complete the trade-off in the most optimal way. For the airship, it was found that at a cruise speed of 100 km/h, a range of 480 km was achieved. Naturally, this is not ideal considering the requirements of a cruise speed of 400 km/h and a range of 1000 km, however, the airship does come with several other advantages.

First of all, it is easily assembled. Essentially, the skin would only require inflating with hydrogen gas. Secondly, it has VTOL capabilities and can thus land anywhere on Mars without the need for securing a long landing strip. Finally, hydrogen can be obtained through electrolysis of water or ice, available in the Martian soil, which also produces oxygen as a byproduct. Moreover, hydrogen is a very safe gas to use in the Martian atmosphere since it cannot react with carbon dioxide. It is, therefore, not the ideal option in terms of performance, but it does provide other advantages that could make it a viable option. How it compares to the other design options is analyzed in the trade-off.

## E.5. Trade-off

The trade-off process began by determining the main criteria along which the designs should be graded. Among a variety of potential criteria, the final selected ones were:

- **Range at 350 kg payload:** Although the minimum range is of 1000km, improvements in this department will allow for longer missions and increased mission performance.
- **Landing/Take-off distance:** Longer distances in these maneuvers lead to increased risk of colliding with rocks or other topological features. Vertical Take-off and Landing, VTOL, would negate this risk along with removing the need for extended, flat areas of land to perform these maneuvers.
- **Sustainability:** The sustainability criterion was broken down into a rubric with 4 categories:
  - Emission of foreign molecules from the engine
  - Emission of foreign molecules from the lift system
  - Recyclability of the systems' structure
  - Use of batteries, as this technology is simultaneously applicable to Earth, sources its energy from renewable sources and, when degraded, can be used as static energy storage.
- **Feasibility:** The feasibility of the design is broken down mainly into the Technology Readiness Level, assessing at what development stage a technology is. This scale from 1 to 9 could lead to draws between designs, in which case the number of designs produced will be used to separate these draws.

In all of these criteria, the designs were scored from 0 to 4, with the latter being the highest, leading to a maximum achievable score of 16. This score was stretched to 100 to allow for comparison. The results of the trade-off can be found in Table E.2

**Table E.2:** Trade-off summary including criteria values and scores. The total weighted score in the last column indicates the overall goodness of the design. The tiltrotor design has the highest score and is selected.

Weight	Range at 350 kg payload [km]	Landing/take-off distance [m]	Feasibility	Sustainability	Score
	1	1	1	1	
Blended wing	1779	2000	Min. TRL of 4 (Power) and <1000 existing designs	Emits carbon, and the energy source is not renewable	44
Biplane aircraft	2157	2000	Min. TRL of 4 (Power) and >1000 existing designs	Emits carbon, and the energy source is not renewable	56
✓ Tiltrotor	1885	0	Min. TRL of 6 (Control)	Rotor blades are not recyclable	81
Multicopter	1270	0	Min. TRL of 4 (Power) and <1000 existing designs	The energy source is not renewable, and rotor blades are not recyclable	62
Airship	480	0	Min. TRL of 4 (Power) and <1000 existing designs	Emits carbon and hydrogen, and the energy source is not renewable	38

As part of a sensitivity analysis, the weights of each category were varied as the uncertainty when selecting these weights is not negligible. This led to the decision to vary the weights by a factor of 0.5 and 2 in order to assess the impact of the decision. This led to Figure E.4, where the results of these variations do not affect the outcome of the trade-off.

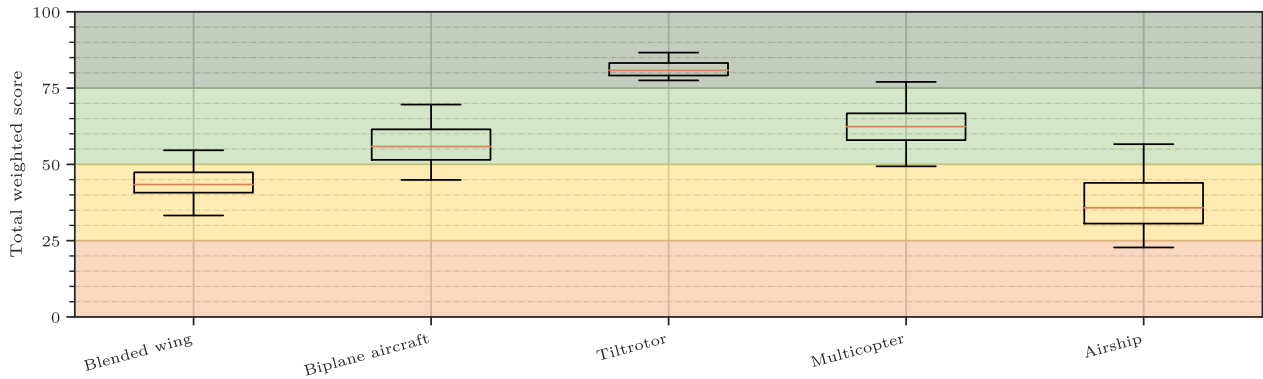


**Figure E.4:** Sensitivity analysis for trade-off weights.

## E.6. Verification and Validation plan

The verification and validation process for this report can be broken down into two parts. First, all verification and validation procedures are included in the Design Synthesis Exercise, followed by the verification and validation procedures that will occur after the Design Synthesis Exercise. The models and tools used in the process of sizing each design were verified and validated by the developing teams. This process will endure in the next phase of the design as each member specializes more and more within their role and develops the necessary tools.

Nonetheless, the models have and will be verified by a combination of unit tests, module tests, subsystem tests, and system tests. Regarding the validation of these models, during the DSE, experimental data will be used, when available, to compare the model outputs. Going past the DSE, the use of models, wind tunnel tests, and prototyping will ensure the tools are validated.

Regarding the final product, the fulfillment of driving requirements will be validated through a combination of testing, demonstration, analysis, and inspection in the phases following the end of the Design Synthesis Exercise.

## E.7. Operations and logistics

The flow in Figure E.5 shows what needs to be done to get the aircraft flying on Mars. It also shows the operations on Mars needed for doing the operations, this includes recharging, checkouts, and maintenance. Checkouts will be done with the same equipment that is used to check and assemble the parts shipped to Mars. The system will not be dependent on regular shipments from Earth, only for big fixes or battery life problems leading to limited performance.

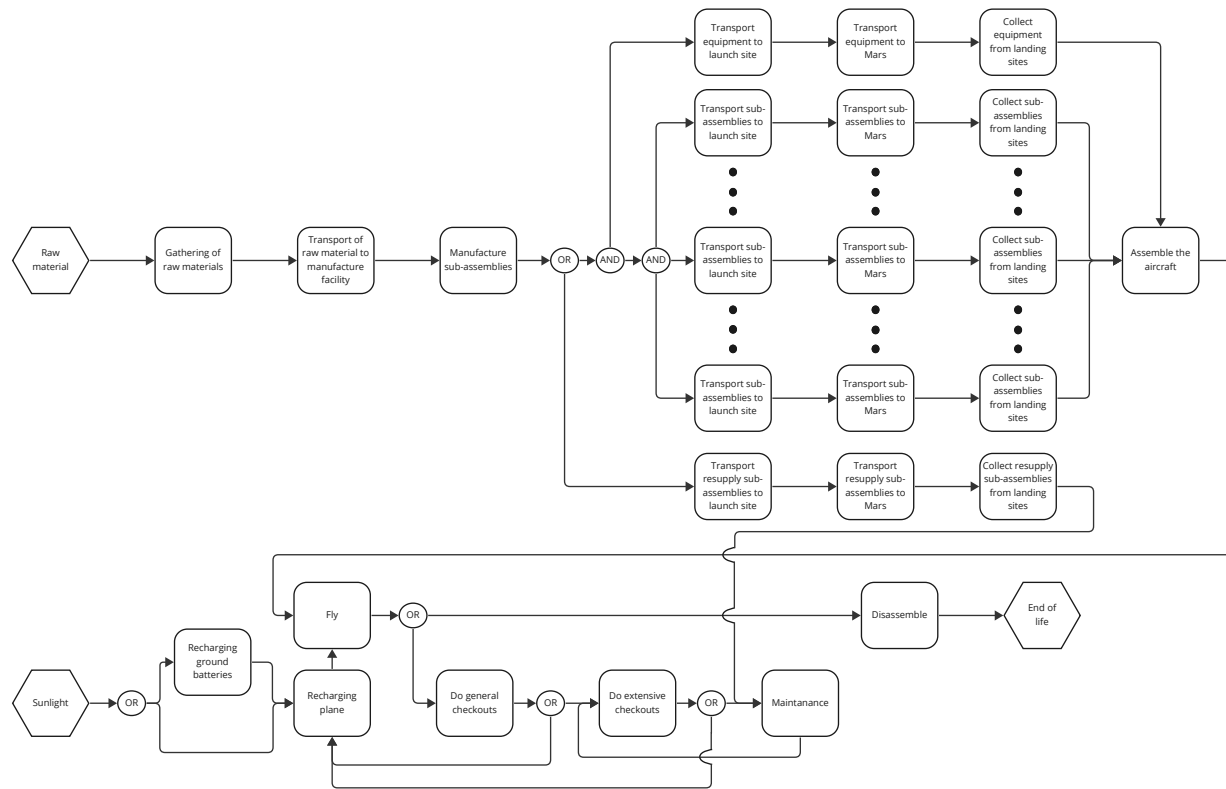


**Figure E.5:** Operations and logistics flow chart

## E.8. Technical Risk Assessment

From the chosen design, an analysis of technical risks was conducted. This allowed us to discover potential limitations of the design along with the required elements to mitigate these risks. The process revealed 15 different risks. These were ranked from 1 to 5 for both the likelihood of occurrence, with 5 indicating a probability of more than 95% and 1 indicating a probability of less than 1%, and impact, where 1 indicates negligible impact, and 5 indicates total mission failure.

**Table E.3:** Additional Risks and their mitigation techniques

Risk ID	Description	Mitigation	Probability (1-5)	Impact (1-5)
R-AR-01	Faulty Batteries	Isolate battery storage and regularly inspect	1	5
R-AR-02	Transmission Failure	Redundancy	1	4
R-AR-03	Gearbox Failure	Redundancy	1	4
R-AR-04	Hydraulics Failure	Redundancy	1	4
R-AR-05	Avionics Failure	Redundancy	1	3
R-AR-06	Brownout	Infrared Imaging	4	3
R-AR-07	Short-circuiting	Fuses and surge protectors	1	4
R-AR-08	Rotor failure	Ensure Rotor and Cockpit aren't aligned	1	4
R-AR-09	Autopilot failure	Install alert system and manual override	1	2
R-AR-10	Instrument failure	Redundancy	1	3
R-AR-11	Temperature control failure	Redundancy	1	3
R-AR-12	Astronauts unresponsive	Automatically engage autopilot	1	5
R-AR-13	Battery Ageing	Monitor battery health and performance	5	3
R-AR-14	Vortex Ring State	Set limit on descent rate and train pilots in Vuichard Correcting Technique	3	3
R-AR-15	Center of gravity shift	Calculate when loading payload and alert if too close to neutral point	2	5

From Table E.3, the risk mitigation will decrease the probability and/or the impact of each event, leading to the final risk matrix seen in Table E.4.

**Table E.4:** Design risk matrix

		Probability				
		Very Low (1)	Low (2)	Moderate (3)	High (4)	Very High (5)
Impact	Catastrophic (5)	R-AR-13, R-AR-15				
	Critical (4)					
	Moderate (3)	R-AR-01, R-AR-07, R-AR-11, R-AR-12				
	Marginal (2)	R-AR-03, R-AR-08				
	Negligible (1)	R-AR-02, R-AR-04, R-AR-05, R-AR-09, R-AR-10	R-AR-14		R-AR-06	

## E.9. Sustainable development strategy

The sustainable development strategy slowly moves towards a more technical and detailed approach. Whereas before sustainability was mainly focused on organizational sustainability within the group and ensuring that a definition was chosen for sustainability to comply with, the sustainability strategy now focuses on how the designs approach sustainability and how sustainability is enforced during the detailed conceptual design phase. Each concept has to result in a design that will at least fulfill the customer's requirement to only use in-situ available resources. Furthermore, during the trade-off, sustainability was also considered one of the final trade-off criteria. This meant that every concept strived for the highest score possible in this category.

For the next phase of the project, sustainability will become increasingly important. Each subsystem will have to consider sustainability and comply with the requirements set earlier. This includes but is not limited to, material choice, recyclability, manufacturing processes, assembly process, and end-of-life plan. The sustainability manager will ensure these goals are met and that the sustainability strategy is enforced.

# Contents

Executive Overview	i
Acronyms	ix
1 Introduction	1
2 Organization Update	2
3 Turbojet Propulsion System	3
3.1 Propulsion system characteristics estimation . . . . .	3
3.2 Verification . . . . .	5
4 Preliminary Sizing	6
4.1 Design concept 1+2: Fixed-wing aircraft . . . . .	6
4.2 Design concept 3: Tiltrotor aircraft . . . . .	15
4.3 Design concept 4: Multicopter . . . . .	20
4.4 Design concept 5: Airship . . . . .	28
5 Verification and Validation of Design Concepts	31
5.1 Fixed-Wing Aircraft: Flying Wing & Biplane . . . . .	31
5.2 Tiltrotor . . . . .	33
5.3 Multicopter . . . . .	37
6 Verification and Validation Plan Preliminary Design	42
6.1 Responsibilities. . . . .	42
6.2 Verification and Validation methods . . . . .	42
6.3 Model Verification and Validation. . . . .	42
6.4 Product Verification and Validation. . . . .	43
7 Trade-Off	44
7.1 Methodology . . . . .	44
7.2 Results. . . . .	47
8 Technical Risk Assessment	50
8.1 Methodology . . . . .	50
8.2 Risks from previous reports . . . . .	50
8.3 Additional risks. . . . .	51
9 Sustainable Development Strategy	53
10 Project Logic	54
10.1 Project description & development logic . . . . .	54
10.2 Operations and logistics description . . . . .	54
10.3 N2 charts . . . . .	55
10.4 Work Breakdown Structure . . . . .	56
10.5 Work Flow Diagram . . . . .	56
10.6 Gantt chart . . . . .	56
Bibliography	61

# Acronyms

**AC** aerodynamic centre.

**CFRP** Carbon Fiber-Reinforced Polymer.

**CG** center of gravity.

**EEE** Equivalent Earth Engine.

**HTOL** Horizontal Take-Off and Landing.

**IQR** inter-quartile range.

**ISRU** in-situ resource utilization.

**MAC** mean aerodynamic chord.

**MTOM** maximum take-off mass.

**OWE** Operational Empty Weight.

**PD&DL** Project Description & Development Logic.

**RC** Rate of Climb.

**SFC** Specific Fuel Consumption.

**TRL** Technology Readiness Level.

**VTOL** Vertical Take-Off and Landing.

**WBS** Work Breakdown Structure.

**WF** Fuel Weight.

**WFD** Work Flow Diagram.

**WPL** Payload Weight.

# Introduction

By Thomas van de Pavoordt

Private and public organizations have the goal of making humanity a multi-planetary species. Mars as our next neighbor will be our first destination possibly as soon as a decade. The first astronauts will be scientists, which will explore wide regions of the red planet. Currently, no feasible solution exists for human transportation on Mars over vast ranges and in a fast manner. While surface rovers may be adapted for human transportation, only airborne transportation will be able to meet the need of true mobility. This midterm report is the third in a series of reports to describe the conceptual design of a two-astronaut Martian aircraft.

Previously, the project plan showed the organizational aspects of this project, including task division and scheduling. The baseline report represented the first technical report of the project. It outlined the functional description of the system that should fulfill the mission and inventoried all requirements. From this, the design option tree was created, exploring every possible option of the design. The baseline report concluded with 5 different feasible options, to be further explored in this midterm report. The goal for this phase is to evaluate the options quantitatively, perform high-level estimations on the to-be-determined trade-off criteria, and decide on the preferred design option.

The design options remaining from the baseline report were limited to 5 concepts. The first two options consider an aircraft with a wing, where one explores a flying wing or a tailless option and the other explores a more conventional type of aircraft with a tail. The third option considers a blend between a helicopter and an aircraft, more conventionally known as a tiltrotor. The fourth investigates the possibility of a drone-style aircraft, with multiple rotors placed around the main body. The final design option that is considered is an airship, which utilizes a lighter-than-air gas to produce lift. Artist's impressions of all design options can be seen in Figure 1.1:

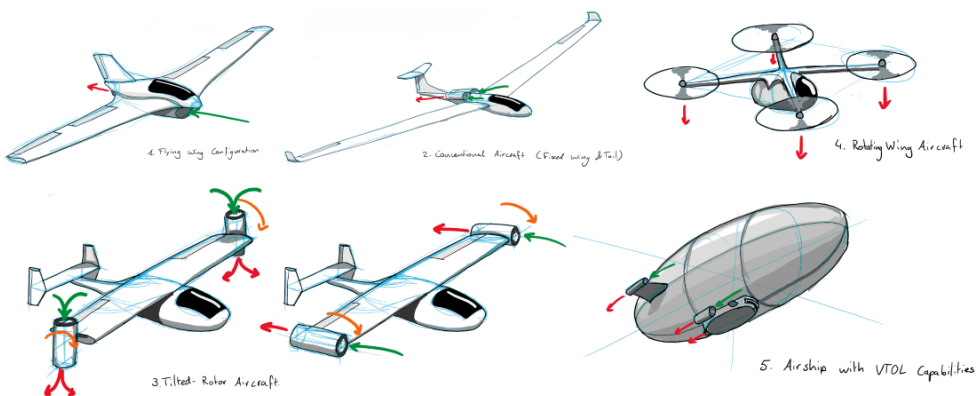


**Figure 1.1: Artist's impression of design concepts.**

This midterm report is structured as follows. Chapter 2 readdresses the team roles for the final phases of the project. Chapter 3 dives into a literature review on the Magnesium-CO<sub>2</sub> engine in preparation for the analysis of each design concept, which is done in Chapter 4. Naturally, before a trade-off between the concepts can be done, they need to be verified and validated, which is done in Chapter 5. Chapter 6 briefly describes the verification and validation plan for during and after the final design phase. Thereafter, a trade-off is performed in Chapter 7 to determine the most optimal concept. Closing off, Chapter 8 will assess the technical risks associated with the final design and proposes mitigation measures. Chapter 9 will review the sustainability approach and, finally, Chapter 10 will show the updated Project Description & Development Logic with all associated diagrams, including the N2-chart purposed to guide the iteration of the final design phase.

Source code for Chapters 4 to 7 can be found at <https://github.com/DominikStiller/tudelft-dse>.

# Organization Update

By Freek Braspenning

This chapter serves the purpose of documenting the change in organizational and technical roles within the team. Table 2.1 shows the switch in responsibility between the graphics design manager and the sustainability manager. Table 2.2 notes the switch in responsibility between the power and hydraulics engineer and the materials engineer. The new role division is summarized in Table 2.3.

**Table 2.1:** Overview of the changes within the organizational role division

Organizational Role	Person	Description
Graphics Design Manager	Thomas	Responsible for compliance and consistency regarding the visual elements of all deliverables. The individual shall ensure all graphics are of the same style and of high quality.
Sustainability Manager	Patrick	Ensures that all aspects of the group's work and the development of the product are performed in a sustainable manner (e.g. using sustainable materials, being ethically sustainable, operational sustainability, etc.).

**Table 2.2:** Overview of the changes of the technical roles in the team.

Technical Role	Person	Description
Power and Hydraulics Engineer	Timo	Responsible for the design's power, electrical systems and hydraulics.
Materials Engineer	Freek	Responsible for the selection of suitable materials for the design's different components.

**Table 2.3:** Technical and organizational roles for each of the team members

Name	Organizational Role	Technical Role	Deputy Technical Role
Dominik	IT and File Manager	Flight Performance Engineer	Ground Operations Engineer
Sebastian	Team Leader	Aerodynamics Engineer - Main Body	Power and Hydraulics Engineer
Freek	Budget Manager	Materials Engineer	Propulsion Engineer
Joachim	Deliverable Compliance Manager	Chief/Integration Engineer	Aerodynamics Engineer - Main Body
Javier	Secretary	Structures Engineer	Materials Engineer
Pedro	Systems Engineer	Propulsion Engineer	Chief/Integration Engineer
Adrian	External Affairs Manager	Aerodynamics Engineer - Lift Devices	Flight Performance Engineer
Patrick	Sustainability Manager	Stability and Controllability Engineer	Structures Engineer
Timo	Project Manager	Power and Hydraulics Engineer	Aerodynamics Engineer - Lift Devices
Thomas	Graphics Design Manager	Ground Operations Engineer	Stability and Controllability Engineer

# Turbojet Propulsion System

By Pedro Coimbra Dos Santos

The Martian atmosphere is predominantly composed of CO<sub>2</sub>, hence a Martian turbojet engine would need to use CO<sub>2</sub> as oxidizer. Many fuels might be possible, but a jet engine that uses magnesium as fuel and CO<sub>2</sub> as oxidizer has been the one with the most research data available [3]. While this technology is still in its infancy, some advantages and disadvantages can already be identified:

**Table 3.1: Advantages and disadvantages of using a magnesium + CO<sub>2</sub> engine**

Advantages	Disadvantages
High thrust-to-weight ratio.	Only small prototypes have been tested.
Martian regolith can be processed into Mg powder, which assures sustainability.	Jet engines typically need more maintenance than electric engines.
	During tests, soft carbon flakes clogged the engine, as seen in Figure 3.2. Scaling up the prototype may mitigate this.
	A carrier gas is needed to pump the Mg powder to the combustion chamber [4]. Different gases are considered in Figure 3.1.

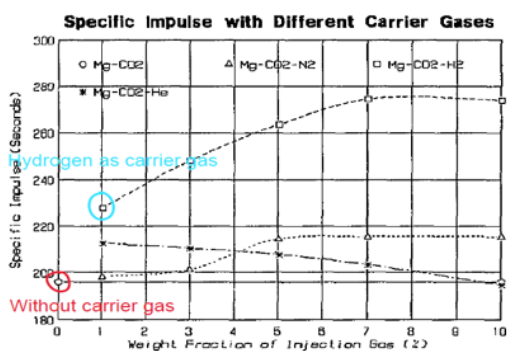


**Figure 3.1: Influence of carrier gas on specific impulse [4].**

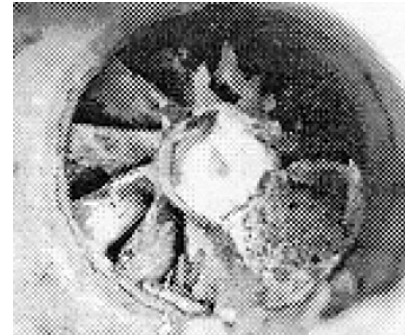


**Figure 3.2: Clogged rear blades after engine test due to the accumulation of carbon flakes [4].**

## 3.1. Propulsion system characteristics estimation

A computational tool for estimating the propulsion system's size and performance has been developed, with the objective of being rapidly iterable, where methods and equations found in literature have been implemented. This methodology will be discussed in this chapter.

### 3.1.1. Engine sizing

The first step was to size the engine itself, then use its characteristics in order to size the rest of the propulsion system.

**Estimating in- and outlet size** Figure 3.3 below shows the expected inlet and outlet diameter that such a Martian engine would have, depending on its maximum thrust [3]. The Excel tool has been programmed to use this table's underlying formula in order to estimate those parameters.

**Estimating fuel consumption and thrust** The Specific Fuel Consumption (SFC) has been estimated with the help of Figure 3.4 from the same paper (the image has been edited by the authors of this re-

port), where an Mg + CO<sub>2</sub> engine is compared with an Earth engine using JP-4 + O<sub>2</sub>. It can be noted that, between Mach 0.5 and 0.7, the SFC of the Martian engine is roughly 4 times larger than its Earth counterpart. Considering that the F135 (the engine that powers the F-35) is one of the most advanced turbojets there are and that its SFC is  $2.5 \times 10^{-5}$  kg/Ns, the Martian engine's SFC can confidently be assumed to be  $10 \times 10^{-5}$  kg/Ns [5].

I <sub>a</sub> [s]	80.4			
SFC [kgf/(hr·kgf)]	5.06			
F [N]	1500	1000	500	100
m <sub>CO<sub>2</sub></sub> [kg/s]	1.38	0.921	0.460	0.0921
D <sub>i</sub> [cm]	83.6	68.2	48.2	21.6
D <sub>n</sub> [cm]	78.6	64.2	45.4	20.3

**Figure 3.3:** Diameters and mass flow estimation for a certain thrust [3].

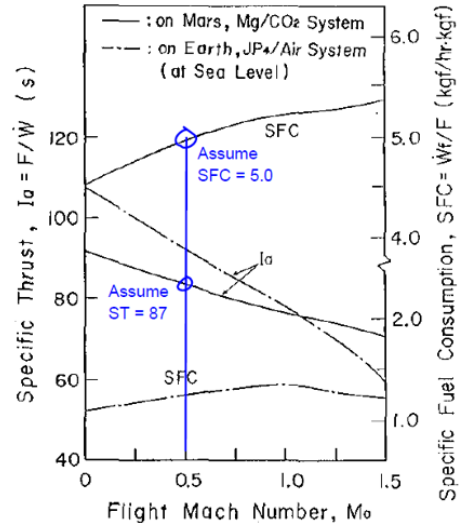


**Figure 3.4:** Comparison of specific thrust and specific fuel consumption of turbojet engines used in the atmospheres of Mars and the Earth as a function of Mach number [3].

By looking at Figure 3.4 again for the values between Mach 0.5 and 0.7, it can also be noted that the specific thrust of the Martian engine is roughly 4% worse than its Earth counterpart. Due to that, a thrust equally worse has been assumed.

**Sizing Equivalent Earth Engine** With these performance relations with respect to the Earth engine in mind, the strategy was then to translate this Martian engine into an "**Equivalent Earth Engine (EEE)**". With this strategy, classic statistical relations for Earth engines can be used for weight estimation, such that the sizing of the Martian engine is actually performed in the EEE, and the known drop in performance is then subsequently applied.

The mass for the EEE without the in- and outlet masses can be found using the statistical formula Equation (3.1) below with some adjustments for unit conversion [6]:

$$W_{lbs} = 250 + 0.175 \cdot T_{lbf} \quad W_{kg} = \left( 250 + 0.175 \cdot \frac{T_{lbf}}{4.44822} \right) \cdot \frac{1}{2.20462} \quad (3.1)$$

Where  $W_{lbs}$  and  $W_{kg}$  are the estimated masses of the engine in pounds and kilograms respectively, and  $T_{lbf}$  is the maximum thrust provided by the engine in pound force. Conversion factors have been used in the second formula so that the mass is returned in kilograms.

Subsequently, the mass of the in- and outlet can then be computed and added to the mass previously found using the formula below [7]:

$$M_i = 29.26 \cdot (l_d N_i A_i^{0.5} k_{geo})^{0.7331} \quad M_n = 14.63 \cdot \frac{\pi D_n^2}{4} \quad (3.2)$$

Where  $M_i$  and  $M_n$  are the in- and outlet masses respectively, both in kilograms. Furthermore,  $l_d$  is the duct length,  $N_i$  is the number of engines,  $A_i$  is the area of the inlet,  $k_{geo}$  is a statistical factor with a value 0.5, and  $D_n$  is the outlet's diameter. All variables use standard metric units. This way, the final Martian engine total mass is obtained.

### 3.1.2. Main fuel tank sizing

With the SFC of  $10 \times 10^{-5}$  kg/Ns previously discussed, the fuel consumption is then estimated based on the flight profile phases' required thrust. With this information, the fuel tank has been sized.

Since the magnesium powder does not need to be pressurized and it is relatively dense compared to liquid propellants, its tank's dimensions will be relatively small, and its thickness will be mainly constrained by thermal stresses. Due to this very low contribution to the total propulsion system's mass, it is neglected in this design phase.

### 3.1.3. Carrier gas storage and processing

A carrier gas is necessary to transport the magnesium powder to the interior of the engine's combustion chamber. The main idea is to use a pneumatic conveying system in order to capture Martian air mid-flight and pressurize it in a storage tank<sup>1</sup>.

Although the gas will be obtained mid-air, a sufficiently large storage tank is needed in order to ensure redundancy and a certain flight autonomy in case the pneumatic conveying system fails. An autonomy of 20 minutes of flight would arguably be ideal.

By determining a weight fraction of 1% for the carrier gas flow with respect to the magnesium powder, which would be enough to ensure proper flow [4], a CO<sub>2</sub> storage mass required can be derived. Then, using its molar mass and corresponding volume according to the ideal gas law, the tank's volume can be estimated depending on the pressurization factor chosen.

A cylindrical shape has been chosen for the tank for simplicity. Its thickness has been found by using the pressurization stress formula with thin-walled assumption, shown by Equation (3.3) and Equation (3.4) below:

$$\sigma_L = \frac{PD}{4t} \quad (3.3)$$

$$\sigma_C = \frac{PD}{2t} \quad (3.4)$$

Where  $\sigma_L$  is the longitudinal stress on the cylinder's walls,  $\sigma_C$  is the circumferential stress on the walls,  $P$  is the pressure differential between the inside and outside of the cylinder,  $D$  is the diameter of the cylinder, and  $t$  is the thickness of the tank's walls. Furthermore, it is known that for a classic fuel tank with pressurized fuel, the circumferential stress is dominant for the required thickness by looking at the equation's denominator.

## 3.2. Verification

Verifying a theoretical engine is quite hard, especially when the prototypes built have not been to scale. A good idea would be to compare its computed performance with that of Earth engines and see if this relation matches expectations described in scientific papers that report actual prototype testing.

Using the computational tool, a 125 kN Martian engine ends up having a thrust-to-mass ratio of 50 N/kg. The F135-100W engine has a value of 112 N/kg for that. This means that the assumptions made during the design of the tool were probably conservative, in the sense that taking into account the challenges this engine must overcome and its increased mass and decreased efficiency compared to the F135-100W, the final product is less than half as powerful proportional to its mass and about 4 times less fuel efficient than the Earth engine that is the best jet engine of its category [5].

Better performance might still be conservatively assumed given possible future advances in this technology. But this is something that would need more thorough analysis in the next design stages if this propulsion system is selected.

<sup>1</sup>URL: <https://www.iqsdirectory.com/articles/pneumatic-conveyor.html> [cited 2023-05-24]

# Preliminary Sizing

Five concepts were deemed promising in the baseline phase. To determine which one is the best to fulfill the mission, a quantitative trade-off will be performed. The preliminary sizing serves as a first-order estimation of values for trade-off criteria and is discussed in Sections 4.1 to 4.4.

To make the values comparable between designs, some common conditions were agreed upon. The design density for aerodynamic surfaces is  $0.01 \text{ kg/m}^3$ , which is the worst-case density at zero elevation and average density at 5 km altitude. The design payload mass is 350 kg, which corresponds to two suited astronauts of 250 kg and cargo of 100 kg. The lifting capability is based on a mass of 3000 kg, the maximum take-off mass (MTOM) requirement, while the target MTOM is 2700 kg (due to a 10 % margin). If the mass is below 2700 kg, the fuel mass is increased by the difference to obtain a higher range. This range will ultimately be compared in the trade-off.

## 4.1. Design concept 1+2: Fixed-wing aircraft

*By Joachim Bron*

In the following subsections, the two designs for the fixed-wing aircraft will be described. These designs consist of a flying wing aircraft and a biplane aircraft. First, in Section 4.1.1, definitions of what exactly is meant with each design are given. Then, in Section 4.1.2, the preliminary sizing approach for both fixed-wing aircraft is given. For each part, this is first described qualitatively, followed by numerical results for both concepts.

### 4.1.1. Definitions

*By Joachim Bron*

For the fixed-wing aircraft concepts, two designs were chosen: a flying wing aircraft and a biplane. As opposed to the other three options, these fixed-wing concepts use Horizontal Take-Off and Landing (HTOL). The flying wing aircraft consists of a (large) wing, a fuselage to carry the astronauts and payload, and potentially some control surfaces such as elevons at the end of the wings and a rudder. It does not have a horizontal stabilizer similar to conventional aircraft, which is the main difference from the biplane design. In general, the flying wing is advantageous as it is a simpler design; on the downside, it suffers on the stability side.

The biplane design consists of two wings stacked one on top of the other. It also contains a fuselage to carry astronauts and payload. It will potentially also have control surfaces such as ailerons and a rudder. Finally, its main difference from the flying wing concept is that it has a horizontal and vertical stabilizer. The biplane design comes at a lower weight than the flying wing due to its smaller wings and smaller structural requirements.

### 4.1.2. Preliminary sizing and main assumptions

*By Joachim Bron, Adrien Beňo, Timo de Kemp, Freek Braspenning*

The preliminary sizing for the fixed-wing concepts was performed as follows:

1. Research low Reynolds' number aerodynamic effects, as these will form the basis for the wing sizing.
2. Determine the minimum needed wing area and design wing plan-form.
3. Determine the fuselage volume and dimensions.
4. Calculate the drag due to the wing and fuselage.
5. Determine needed thrust based on maximum drag.
6. Size engines and compute their weight.
7. Perform class I weight estimations and iterate
8. Size structural aspects.
9. Perform stability calculations

**Aerodynamic considerations** The following provides an overview of the research concerning the aerodynamics of wings at low Reynolds' numbers. The discussed aspects include the coefficient of lift, coefficient of drag, taper ratio, aspect ratio, ground effect, vortex generators, staggered wings, and unconventional wing designs, such as box wings and biplanes.

The design of conventional and flying wing concepts is highly dependent on the lift and drag coefficient of its wings as no other force in the lifting direction is readily available. Preliminary analysis shows that the approximate Reynolds' number which any of the two concepts would experience is in the order of magnitude  $10^5$  (see Equation (4.1)), which puts the aircraft in a regime when viscous forces are dominant over inertial.

$$Re = \frac{uL}{\nu} = \frac{111 \cdot 1}{5.17 \cdot 10^{-4}} = 214700 \quad (4.1)$$

This limits the research of airfoils to specialized low Reynolds' number airfoils. Selig and Guglielmo [8] provide a selection of high lift low Reynolds' number airfoils. For the preliminary design analysis, we will assume the best-performing one - S1223. This airfoil has  $C_{l_{max}} \approx 2.3$ , and its lift curve can be slightly adjusted by the use of vortex generators or high-lift devices. The former could potentially provide additional  $\Delta C_{vg} = 0.3$  and the latter can adjust the shape of the lift curve [9].

According to the experimental and theoretical work of [?], the taper ratio almost does not affect the lift curve, but higher airfoil efficiency can be achieved with a straight planform. Hence, for the purposes of the preliminary research, taper ratio  $\lambda = 1$  will be assumed. An aspect ratio of higher than 10 suffices to reach the saturation part of the range and endurance curves for most low Reynolds' number airfoils [10], hence this value is assumed. According to Gross and Traub [11], the ground effect does not provide any additional noticeable lift. Even worse, ground proximity increases drag. Hence, we assume that the aircraft will not make use of the ground effect.

One of the problems encountered in low Reynolds' number flight is early flow separation. One of the design options which could help mitigate this phenomenon is staggered wing design, as shown in Figure 4.1. Unfortunately, XFLR5 (which runs on XFOIL) could not analyze this configuration and hence it will be omitted from the current design stage and left for further analysis in the detailed design stage.



**Figure 4.1:** Staggered wing design helps to direct the flow, which would have otherwise separated, according to the shape of the wings staggered behind the first wing. [own work]

The drag estimations form one of the driving performance characteristics of the wing design as thrust is also very limited in the Martian atmosphere. "Unconventional" wing designs, such as biplane or box wing planes must be explored by default, as conventional wing designs do not provide necessary drag characteristics. The induced drag estimation is based on the induced drag formula, given in Equation (4.2). According to Somerville et al. [12], the induced drag of unconventional wings can substantially decrease drag, as shown in Figure 4.2.

$$C_{D_i} = \frac{C_L^2}{\pi AR} (1 + \delta) \quad (4.2)$$

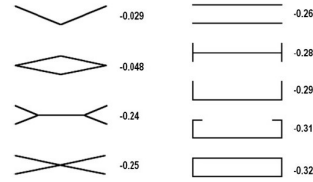


**Figure 4.2:** Negative induced drag factor for unconventional wings  $\delta$  [12]

For structural reasons and the need for ease of assembly at the site, some of the above designs are considered unfeasible. Moreover, the need for two wings is justified by otherwise too large wing area for single wing. This leaves biplane and box configuration. For ease of assembly, we will assume  $\delta = -0.26$ .

**Wing sizing** In order to size the wings, their area was estimated first. This was done for the worst case scenario, which occurs at MTOM and stall speed. The required wing gross surface area is given by Equation (4.3)

$$S = \frac{W_{MTOM}}{C_{L_{max}} \frac{1}{2} \rho V_{stall}^2} \quad (4.3)$$

where  $W_{MTOM}$  is maximum take-off weight and  $V_{stall}$  is the stall speed. MTOM was taken from the requirements with a value of 3000 kg,  $V_{stall} = 70 \text{ m/s}$  was assumed based on typical values for stall speed, and  $\rho = 0.01$  was taken as it is a conservative estimate.  $C_{L_{max}}$  was taken as described under "Aerodynamic considerations".

Once the necessary surface area was calculated, the wing parameters were chosen to shape the wing. The parameters that had to be chosen are the aspect ratio  $AR$ , the taper ratio  $\lambda$  and the quarter chord sweep  $\Lambda_{0.25}$ . These are mostly important for the flying wing to ensure stability, and thus are less important for the biplane (as shown in Table 4.1). From these parameters, the wingspan, root chord length, tip chord length as well as the mean aerodynamic chord (MAC) can also be calculated. Furthermore, the wing planform can be shaped and the geometry of the wing designed, which will be useful to calculate the center of gravity.

**Fuselage sizing** To provide space to carry the astronauts and payload, a fuselage / main body is needed. The minimum volume needed for the astronauts was found using standard cabin sizes. This cabin was assumed to be have internal dimensions of  $1.5 \times 1.5 \times 1.9 \text{ m}^3$ . Around this a cylindrical fuselage with a diameter of 2.5 m was fit. Using values given by Torenbeek [7], a payload density of  $160 \text{ kg/m}^3$  was assumed. Assuming a loading efficiency of 85% and a payload mass of 100 kg, this meant that  $0.9 \text{ m}^3$  of volume was needed for the payload. Furthermore, to enhance the aerodynamics of the fuselage, it was chosen to add parabolic-shaped nose and aft cones, which also provide more storage space in case this would be needed for other systems.

With these dimensions known, the fuselage geometry and center of gravity could be determined, and could be connected to the wing geometry. For simplicity, the fuselage designed (presented later) was the same for both the flying wing and the biplane. Its placement relative to the wing is still preliminary, but an effort was made to put it as forward as possible to ensure enough stability margin later on and make sure the aircraft center of gravity (CG) is in front of the aircraft aerodynamic centre (AC).

**Weight estimations** The weight is being divided into the following three categories: Operational Empty Weight (OEW), Fuel Weight (WF), and Payload Weight (WPL). In the lecture slides by R. Vos et al. [13] a method is presented to determine these weights. For the OEW a statistical estimation was proposed, however, no comparable aircraft have been designed for Mars. Consequently, a different estimation method was needed to estimate the OEW. This method is the one from Torenbeek [7], which provides a way to estimate different parts of the OEW. The final part of the OEW that needed to be accounted for was the trapped oil and fuel. This was taken to be 1% of the targeted weight. Weight fractions were used to

describe the fuel used in each stage of the flight. For ground operations, take-off, climb, descent, and landing the weight fractions proposed by the slides from R. Vos et al. [?] were used. The Breguet range equation was used to determine the fuel fractions for range. Furthermore the same design mission was used as in the lecture slides, except for the loiter phase as no loitering for an airport was necessary on Mars. Finally the payload weight is the weight of the two astronauts including their suits and an additional 100 kg were assumed to be taken to do their research.

Note that initially, the wing's weight was estimated based on the same weight loading as the Raymer aircraft [14]. After the class I weight estimation was completed, this estimate turned out to be quite accurate.

Using the weights calculated and the placing of the different components, the CG of the aircraft could be found. Regarding the weight of the fuel, the volume needed to carry it was found to be much smaller than the volume available to carry fuel in the wings, and thus the fuel was assumed to be spread along the wings as a preliminary estimate.

**Engine sizing** Based on the thrust required at cruise, the thrust required for the climb performance requirements, and the thrust required at TO and landing, the maximum thrust required can be found and used to size the engines. For the fixed-wing concepts, only the Mg-CO<sub>2</sub> engines are used, since preliminary calculations using propellers and batteries demonstrated the design to be too heavy and impossible to perform any ground operations. Using the required thrust, the engines can be sized and their weight estimated, and more accurate estimates of the fuel needed can be obtained. More details on the engine sizing can be found in Chapter 3. It was chosen to use two engines for reliability purposes, placed on the wing (the placement will be investigated further in the detailed design).

**Drag estimations** Drag estimations are produced based on the formulas from Torenbeek [7]. Equation (4.4) helps with conceptual understanding of the process.

$$C_D = C_{D_0} + C_{D_i} = C_{D_0} + \frac{C_L^2}{\pi e AR} \quad (4.4)$$

$C_{D_0}$  can be further decomposed as a function of fuselage dimensions and different aerodynamic correction factors as given in Torenbeek [7]. Oswald efficiency factor is given by the results of the research on aerodynamic provided before,  $e = \frac{1}{1+\delta} = 1.35$ . It may seem erroneous that the Oswald efficiency factor is above 1, since elliptical wing has  $e_{elliptical} = 1$ . However, it is in fact correct due to the interaction between the upper and lower wings which contribute to  $e$ . Drag is then equal to:

$$D = C_D \cdot q \cdot S \quad (4.5)$$

where  $q$  and  $S$  correspond to dynamic pressure and surface area. These values are specific to the two concepts and are left to be evaluated in their respective chapters.

**Structural considerations** A preliminary structural analysis was performed on the wing subsystem. First a wingbox representation of the airfoil was made. The geometry of the wingbox was estimated, as seen in Figure 5.2b. From the geometry, the moments of inertia were computed by Equation (4.6), Equation (4.7), and Equation (4.8).

$$I_{xx} = \frac{ta^3 \sin^2 \beta}{12} \quad (4.6) \qquad I_{zz} = \frac{ta^3 \cos^2 \beta}{12} \quad (4.7) \qquad I_{xz} = \frac{ta^3 \sin \beta \cos \beta}{12} \quad (4.8)$$

With this the internal stresses can be computed using Equation (4.9).

$$\sigma_y = \frac{(M_x I_{zz} - M_z I_{xz}) z + (M_z I_{xx} - M_x I_{xz}) x}{I_{xx} I_{zz} - I_{xz}^2} \quad (4.9)$$

Where the moment distributions were obtained from the lift and drag distributions given by simulation results from XFLR5.

#### 4.1.3. Performance calculations

By Freek Braspenning, Joachim Bron

**Mission profile** The mission profile considers the main mission (2-5) as well as possible diversions (5-8). The mission profile for both the flying wing and the biplane is given in Figure 4.3.



Figure 4.3: Mission profile

**Thrust and maximum speed calculations** After the maximum thrust has been found, the (horizontal steady) maximum speed that can be flown can be computed by using Equation (4.10):

$$T = D \implies T = C_{D0} \frac{1}{2} \rho V^2 S + \frac{W^2}{\pi A e} \frac{1}{\frac{1}{2} \rho V^2 S} \quad (4.10)$$

Equation (4.10) can be solved for  $V$  for various thrust settings until the maximum  $V$  is found. Note that the maximum speed was calculated for the worst case scenario of MTOM = 3000 kg. The maximum speed is assumed to be Mach 0.7 even if the propulsion system allows for a higher speed, to avoid compressibility effects.

**Maximum altitude** The theoretical maximum altitude that can be flown can crudely be approximated by finding the minimum air density at which the aircraft can fly, given by Equation (4.11):

$$\rho_{h_{max}} = \frac{W}{C_{L_{max}} \frac{1}{2} V_{h_{max}}^2 S} \quad (4.11)$$

This is computed for the highest weight. Using the density calculated and the atmospheric model of Mars, the altitude can be computed.

**Cruise condition calculations** The cruise condition  $C_L$  was checked to verify previous calculations and checked whether the approximated values were in accordance with this calculation. The value of  $C_{L_{cruise}}$  was found using Equation (4.12):

$$C_{L_{cruise}} = \frac{MTOM \cdot g_{mars}}{q_\infty S} \quad (4.12)$$

where  $q_\infty$  is the free-stream dynamic pressure. Finally, the drag at cruise condition is needed to determine how much thrust is required.

**Climb performance** The aircraft needs to achieve a required climb angle in order to avoid obstacles or get out of a crater. Based on statistical data of Martian craters' dimensions, it was decided that the aircraft shall have a minimum climb angle of  $\gamma = 30^\circ$ . The amount of thrust required to meet this minimum climb angle is then determined using Equation (4.13):

$$T = D + W \sin \gamma \quad (4.13)$$

where  $W$  is the maximum take-off weight. Based on this, the maximum Rate of Climb (RC) can be found using Equation (4.14).

$$RC = \frac{TV - DV}{W} \quad (4.14)$$

**Take-off and landing performance** Take-off and landing is mostly determined by the take-off and landing distance. For take-off, the thrust required is given by Equation (4.15):

$$T = \frac{V_{LOF}^2 W}{2d_{TOg}} + \bar{D} + D_g \quad (4.15)$$

where  $V_{LOF} = 1.05V_{stall}$  is the liftoff speed,  $d_{TO}$  is the take-off distance, and  $W$  is the maximum take-off weight.  $\bar{D} = C_{D,TO} \frac{1}{2} \rho \bar{V}^2 S$  is the average aerodynamic drag during take-off and  $D_g = \mu(W - \bar{L})$  is the drag due to the ground friction. The landing performance was always found to be less critical than take-off performance, hence we only present the take-off related equation.

#### 4.1.4. Structural considerations

By Freek Braspenning, Timo de Kemp

**Flying wing structural performance** The aerodynamic loads exerted on the wing are given in Figure 4.4. The loads were estimated by simulation results from XFLR5. The wingbox shape is assumed to approximately follow the airfoil, as shown in Figure 4.5b. The maximum tensile stress in the wingbox occurs at the root and is equal to 282.5 MPa. This occurs at point 4, as shown in Figure 4.5a. The maximum compressive stress in the wingbox occurs at the root and is equal to 282.0 MPa. This occurs at point 2, as shown in Figure 4.5a.

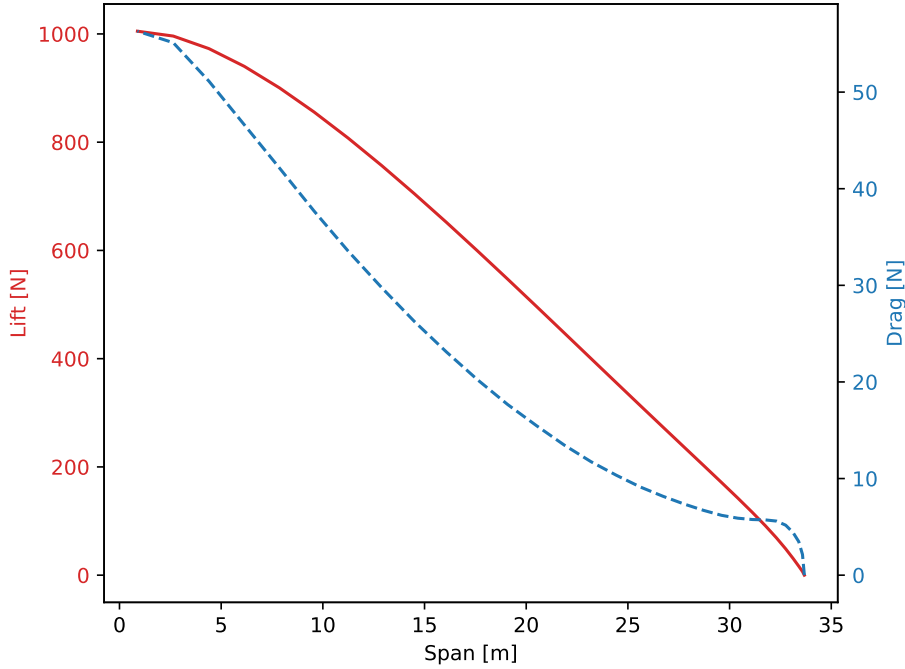
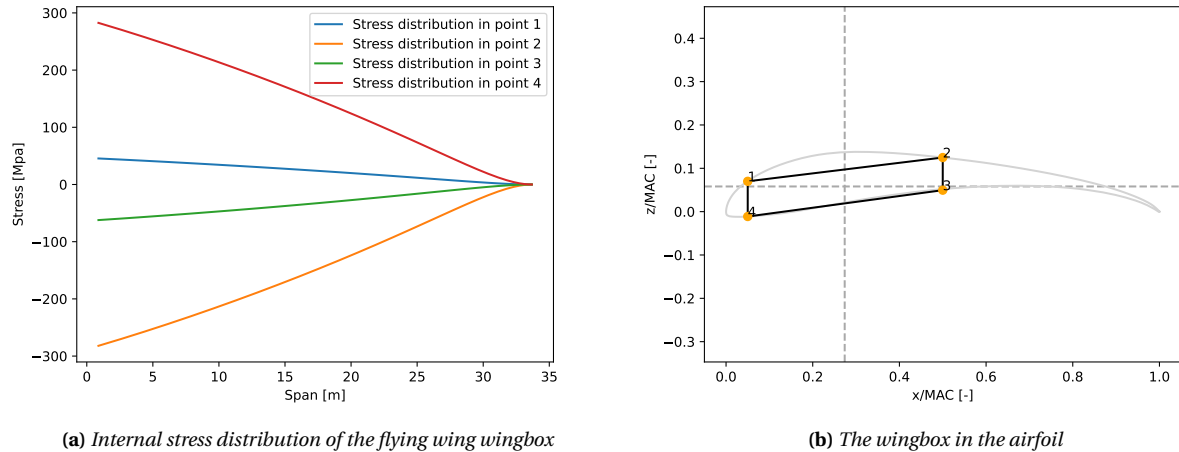
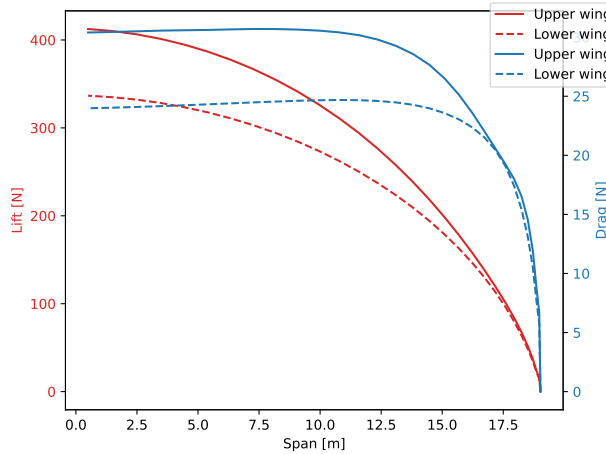


Figure 4.4: Applied loads on the wing of the flying wing



**Figure 4.5:** Internal stress distribution in the wingbox

**Biplane structural performance** The aerodynamic loads exerted on the main wings are given in Figure 4.6. The loads were estimated by simulation results from XFLR5. The wingbox shape is assumed to approximately follow the airfoil, as shown in Figure 4.7b. The maximum tensile stress in the wingbox occurs at the root of the bottom left stringer, see point 4 in Figure 4.7b, and is equal to 283.3 MPa, as shown in Figure 4.7a. The maximum compressive stress in the wingbox occurs at the root of the top right stringer, see point 2 in Figure 4.7b, and is equal to 282.6 MPa, as shown in Figure 4.7a. It should be noted that the average applied loads on the wings of the flying wing are higher than the average applied loads on the wings of the biplane, yet the maximum tensile stresses are approximately the same. This is due to their respective wing planform.



**Figure 4.6:** Applied loads on the wings of the biplane

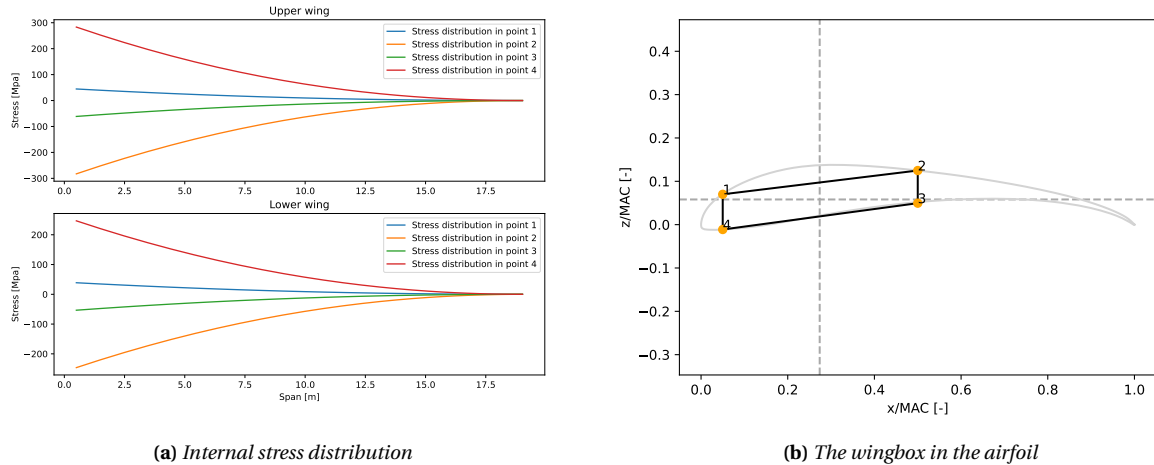


Figure 4.7: Internal stress distribution in the wingbox

#### 4.1.5. Stability and control

By Joachim Bron and Adrian Beňo

**Flying wing stability** Stability is a common problem among flying wings. Commonly, reflex airfoils or large sweep angles are needed to achieve stability. Here, a simple stability model was set up to check if stability can be achieved using elevons and an arbitrary airfoil.

The flying wing was modeled by a CG, in which the weight ( $W$ ) acts, an AC (behind the CG for stability) in which the moment  $M_{ac}$  and normal force  $N$  of the wing and aircraft act and the elevon's AC, where the elevon's normal force  $N_e$  acts. The distances between these different points are given in Figure 4.8.

Setting up moment and force equilibrium and assuming steady flight, the following equations were obtained:

$$M_{cg} = 0 \implies M_{ac} - N(x_{ac} - x_w) - N_e l_e = 0 \quad (4.16)$$

$$F_y = 0 \implies N = W \quad (4.17)$$

Both can be rewritten as:

$$C_{m_{ac}} - C_N \frac{x_{ac} - x_w}{\bar{c}} - C_{N_e} \left( \frac{V_e}{V} \right)^2 \frac{S_e l_e}{S \bar{c}} = 0 \quad (4.18)$$

$$C_N = \frac{W}{\frac{1}{2} \rho V^2 S} \quad (4.19)$$

Assuming  $V_e/V = 1$ , the first equation can be rewritten as:

$$C_{N_e} \frac{S_e l_e}{S \bar{c}} = C_{m_{ac}} - C_N \frac{x_{ac} - x_w}{\bar{c}} \quad (4.20)$$

This equation was then used to size the elevons and ensure moment equilibrium. Later on, a deeper analysis can be performed to investigate static stability using control derivatives.

**Biplane stability** The approximate size and weight of the horizontal tail had to be approximated based on the stability constraints. One additional constraining factor was the need for symmetrical airfoil. Unfortunately, these have lowered maximum coefficient of lift. For the purposes of the preliminary design,

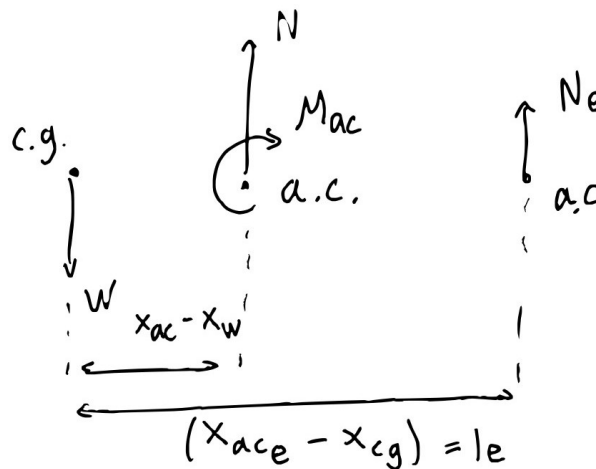


Figure 4.8: FBD of simplified flying wing

NACA0012 airfoil was assumed. The force needed to be exerted by horizontal tail is given in Equation (4.21). The surface area required is then given by Equation (4.22). The horizontal tail surface area was evaluated for take-off, cruise and landing conditions separately, in order to find the limiting size. The weight of the horizontal tail was estimated using formula from [7], given in Equation (4.23).

$$N_h \approx \frac{1}{l_h} \left( C_{m_{ac}} \frac{1}{2} \rho V^2 S c + W(x_{cg} - x_w) \right) \quad (4.21)$$

$$S_h = \frac{N_h}{C_{l_h} \frac{1}{2} \rho V^2} \quad (4.22)$$

$$M_t = 0.64(n_{ult} S_{tail}^2)^{0.75} \quad (4.23)$$

#### 4.1.6. Preliminary design concept 1 summary: Flying wing

By Adrian Beňo and Joachim Bron

The defining characteristics of the flying wing concept is that it lacks a tail. This reduces the total drag and decreases the amount of fuel needed, which makes the concept more sustainable. At the same time, the area of the wing causes high wingspan and high average structural loads, which require more material. Furthermore, the geometry of the flying wing makes it hard to maneuver close to the ground. The defining design characteristics regarding the flying wing concept can be found in Table 4.1. The planform of the flying wing can be seen in Figure 4.9.

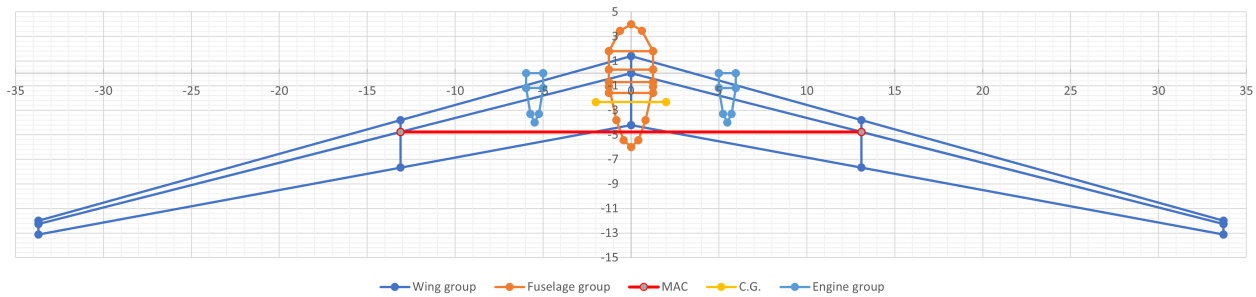


Figure 4.9: Top view of the flying wing concept

#### 4.1.7. Preliminary design concept 2 summary: Biplane

By Adrian Beňo and Joachim Bron

The defining characteristic of the biplane concept is an Oswald efficiency factor greater than 1, which substantially reduces the induced drag. Moreover, the biplane design distributes the necessary wing area over two wings and thus, effectively reduces the wingspan by a factor of 2. As mentioned before, this does not decrease the maximum stress in the wing, but the stress distribution over the wingspan results in lower structural loads on average, decreasing degradation due to fatigue. It is also easier to maneuver due to its geometry. The defining design characteristics regarding the biplane concept can be found in Table 4.1. The planform of the biplane can be seen in Figure 4.10.

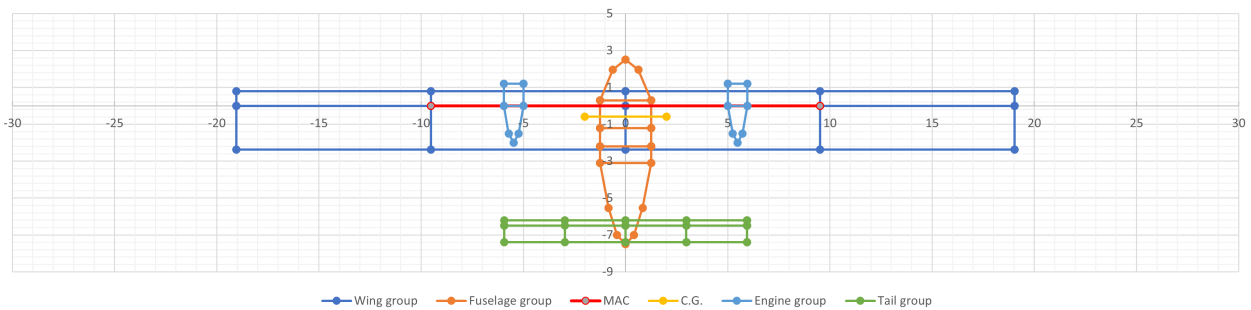


Figure 4.10: Top view of the biplane concept

**Table 4.1:** Selection of the defining parameters of the flying wing and biplane concepts.

Parameter	Flying wing	Biplane	Parameter	Flying wing	Biplane
$C_{l_{max}}$	2	2	$V_{cruise}$ [m/s]	111	111
$C_{l_{cruise}}$	0.79	0.79	$MAC$ [m]	3.37	3.17
$C_{l_{takeoff}}$	1.8	1.8	$f_d$ [m]	2.5	2.5
$C_{l_{landing}}$	2	2	$f_l$ [m]	10	10
$\lambda$	0.2	1	$OEW$ [N]	6270	5314
$AR$	20	12	$WF$ [N]	2318	3355
$e$	0.75	1.35	$WP$ [N]	1298	1298
$C_{D_0}$	0.034	0.034	$V_{max}$ [m/s]	154	154
$D$ [N]	478	483	$RC$ [m/s]	32.18	32.69
$S$ [ $m^2$ ]	227	227	$e_d$ [m]	0.96	0.96
$V_{stall}$ [m/s]	70	70	$e_t$ [m]	1.2	1.2
$b$ [m]	67.4	38.1	$T_{max}$ [N]	4550	4539
$W_{engine}$ [N]	816	712	$c_{root}$ [m]	5.61	3.17
$\lambda_{1/4} [deg]$	20	0	$c_{tip}$ [m]	1.12	3.17
$d_{take-off}$ [m]	2000	2000	$d_{landing}$ [m]	1949	1960
$R$ at 350 kg payload [m]	1779	2157	-	-	-

## 4.2. Design concept 3: Tiltrotor aircraft

By Sebastian Harris, Javier Alonso

The tiltrotor configuration requires the combination of a wing and the lift capacity of a rotorcraft. Regarding the rotor configuration, it was chosen to use a set of counter-rotating rotors at the tip of each wing in order to reduce the required rotor radius for take-off.

### 4.2.1. Main Rotor Sizing

By Sebastian Harris

The process for sizing the main rotor is based on the combination of momentum and blade element theory, as detailed in the book *multicopter Performance, Stability, and Control* by Prouty [2]. The process requires a blade number, blade radius, chord, twist, cutout, airfoil data, and the relevant test conditions as input. The initial conditions were set to contain the number of blades per rotor, determined to be 6, the chord, calculated as a twentieth of the radius, the twist, assumed to be ideal, the blade cutout, determined to be the chord divided by the radius, and finally the data of the airfoil in this case S1223. The rotation of the chord is calculated to always lead to a tip speed of Mach 0.92.

The blade is separated into up to 15 elements along the radius, each of equal length. For each of these elements, the chord is calculated as well as the local Mach number. The latter is done by the following relation, also leading to the lift curve slope:

$$M_{local} = (r/R) \left( \frac{\Omega R}{V_{sound}} \right) [2] \quad a_{local} = \frac{a}{\sqrt{1 - M_{local}^2}} [2]$$

Subsequently, the local twist of the blade can be calculated for each element boundary as  $\Delta\theta$ . Thus, the pitch at the blade element is calculated as

$$\theta = \theta_0 + \Delta\theta - \alpha_0 [2]$$

Where  $\alpha_0$  is the zero lift angle of attack for the airfoil selected.

Due to the twist and rotation of the blade, each element has a separate angle with respect to the flow, part of which is called the local inflow angle. The local inflow depends on the twist amongst other parameters

and is calculated as

$$\frac{v_1}{\Omega r} = \frac{ab\frac{c}{R}}{16\pi\frac{r}{R}} \left[ -1 + \sqrt{1 + \frac{32\pi\theta\frac{r}{R}}{ab\frac{c}{R}}} \right] [2]$$

Finally, the local angle of attack can be calculated as  $\alpha = \theta - \arctan \frac{v_1}{\Omega r}$ . For the sake of design simplicity in these first stages, it was assumed the local angle of attack would be constant at 6°, a value that matches that of rotorcraft on Earth. [2].

Given this angle of attack, the local values for lift and drag coefficients can be calculated using the previously mentioned lift curve slopes.

With these values in mind, the thrust coefficient can be calculated by first determining the running thrust loading, followed by integrating over the length of the blade, starting from the cutoff point in order to provide the thrust coefficient without tip loss:

$$\frac{dC_t}{d\frac{r}{R}} = \frac{b(\frac{r}{R})^2 \frac{c}{R} c_l}{2\pi} [2] \quad C_{T_{notiploss}} = \int_{x_0}^1 \frac{dC_T}{d\frac{r}{R}} d\frac{r}{R} [2]$$

The tip loss factor, B, is calculated, from which the final thrust coefficient follows:

$$B = 1 - \frac{\sqrt{2C_{T_{notiploss}}}}{b} [2] \quad C_T = C_{T_{notiploss}} - \int_B^1 \frac{dC_T}{d\frac{r}{R}} d\frac{r}{R} [2]$$

In parallel, the required torque for the blade to rotate can be found via the running profile torque, calculated as follows:

$$\frac{dC_{Q_0}}{d\frac{r}{R}} = \frac{b(\frac{r}{R})^3 \frac{c}{R} c_d}{2\pi} [2] \quad C_{Q_0} = \int_0^1 \frac{dC_{Q_0}}{d\frac{r}{R}} d\frac{r}{R} [2]$$

Similarly, the running-induced torque loading:

$$\frac{dC_{Q_i}}{d\frac{r}{R}} = \frac{b(\frac{r}{R})^3 \frac{c}{R} c_l \frac{v_1}{\Omega r}}{2\pi} [2] \quad C_{Q_i} = \int_{x_0}^B \frac{dC_{Q_i}}{d\frac{r}{R}} d\frac{r}{R} [2]$$

The disk loading of the rotor can be calculated as:

$$D.L. = C_T \rho (\Omega R)^2 [2]$$

Finally, the thrust generated by the rotor can be calculated as:

$$T = \rho A (\Omega R)^2 C_T [2]$$

In order to understand the power required by the rotor, the thrust and area of the rotor can be combined to find:

$$P = T \sqrt{\frac{T}{2\rho A}} [2] \quad (4.24)$$

The required radius can be found for a specified mass by iterating this process until the lift produced is sufficient.

The result of the iteration leads to the following values for both rotor and power sizing:

- Rotor Radius: 10.4 [m]
- Rotor Thrust: 2789.72 [N]
- Power Required per Rotor: 56522 [W]

It is important to note that this value of power applies for maximum thrust during vertical take-off, during cruise, and other flight states, this value will be lower due to the action of the wing.

To minimize the mass of the rotor, a study was conducted relating the weight of the rotor with respect to its loading. This led to the calculation of the lowest possible rotor mass. As a first estimate, a rotor fill of 9% was used, leading to a mass of 265 kg per set of rotors.

### 4.2.2. Geometry sizing

By Javier Alonso

The sizing of the wing is set up in order to minimize wing area when in cruise. This is done by first determining the maximum mass to be lifted, in this case, 3000 kg. Next, the lifting coefficient was determined to be the same as that of the rotor. That is, the value of the S1223 airfoil at an angle of attack of 6°, which is 1.6. As such, the required surface area can be calculated as:

$$S = \frac{MTOMg_{mars}}{C_L \frac{1}{2} \rho V_{cruise}^2} [15]$$

The total wing area required is 112.7 m<sup>2</sup>. Regarding the shape of this wing, two factors determine its size. The first is the rotors having enough space to rotate without interfering with each other. As a first estimate, it was determined that one rotor radius of space between the tips would be sufficient, therefore, the wingspan would have to be three times the rotor radius. Furthermore, the low viscosity of the Martian atmosphere leads to a requirement for an aspect ratio to be larger than 10, as mentioned in Section 4.1. From the surface area, the induced drag can be calculated via the formula:

$$C_{D_{wing}} = C_{D_0} + \frac{C_L^2}{\pi ARe} [15]$$

Additionally, the drag of the fuselage, engines and undercarriage can be calculated through statistical relations as described by Torenbeek [7].

The first step was to determine the relevant dimensions, for this, the cockpit was determined to have a length of 1.78 m as this value is average in aircraft[7]. Next, the fuselage was assumed to be a cylinder of 1.5 m diameter. Although this value does not allow for the astronauts to stand, it should nonetheless allow for ample operating room. Finally, to the length of the cockpit, the wing chord was added in order to ensure sufficient structural load paths. As there is no need for the fuselage to extend all the way back, the tail was assumed to be connected via a set of booms to the fuselage, thus reducing the fuselage's total length. The relationships for the drag of the fuselage and engines can be seen below:

$$C_{D_{fuselage}} = 0.0031 l_{fuselage} (h_{fuselage} + b_{fuselage}) [7] \quad C_{D_{engine}} = 2 \cdot 0.08 \cdot 0.07 [7]$$

For the engines, the value was hard to estimate as the shape of the engines is not yet known. However, the drag was still calculated not to neglect the contribution. Regarding the undercarriage, the exact design was not yet known, leading to an assumption the main gear would retract into the streamlined fairing, which results in a correction factor:  $r_{uc} = 1.08$  [7].

Next, the drag must be corrected according to the Reynolds number around the fuselage, leading to a correction factor:

$$r_{Re} = 47 \left( \frac{V_{cruise} l_{fuselage}}{\mu_{cruise}} \right)^{-0.2} [7]$$

Finally, the tailplane correction factor is  $r_t = 1.24$  [7]. Combining these factors leads to a drag coefficient, after which the total drag is calculated.

$$C_{D_0} = r_{Re} \cdot r_{uc} \cdot \frac{r_t (C_{D_{fuselage}} + C_{D_{engine}})}{S_{wing}} [7] \quad D = \frac{1}{2} \rho S_{wing} V_{cruise} (C_{D_0} + C_{D_{wing}})$$

During the cruise, this drag must be counteracted by thrust, thus providing a value for cruise thrust,  $T_{cruise}$ , which, after implementing all the formulas above, comes to a value of 739.5 N.

### 4.2.3. Power budget

By Javier Alonso

A different power will be required during cruise and vertical climb. During cruise, the power output of the propeller can be calculated by multiplying the thrust required during cruise and the cruise velocity, which lead to a required power of:

$$P = T_{cruise} V_{cruise} = 739.5 \text{ N} \cdot 112 \text{ m/s} = 82.163 \text{ kW} \quad (4.25)$$

The minimum cruise time required, stemming from the cruise speed and minimum range, was 2.5 hours. This value was then multiplied to the power obtained in Equation (4.25) in order to obtain the energy that needs to be stored in the aircraft for cruise. Two significantly different values can be found for electrical and thermal engines since the former have an efficiency of up to 95% but modern thermal engines have an efficiency of just 50%<sup>1</sup>.

As mentioned before, with a thrust of 739.5 N, the power output of the engines will be 82.163 kW. The situation during lift-off and landing are very different, however. The required thrust in these scenario was 11.13 kN; therefore, the total power output could be calculated using Equation 4.24 which yielded a value of 226.1 kW. As an initial estimate of take-off procedures, the time for this maneuver was determined to be five minutes.

Thus, the values of energy and power consumption were calculated by multiplying the power by the time during which the power is applied. The results of this can be seen in Table 4.2.

**Table 4.2: Energy and Power consumption at various maneuvers**

Maneuver	Power [W]	Energy[Wh]
Take-off	226088	18840.7
Cruise	82163.7	205409.3

By using an energy density of 437 Wh/kg, a power density of 1317 W/kg [16] and applying a 30% margin to account for battery degradation, the total battery mass comes up to 878 kg.

To increase the range and the ability to fly to remote areas, the installation of solar panels on the wing's surface would decrease the power consumption during flight as well as allow recharge once landed. The solar irradiance on Mars is 586.2 W/m<sup>2</sup><sup>2</sup>, and the available wing area is 112.7 m/s<sup>2</sup>. Using a total area of 56 m<sup>2</sup> the average collecting power would be 32.8 kW. Space-degree solar panels have an efficiency of 34%<sup>3</sup>. Therefore, they would be able to provide 11.1 kW with a 90° angle of incidence and maximum irradiance, which represents around an eighth of the power consumption in cruise.

#### 4.2.4. Weight Calculation

By Sebastian Harris

Once certain dimensions of the aircraft were known, it was possible to determine the weight of the relevant structures along with more detailed dimensions of the aircraft. The formulas used were sourced from statistical relations by Torenbeek [7].

The first step was to determine the dimensions of the fuselage. The cockpit area was set to have a length of 1.78 m [7]. The fuselage was assumed to be cylindrical in order to facilitate calculations. For the cross-sectional dimensions of the fuselage, the diameter of the fuselage was set to be 1.5 m based on the 0.75 m distance between seats specified by Torenbeek [7]. The length of the fuselage was set to be the length of the cockpit plus the length of the chord.

With these dimensions the value of the wing group can be calculated with the following relation:

$$\frac{m_{wing}}{m_{TO}} = 4.910^{-3} b^{0.75} \left( 1 + \sqrt{\frac{1.905}{b}} N_{ult}^{0.55} \frac{\frac{b}{c}}{S_{wing}} \right)^{0.3} [7]$$

Additionally, the use of a wing brace, a structure relieving the wing from its own weight, was used to further reduce this weight by 30%.

<sup>1</sup>URL: <https://simpleflying.com/electric-aircraft-power-chain-efficiency-guide/> [cited 2023-05-16]

<sup>2</sup>URL: <https://mars.nasa.gov/all-about-mars/facts/> [cited 2023-05-01]

<sup>3</sup>URL: <https://www.spectrolab.com/DataSheets/Panel/panels.pdf> [cited 2023-05-24]

The tail of the aircraft was then sized. In order to provide some first estimates, it was determined the rear tail would be sized as:

$$S_{tail} = \frac{S_{wing} c}{1.5R} [7] \quad m_{tail} = 0.64(N_{ult} S_{tail}^2)^{0.75} [7]$$

Next, the fuselage weight was calculated. This is dependent on the gross surface of the fuselage and the dive speed. The dive speed was determined to be 110% of the cruise speed as the cruise speed should be the aircraft's maximum speed.

For the gross fuselage area, it was assumed to be a cylinder capped by a half sphere at each end, leading to the calculation as:

$$S_{gross} = 4\pi r^2 + 2\pi r * l_f [7] \quad m_{fus} = 0.23 \sqrt{\frac{V_{dive} l_t}{(b_f + h_f)}} S_{gross}^{1.2} [7]$$

The total weight of the aircraft was then used to determine the weight for the next iteration, calculated as follows:

$$m_{total} = m_{wing} + m_{tail} + m_{rotor} + m_{payload} (+m_{solar})$$

Finally, the volume of the aircraft could be calculated based on these dimensions. This volume was divided into the volume of the wings, the rotor blades, the fuselage and the tail. In addition to this, a safety factor of 50% was added to account for elements needed for the assembly such as the tail pole.

The fuselage was sub-divided into a conical cockpit and a cylindrical fuselage section. Its volume can be calculated as shown in Equation (4.26).

$$V_f = \frac{1}{3} l_{cockpit} \left( \frac{f_w}{2} \right)^2 \quad (4.26)$$

In order to size the wings, the cross-sectional area of the airfoil was computed using Python and multiplied by the wingspan. The same procedure was applied to the rotor blades.

Finally, the density of the tail was assumed to be the same as the wing, such that the volume was obtained by multiplying the wing volume by the mass fraction.

#### 4.2.5. Performance

*By Sebastian Harris*

The performance of the design was mainly calculated based on RC and the payload-range diagram. Regarding RC, this was calculated at cruise, allowing for a better understanding of performance in operational capabilities.

When calculating RC, the first step was to determine the climb angle during the cruise. This angle depends on the maximum thrust available during the cruise. This is done by calculating it from the power relation:

$$T_{max} = \frac{P_{available}}{\sqrt{\frac{1}{2\rho\pi R^2}}}^{\frac{2}{3}}$$

From which the climb angle was found, in turn leading to the rate of climb.

$$\gamma = \arctan \left( \frac{T}{m_{total} g_{mars}} - \frac{C_l}{C_d} \right) \quad ROC_{cruise} = V_{cruise} \sin \gamma$$

Regarding the vertical configuration, the climb performance was dependent on the difference in horsepower between the maximum performance and that required to hover. As the maximum power and hover power are known, the rate of climb could be found by solving the following equation for rate of climb.

$$\Delta hp = \frac{MTOM}{550} \left( \frac{V_{climb}}{2} + \sqrt{\frac{V_{climb}^2}{2} + V_{induced,hover}^2} - V_{induced,hover} \right)$$

It must be mentioned that the formula above is in imperial units, and as such the values must be converted. The result is an iteration on rate of climb until the difference in horsepower is smaller than 1%.

**Table 4.3:** Climb rate in the two main configurations of the tiltrotor

Configuration	Rate of Climb [m/s]	Climb Angle [deg]
Aircraft in cruise	62.5	34.24
Rotorcraft	2.3	90

Regarding the Payload range diagram, the difference between the design mass and the calculated mass from the weight estimation was made use of. This difference would be either filled by batteries or by payload. This process is repeated for a set of payload masses and calculates the range, leading to Figure 4.11.

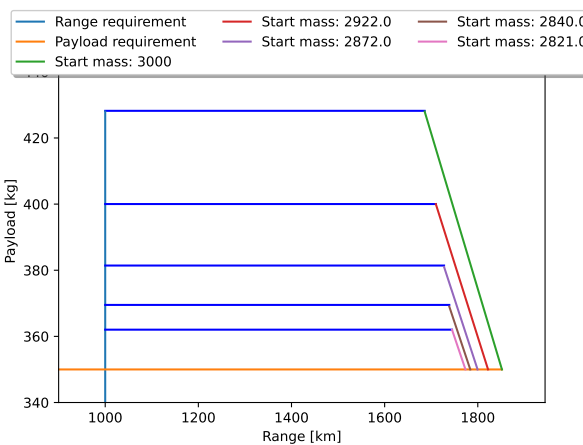


**Figure 4.11:** Payload to Range diagram of the Tiltrotor design

## 4.3. Design concept 4: Multicopter

By Patrick Kostelac, Dominik Stiller

We define a multicopter as a rotorcraft with fixed rotors and no additional lifting surfaces, unlike a tiltrotor aircraft. This concept is the only flight-proven on Mars through Ingenuity, a 1.8-kg demonstrator with a coaxial rotor. The vehicle consists of a multicopter-like fuselage connected to the rotors via spars. Key challenges include the creation of sufficient lift to hover in the thin Martian atmosphere and preventing supersonic tip speeds.

A multicopter is characterized by the number of rotors, blades per rotor, rotation speed, and blade properties. Blade properties include the radius, chord, airfoil, and twist distribution. Rotors can be coaxial, meaning two counterrotating rotors stacked on each other but driven by the same engine.

### 4.3.1. Preliminary sizing

By Dominik Stiller, Patric Kostelac

The preliminary sizing approach for multicopters is as follows:

1. Enumerate radius–rotation speed combination for a range of numbers of blades and rotors.
2. Find the combination with the minimal blade radius such that the vehicle weight can be sustained in hover and the tip Mach number is below 0.85.
3. Size the spars for each combination such that they can sustain rotor thrust and provide sufficient rotor clearance.
4. Estimate the vehicle mass for each combination using statistical and physical approaches.

5. Choose the lightest combination and proceed with detailed sizing.

To simplify the preliminary sizing, we make a range of assumptions:

- Hovering during take-off/landing is the critical sizing condition since forward flight helps with lift.
- The design lift should sustain the weight of 3000 kg.
- The tip speed should not exceed  $M = 0.85$ , similarly to [17].
- The blades have a constant chord and cross-section.
- The blades are 60 % hollow/40 % solid.
- The airfoil geometry follows the cl5605 airfoil of Ingenuity [18]. This thin airfoil supports laminar flow even at low Reynolds numbers.
- The lift curve is linear at a slope of 6 1/rad.
- The pitch angle of the blade changes linearly with radial position from 25° at the root to 8° at the tip.
- The chord-to-radius ratio is 1/20.
- Carbon Fiber-Reinforced Polymer (CFRP) with an allowable tensile stress of 600 MPa is used for rotors and spars.
- Spars are thin-walled cylinders with a thickness of 2 mm.
- The design air density is 0.01 kg/m<sup>3</sup>, corresponding to the lowest expected temperature at zero elevation. At cruise altitude, the forward speed will help with lift generation.

### Rotor sizing

The thrust of each rotor is then found using the equation from Kaya and Kutay [1]:

$$T = t_1 \Omega^2 + t_2 (V \cos \alpha)^2 + t_3 \Omega (\nu_i + V \sin \alpha)$$

where  $\Omega$  is the rotation speed,  $V$  is the multicopter's velocity,  $\alpha$  is the multicopter's angle of attack and  $\nu_i$  is the vertical induced velocity due to rotor downwash. Expressions for  $t_1$ ,  $t_2$ ,  $t_3$  and  $\nu_i$  depending on the geometry are given in [1]. The equation is based on an analytical evaluation of the blade element method.

After initial experiments, the thrust was too low to sustain the multicopter's design weight despite the large blade radius. Therefore, we considered coaxial rotors, which can greatly increase lift without increasing the rotor footprint. Compared to two individual rotors, the lift of two coaxial rotors is about 88% of that. This empirical factor is estimated from results of Coleman [19].

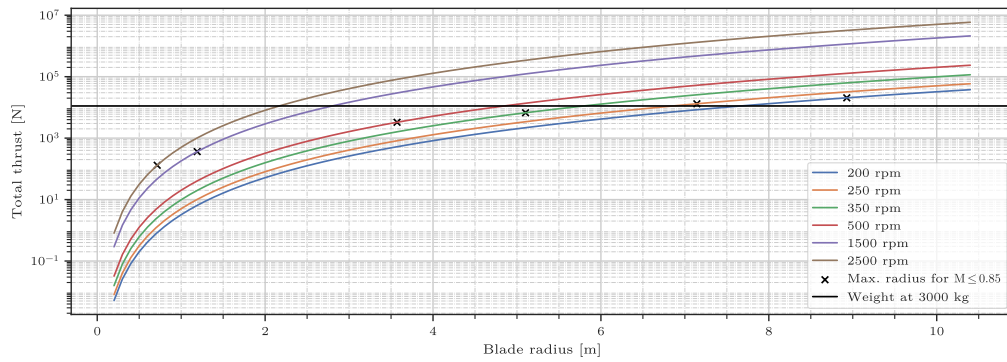


**Figure 4.12:** Radius–rotation speed combinations for six blades and four coaxial rotors.

An example of the resulting radius–rotation speed combinations is shown in Figure 5.7. Above a rotation speed of 250 rpm, the tip Mach number would be too high for any blade radius (i.e., the scatter point is below the black line). At 200 rpm, a radius of 7.8 m would be feasible. However, the minimum blade radius is 7 m, achieved at 250 rpm.

We calculated several combinations of 2–8 rotors with 3–6 blades. The resulting radii are 9.5 m to 5.5 m, the rotation speeds 200 rpm to 300 rpm. The next step is to find the option that results in the lowest total vehicle mass.

### Engine and fuel sizing

In chapter Section 4.3.3, the torque required for each coaxial blade pair at different stages of the flight profile is derived. The critical condition with the highest required torque is the vertical ascent at the lowest density ( $\rho = 0.01 \text{ kg/m}^3$ ), during which the torque of each rotor is  $\tau_t = 3536 \text{ Nm}$ , with the rotational speed  $\omega_t = 250 \text{ rpm} = 26.2 \text{ rad/s}$ . From this, the required horsepower can be derived as follows:

$$P[\text{hp}] = \frac{\tau \cdot \omega}{745.7} = 115 \text{ hp}$$

A 115 hp engine is necessary to rotate one set of coaxial rotors. Due to the need for in situ resource utilization, standard engines are not an option. The battery mass for four 115-hp engines is too high, so the carbon dioxide engine concept is used. That engine is still under development. To account for TRL, it is assumed that it will be twice as heavy as the exact horsepower counterpart. To estimate the mass of the earth's counterpart, a statistical analysis on Pratt and Whitney<sup>4</sup> series of engines. The engine masses are compared to the horsepower produced, and a relationship is found. The estimated lower bound for engine mass is 41 kg, and the upper bound for engine mass is 81 kg.

With the cruise speed of 111 m/s and the range of 1000 km as mentioned in the requirement, the cruise will take two and a half hours  $t_c = 2.5 \text{ hrs}$ . Adding thirty minutes for take-off and landing  $t_l = 0.5 \text{ hrs}$ . The total energy used by all four engines during the flight can then be calculated to be:

$$E[\text{kWh}] = \tau_t \cdot \omega_t \cdot \frac{t_t}{1000} \cdot n_{\text{engines}} = 1110 \text{ kWh}$$

Based on the same Pratt and Whitney series of engines, it was found that the average fuel consumption is  $0.00195 \text{ g}/(\text{kWh} \cdot \text{hp})$  equaling  $0.224 \text{ kg/kWh}$  for a 115 hp engine. This value was obtained based on the current fossil fuels used. The magnesium carbon dioxide reaction releases 0.568044 times the energy when compared to fossil fuel reaction in the standard multicopter engines. Meaning that  $\frac{1}{0.568} = 1.76$  times more fuel is needed making the fuel consumption of the magnesium engine  $0.224 \cdot 1.76 = 0.394 \text{ kg/kWh}$ . This means that the total fuel consumption for a three-hour, 1000 km flight is:

$$M_{\text{fuel}} = 0.394 \cdot 1110 = 437 \text{ kg}$$

### Mass estimation

The mass estimation approach is based on a mix of custom physical calculations and empirical relations for helicopters from Prouty [2]. While Prouty [2] has relations for all subsystems, a helicopter's layout is too different from our Martian multicopter to, for example, use their rotor and engine sizing. The system mass is broken down as follows:

$$MTOM = m_{\text{rotors}} + m_{\text{engines}} + m_{\text{hubs}} + m_{\text{spars}} + m_{\text{fuselage}} + m_{\text{legs}} + m_{\text{misc.}} + m_{\text{payload}} + m_{\text{fuel}}$$

Some component masses are taken to be fixed:  $m_{\text{misc.}} = 400 \text{ kg}$  (estimated from remaining components like the fuel system, fuselage interior, electronics, etc.) and  $m_{\text{payload}} = 350 \text{ kg}$  (set as a requirement).

The rotor mass  $m_{\text{rotors}}$  is calculated from the mass of each blade multiplied by the number of total blades. The blade mass depends on the volume and density. The cl5605 airfoil we use has  $t/c = 0.05$  and is approximately triangular in shape. Therefore, the area is  $0.025c^2$ , from which the volume is found by multiplication with the blade length by the constant-cross section assumption. However, we assume that the volume is only filled to 40%, accounting for interior honeycomb structures and foam commonly found in multicopter blades [20]. The mass is then calculated with the density of CFRP. The blades account for roughly 25 % of the mass and may be a promising target for weight optimization. Note that we assume that the blade can sustain in-plane and out-of-plane bending stresses as well as centrifugal loads.

The engine mass  $m_{\text{engines}}$  is just the individual engine mass multiplied by the number of sets of coaxial rotors. Both rotors are driven by the same engine.

<sup>4</sup>URL: <https://www.prattwhitney.com/en/products/helicopter-engines> [cited 2023-05-11]

The hub mass  $m_{\text{hubs}}$  is calculated using Prouty [2]’s relation for a multicopter hub and hinge, which have to support the centrifugal forces of the blades and contain the swashplate assembly. However, our design does not require collective/cyclic control and benefits from more than 30 years of innovation since the publication of the book. Therefore, we use 20% of the estimated value and multiply it by the number of engines.

The spar mass  $m_{\text{spars}}$  is based on a thin-walled cylinder of length 1.2 times the radius for rotor clearance and a thickness of 2 mm. The diameter is set such that bending due to thrust is sustained. The spar is modeled as a cantilever beam made from CFRP with the thrust applied at the tip.

The fuselage mass  $m_{\text{fuselage}}$  is based on Prouty [2]’s relation since we assume the multicopter fuselage to be similar to a helicopter fuselage. The fuselage size is independent of the rotor size, and the wetted area is based on a box of  $5 \times 3 \times 2$  m. The estimated mass is 83 kg for the structure only without interior items, which are part of the miscellaneous mass.

The landing leg mass  $m_{\text{legs}}$  is, again, based on Prouty [2]’s relation for four legs. However, we take 33 % of the value since we do not have wheeled legs. The estimated mass is 41 kg.

The fuel mass  $m_{\text{fuel}}$  is then set such that the total mass is 2700 kg through iteration, which leads to a fuel mass of 603 kg.

A multicopter with four coaxial rotors (i.e., eight rotors in total) of six blades leads to the largest fuel mass and will be used going forward.

#### 4.3.2. Preliminary design

By Dominik Stiller

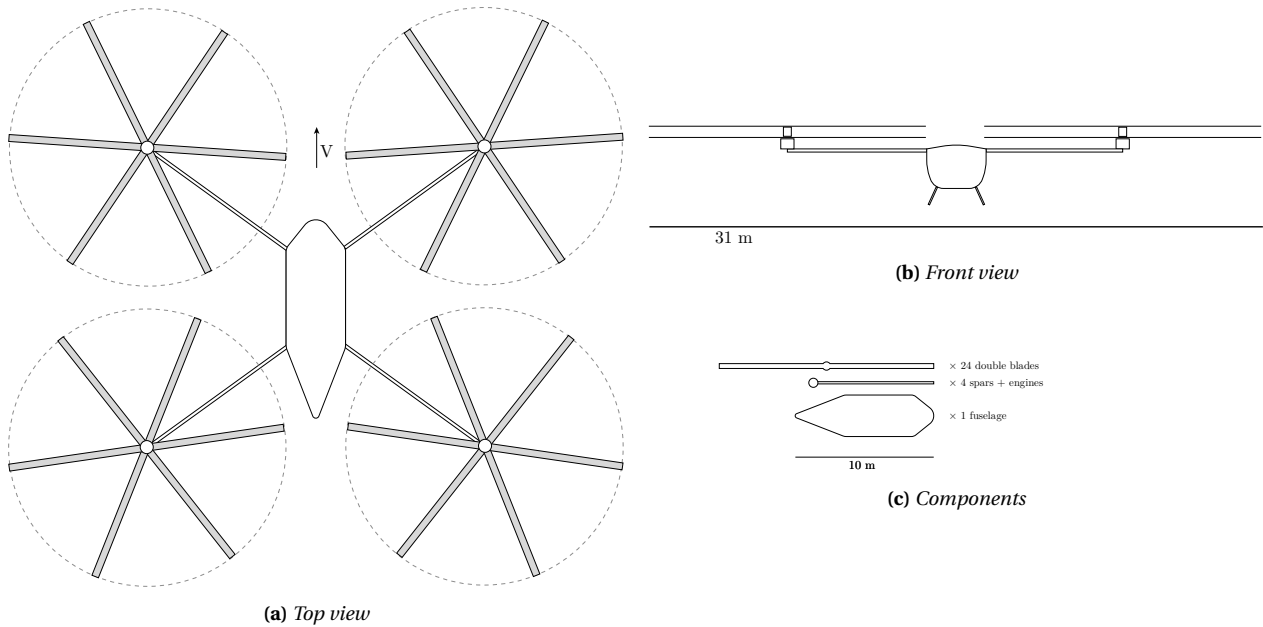


**Figure 4.13:** Scale drawings of the preliminary multicopter design with four coaxial rotors and a radius of 7 m.

The preliminary design of the multicopter is shown in Figure 4.13. The aircraft uses four coaxial rotors, so eight rotors of six blades each. The maximum rotation speed is 250 rpm during take-off. The blade radius is 7 m, with a chord of 0.35 m and a maximum thickness of 18 mm. The spars are 8.4 m long and have a diameter of 16 cm. The fuselage has a length of 10 m and a width of 3 m, although these dimensions should be considered a placeholder. The total dimensions of the multicopter are about 30 m in width and length, depending on the spar angle, and 4 m in height. The spars could be angled upwards for more rotor ground clearance.

The total mass is 2665 kg. Considering the rotor has been sized to sustain a weight of 3000 kg, there is sufficient margin. The blades have the largest contribution at 720 kg (there are 48 blades), followed by engines and hubs, which sum to 442 kg. The spars are relatively light at 58 kg.

The multicopter can be disassembled for transport as shown in Figure 4.13c. Rotor blades are assumed to be transported as double blades (i.e., three per rotor) of 14.5 m in length but could also be packed as single blades. They would then be stacked in a rack. The total disassembled volume is 186 m<sup>3</sup>, compared to an assembled bounding box volume of 3600 m<sup>3</sup>. The maximum height and volume are well within the capabilities of the SLS and Starship launchers.

### 4.3.3. Aerodynamic characteristic

*By Patrick Kostelac*

The aerodynamic characteristics of the aircraft are a crucial part of the design stage. As previously mentioned the gravity field on Mars generates an attraction of 3.71 m/s<sup>2</sup>, meaning that 11130 N of lift is necessary. However, the Martian atmosphere can be as thin as  $\rho = 0.01 \text{ kg/m}^3$ , which requires large lifting surfaces. The multicopter design uses the rotor thrust as the main lifting component. The rotors are sized according to the critical conditions: vertical climb during take-off. The thrust equation from Kaya and Kutay [1] in Section 4.3.1 can be expanded to include the rotor geometry components:

$$T = \Omega^2 \left( \frac{1}{6} \rho A \sigma a \theta_0 R^2 + \frac{1}{8} \sigma a \rho A \theta_{tw} R^2 \right) + (V \cos \alpha)^2 \left( \frac{1}{4} \rho A \sigma a \theta_0 + \frac{1}{8} \sigma a \rho A \theta_{tw} \right) \\ + \Omega (V \sin \alpha + v_i) \left( -\frac{1}{4} \sigma a \rho A R \right)$$

where  $\rho$  is the density,  $A$  is the area covered by the rotor,  $\sigma$  is the rotor solidity,  $a \cdot \theta_0$  and  $a \cdot \theta_{tw}$  represent the lift coefficient of the blade at the root and the tip with  $a$  being the lift curve slope and  $\theta$  the twist angle and  $R$  is the radius of the rotor. The equation is based on an analytical evaluation of the blade element method. Using the analytical expression, the influence of individual blade parameters can be assessed, and thus an optimal blade radius, solidity, and airfoil, which minimize the mass and maximize the thrust, can be found. The thrust is generated due to the rotor's rotational velocity and the rotor blades' lift coefficient. Due to the difference in velocity at the blade root and the blade tip, the twist angle is introduced to distribute the lift along the blade radius evenly. The thrust produced by the blade depends both on the blade radius and the blade rotational velocity, as can be seen in Figure 5.7 but also on the lift coefficient along the blade, which is controlled by changing the before mentioned parameters.

The radius of 7 m and a rotational speed of 250 rpm found in Section 4.3.1 were obtained by using Ingenuity's clf5605 airfoil [18]. The airfoil twist was set to 25° at the blade root and 8° at the blade tip. The reason for such large twist angles is the induced velocity due to the rotor, which makes the angle of attack of the blades lower than the twist angle. The solidity of the blades is 0.095. Lastly, the current rotor configuration uses four coaxial rotors with three blades per rotor. With these parameters, the thrust produced at hover is 11800 N which is more than the multicopter weight allowing for take-off.

Just as the lift coefficient is a non-dimensional characteristic of fixed-wing aircraft, the ratio of thrust coefficient to solidity  $C_T/\sigma$  is the corresponding non-dimensional characteristic of multicopter. The average section lift coefficient  $\bar{c}_l$  is six times this [2]. While our value of  $C_T/\sigma = 0.31$  during hover is quite high compared to existing vehicles (Ingenuity has 0.1), Prouty [2] suggests a maximum of 0.2 prevent blade stall), our blades have  $\bar{c}_l = 1.86$ , which is within a reasonable range for our clf5605 airfoil [18].

The drag coefficient of the multicopter can be divided into rotor torque drag and cruise body drag. The rotor blade rotational velocity generates large amounts of torque, which has to be compensated by the engines. The torque can be calculated using an analytical equation from Kaya and Kutay [1]:

$$Q = \Omega^2 \left( \frac{1}{8} \rho A \sigma \overline{C_d} R^3 \right) + (V \cos \alpha)^2 \left( \frac{1}{8} \rho A \sigma R \overline{C_d} \right) + (\Omega v_i) \left( \frac{1}{4} \sigma a \rho A \theta_0 R^2 + \frac{1}{8} \rho A \sigma a \theta_{tw} R^2 \right) \\ + (\Omega V \sin \alpha) \left( \frac{1}{4} \sigma a \rho A \theta_0 R^2 + \frac{1}{8} \rho A \sigma a \theta_{tw} R^2 \right) + (v_i + V \sin \alpha)^2 \left( -\frac{1}{4} \sigma a \rho A R \right)$$

Where the symbols are the same as in the thrust equation, and the  $\overline{C_d}$  is the average drag coefficient. The rotor blades act as wings and generate both lift and drag. The drag thus has a zero lift drag component and the lift-induced drag component. Both have to be accounted for in the average drag component. Using the blade properties mentioned before and the average drag coefficient of 0.083 found from data in Koning et al. [18], the blade torque was calculated to be 3536 Nm. During cruise, due to the reduced RPM, the torque produced is only 1925 Nm

The cruise body drag also needs to be calculated. During the cruise, the main body, rotor connectors, and the rotors themselves cause drag opposite of the multicopter velocity. For drag purposes, the main body was assumed to resemble the AKTAY helicopter body with the values obtained from Batrakov et al. [21]; the cruise drag coefficient is 0.1. The connector spars are assumed to have an aerodynamic shape and a drag coefficient of 0.04. Additionally, the spars can be used to generate extra lift during cruise if necessary, but in that case, extra lift drag will be created. The blades of the rotors themselves also cause not only the torque but also the drag in the opposite direction of the velocity. The drag coefficient of the blades is 0.083, as assumed before. The cruise speed of the multicopter is 111 m/s, and assuming the worst ground-level conditions for drag. The density is then 0.02 kg/m<sup>3</sup>. The total drag during cruise is 730 N.

As a concluding remark to the aerodynamic chapter, it is worth mentioning that all of the aerodynamic forces were calculated for the worst possible conditions. That means that the lift was calculated for the lowest possible Martian atmosphere density, and the drag was calculated for the highest Martian atmosphere density. It is important to note that these two can never happen at the same time but are given here as the two worst-case scenarios that are considered.

#### 4.3.4. Stability and control

*By Patrick Kostelac*

The multicopter design should be both stable and controllable. The multicopter design is stable if the multicopter can resist environmental disturbances. The multicopter design is controllable if the multicopter can move in any direction once in the air. In order for the multicopter design to be controllable, it does not require any control surfaces, as all of the maneuvers can be performed by throttling the thrust of the rotors. There are four pairs of coaxial rotors; each pair can be tilted, slightly vectoring the thrust of that coaxial pair. The list of maneuvers that can be performed by the multicopter can be seen below:

- **Vertical movement:** The multicopter can move horizontally by throttling all of the rotors. By increasing the angular speed of all the rotors, the thrust is increased, and the multicopter moves upwards. Similarly, the angular speed can be reduced, reducing the thrust, and thus the multicopter moves downwards.
- **Pitch:** The pitch of the multicopter can be controlled by increasing the angular speed of only the forward rotors or only the backward rotors. By producing a larger force in front or behind the center of gravity, the moment equilibrium is disturbed, and the multicopter pitches forward or backward.
- **Roll:** The roll is controlled similarly to the pitch, but instead of throttling the rotors in front or aft of the cg, the pairs of rotors on the left or on the right are throttled, creating a rolling motion.
- **Yaw:** In order to control the yaw, the multicopter rotors need to be able to tilt the rotors. Regular multicopters yaw by increasing the rotational speed of the diagonal rotors as the rotor's two sets of diagonal rotors rotate in different directions. However, in the case of coaxial rotors, throttling, specifically the counterclockwise or clockwise rotating rotors, is impossible, so the rotors' tilting is required. By tilting the rotors, the thrust is vectored, which can be used to induce a yawing moment when necessary. To ensure that the force remains in equilibrium and only the moments change, the diagonal rotors will be tilted simultaneously.
- **Horizontal movement:** The multicopter can move horizontally by either tilting the rotors while the main body remains in the same orientation or by pitching and rolling the body itself without tilting the rotors individually. Both of these actions create a horizontal thrust component, enabling the

multicopter to move horizontally.

The multicopter is statically stable as it generates its lift from the rotors. The multicopter is symmetrical around its longitudinal axis, meaning it will have statically lateral stability. The longitudinal stability is achieved since the forward and aft rotors are at the same longitudinal distance to the center of gravity.

The dynamic stability of the multicopter design can be logically analyzed as a detailed stability analysis is out of the scope of this phase of the project. In case of a pitch-up disturbance, the front rotors will move upwards, reducing their effective angle of attack and reducing the lift that the front rotors produce, simultaneously the aft rotors are moving down, and thus their effective angle of attack is higher, increasing the lift produced by the aft rotors. This will generate a restoring moment. The same can be concluded for roll stability. In case the downwards-moving rotors are close to stalling in cruise, they might stall when moving downwards, which is why a limitation on the twist angle of the rotors needs to be introduced. Due to the even mass distribution, a side slip will only result in a side force rather than a force and a moment; that force will need to be counteracted by using rotor tilt. Thereby, the multicopter design is both statically and dynamically stable.

#### 4.3.5. Performance analysis

*By Patrick Kostelac, Dominik Stiller*

The performance of the multicopter design will be analyzed based on the selected flight profile for the mission. Each aspect of the flight profile will be assessed individually based on the multicopter design capabilities. The selected flight profile can be seen below:

- **Take-off:** The multicopter design concept has the capability to take-off and land vertically, which sets it apart from the standard airplane designs. This capability could be crucial for Mars exploration as it allows the multicopter to take-off and land almost anywhere. The take-off is the most demanding part of the flight profile for the multicopter design. As can be seen in Section 4.3.1, the highest required torque is during the take-off. During take-off the multicopter does not take advantage of horizontal velocity, which generates extra lift, and it requires additional power compared to hover as the multicopter needs to gain height.
- **Climb:** In case of a completely vertical climb, the required torque and power are the same as in the take-off. However, the climb does not have to be vertical. In order to optimize the climb, the multicopter will fly forwards as it climbs. The free stream velocity will help both the rotors and the connectors generate extra lift, which reduces the torque requirement on the rotors. The multicopter has been designed for a climb angle of 10°, but it is capable of a completely vertical climb if necessary. However, the vertical climb does require more power.
- **Maneuvers:** In case of a sand storm or terrain, the multicopter might need to deviate from the pre-determined flight path. The multicopter does not have any control surfaces; rather, it maneuvers by throttling the thrust on its rotors. Throttling the rotors at the front or at the back allows for yaw control, throttling the rotors at the left and right side allows for roll control, and throttling the diagonal rotors allows for yaw control. The multicopter thus has high maneuverability and is able to fly in crosswind conditions.
- **Cruise:** Due to the extremely high torque requirement on take-off, the multicopter is able to cruise at high velocities. As can be seen in Section 4.3.3, when designing for take-off, the available thrust for the cruise is 21 700 N. This allows for cruise speeds of up to Mach 0.7, set as the maximum in the requirements. However, in this case, the limiting factor is not the drag of the multicopter but rather the high Mach number experienced on the rotor blade tips due to the cruise speed and the rotational speed of the blades. Due to the high Mach number, the lift produced by the rotors is reduced, and thus the available thrust is reduced. Because of this, the multicopter will not cruise faster than 111 m/s. In order to fly at the desired speed, the rotors will be throttled down to an angular velocity of 148 rpm. Flying at this rpm and an angle of attack of 5° (nose down), the thrust is sufficient to sustain the weight and overcome drag. This will reduce the torque and the fuel usage

of the engine. Since the limiting factor is the tip mach speed, In order to fly as fast as possible, the rotor should spin as slowly as possible, which is achievable at the highest densities. The design cruise altitude is thus as low as possible since that allows for the highest densities. However, the multicopter design is capable of flying at 5 km, but due to the lower densities at higher altitudes, the rotors will need to spin faster, which reduces the maximum cruise speeds at higher altitudes.

- **Descent:** The descent stage can be performed vertically or with the horizontal component. In case there is a horizontal component, again, extra lift can be generated due to it. During the descent stage, the multicopter will also need to slow down. This will be done by pitching backward and using the rotor thrust to generate a braking force. In the case of vertical descent, the descent speed is limited by the vortex ring state, which happens if the multicopter descends too quickly and its rotor blades get caught in the irregular air calculation.
- **Landing:** Similarly to take-off, the landing needs to be performed vertically. However, during landing, instead of requiring extra power to gain altitude, less power is required as the multicopter is losing altitude. This makes landing less critical than take-off, which justifies the decision to design for take-off rather than for the landing.

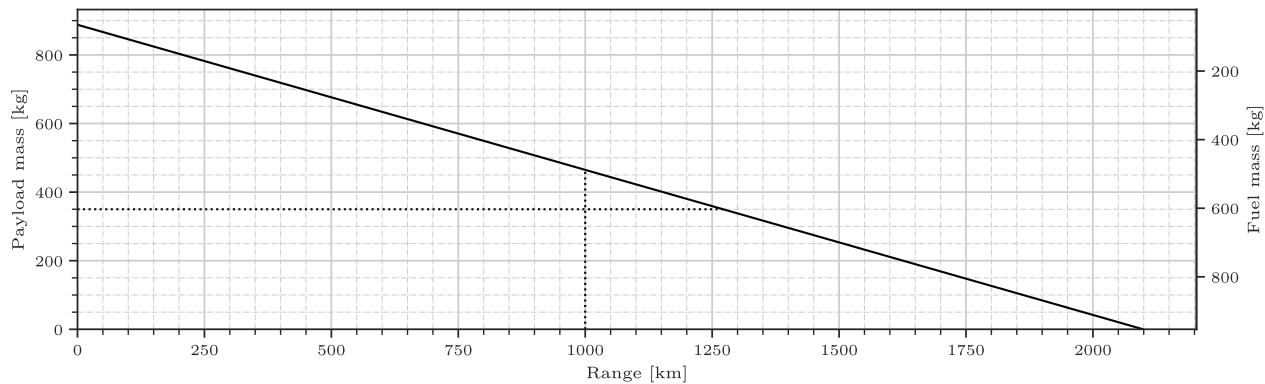


**Figure 4.14:** Payload–range diagram for the multicopter. Payload mass includes both astronauts and cargo. Take-off and landing requires 98 kg of fuel without adding range.

The payload–range diagram for the multicopter is shown in Figure 4.14. There maximum payload is only limited by the MTOM, not by structural considerations. Hence, the relation is linear over the whole range. At the range requirement of 1000 km, the maximum payload mass is 465 kg. At the payload requirement of 350 kg, the maximum range is 1270 km. Note that a safety factor of 1.3 is used for the specific fuel consumption to account for engine uncertainty.

#### 4.3.6. Desing concerns

By Patrick Kostelac

Lastly the design does come with some concerns. The proposed magnesium carbon dioxide engine is still in the development phase and is not yet flight proven, meaning that the engine might not be viable and in case it is viable, its mass and fuel consumption might be higher than anticipated. Additionally, multicopters at the large scale have not yet been used, this comes with a new set of concerns. The large blades could prove to be a weakness in the design as they introduce large forces and moments into the rotor hub structure. The hub structure has not been explored in detail, which can influence the blade flutter and bring the blade structural integrity in question due to fatigue. The stability and controllability of the design could also be a potential hurdle. Currently only drones use throttling of the rotors as a control measure while larger helicopter use swash plates. The proposed design uses a combination of both which adds extra weight. The yaw control is achieved only by tilting the rotors which might not be the most efficient, a potential small tail which adds yawing possibilities could be explored.

## 4.4. Design concept 5: Airship

*By Freek Braspenning, Thomas van de Pavoordt*

The final design option considered was a lighter-than-air vehicle, i.e. an airship. The airship may offer many advantages over the previously mentioned design concepts, as it passively creates lift due to buoyancy.

### 4.4.1. Definition

An airship as a planetary exploration vehicle has been considered in various different mission concepts as a way to cover ground quickly and with a higher efficiency than an ordinary rover [22, 23]. Due to the aircraft being lighter than air, it creates a buoyant force that can provide enough lift to carry the weight of the aircraft. This passive way of providing lift gives the airship a high efficiency. An airship could even offer more advantages since the use of hydrogen is safer in the Martian atmosphere due to the carbon dioxide with which hydrogen does not react. However, a large volume will be required to achieve enough lift. The advantages and disadvantages of the airship will be described in more detail below.

Firstly, the use of hydrogen is highly beneficial on Mars. There is no risk of combustion since hydrogen does not react with carbon dioxide, which is prominently present in the Martian atmosphere. Furthermore, since hydrogen is the lightest known gas, it will create the most buoyant force compared to any other gas. In addition to this, since hydrogen can be obtained through the electrolysis of water, which can be obtained by mining ice on Mars, this fuel is sustainably available. This process will also produce oxygen as a by-product that can be used as breathable air for the astronauts or any habitat present on Mars.

Next to this, the airship also has several advantages in terms of flight performance. Most importantly, the airship has VTOL capabilities. This allows for the exploration of the most remote places, even those that cannot be accessed by conventional airplanes. Furthermore, the low Reynolds number and the low density offer benefits in terms of drag. This will reduce the thrust required and the weight needed for propulsion.

Naturally, the airship also has its disadvantages. First of all, the low density of the Martian atmosphere could pose an issue in providing enough buoyant force. While the relative ratio of the density of the atmosphere and the lighter-than-air gas is approximately the same on Mars as on Earth, the absolute difference might be too little to provide a useful buoyant force. This will result in a massive volume that will cause the weight of the encapsulating skin to increase quadratically. As the skin density can not be meaningfully lowered, without compromising strength, it may end up weighing too much. Furthermore, while the density is much lower than on Earth, the requirement for cruise speed might be unattainable, since the airship will need to withstand the higher pressure that occurs at cruise speed.

In addition, hydrogen is the smallest element and is therefore highly prone to leakage. This will cause very precise tolerances on the skin to prevent leakage, which will likely cause an increase in weight. Due to leakage, the hydrogen will also be refueled often, which puts constraints on the time available to fly and on the production of hydrogen.

It can thus be said that it is worth investigating the concept of an airship on Mars. The Martian atmosphere could provide an environment in which an airship can excel, due to the decreased gravitational acceleration and drag. However, this same environment can pose significant issues due to an increase in required volume and thus mass. The following sections will outline the steps taken to determine key parameters of the airship and their results.

### 4.4.2. Preliminary Sizing

For the preliminary sizing of the airship, several estimation formulas are set up. These formulas provide a first estimate of the mass and performance.

There are several design options when considering an airship, such as the gas used in the blimp, the propulsion type, and the skin materials. Hydrogen was chosen as lighter-than-air gas, as it is more sustainable and lighter than helium. The density of hydrogen was obtained from Equation (4.27):

$$\rho_{H_2} = \frac{p_{H_2}}{R_{H_2} T_0} \quad (4.27)$$

where  $p_{H_2} = 1.005 \cdot p_0$ , and  $R_{H_2} = \frac{R}{M_{H_2}}$ .

The volume of the gas chamber of the airship is obtained from Equation (4.28).

$$V = \frac{m_{MTOM}}{\Delta\rho} \quad (4.28)$$

where

$$\Delta\rho = \rho_0 - \rho_{H_2} \quad (4.29)$$

This equation is based on the force equilibrium between the weight of the airship and the buoyant force provided by the difference in density between hydrogen and the Martian atmosphere. Buoyant force is defined as:

$$F_{Buoyant} = \rho_0 V g_M \quad (4.30)$$

The shape of the balloon is then assumed to be a sphere in order to get a high-level estimation on the surface area needed to encapsulate the gas chamber, as per Equation (4.31) and Equation (4.32).

$$V = \frac{4}{3}\pi r^3 \quad (4.31)$$

$$S = 4\pi r^2 \quad (4.32)$$

The mass of the skin is then estimated using Equation (4.33), where  $\rho_{skin} = \rho_{HDPE} = 940 \text{ kg m}^{-3}$ ,  $t$  the thickness of the skin, and  $S$  the previously calculated surface area. Several skin materials have been considered for high strength and low weight, of which High-Density Polyethylene was assumed.

$$m_{skin} = \rho_{skin} S t \quad (4.33)$$

With the mass of the skin, the total volume required can be calculated again and this process is iterated until it converges. The iteration is then optimized to carry the least amount of skin mass, to be able to leave as much mass for the payload, fuselage, propulsion system, and other subsystems.

#### 4.4.3. Aerodynamic characteristics

Once the preliminary size has been determined, a drag estimation is performed to be able to calculate the required thrust, fuel and range, for example. The drag of an airship can be quantified by Equation (4.34), as given by Li et al. [24].

$$C_D = C_F \left[ 4 \left( \frac{L_a}{D_m} \right)^{1/3} + 6 \left( \frac{L_a}{D_m} \right)^{-1.2} + 24 \left( \frac{L_a}{D_m} \right)^{-2.7} \right] \quad (4.34)$$

Here,  $L_a/D_m$  is the fineness ratio of an airship, which sets up a more ellipsoid shape that induces less drag than a sphere. The skin friction drag coefficient,  $C_F$ , is approximated by Equation (4.35):

$$C_F = 0.045 Re^{-1/6} \quad (4.35)$$

The Reynolds number can be calculated for the characteristic length of the airship, using Equation (4.36) and the dynamic viscosity given by Equation (4.37) [25].

$$Re = \frac{\rho V L_a}{\mu} \quad (4.36)$$

$$\mu = \mu_0 \left( \frac{T}{T_0} \right)^{3/2} \left( \frac{T_0 + S}{T + S} \right) \quad (4.37)$$

where the dynamic viscosity at  $T_0$  is given by  $\mu_0 = 1.37 \times 10^{-5} \text{ Nsm}^{-2}$ , with  $T_0 = 273 \text{ K}$ , and Sutherland's constant is given by  $S = 222 \text{ K}$  [25].

Drag is then easily computed with Equation (4.38):

$$D = 0.5 \rho V_{cruise}^2 SC_D \quad (4.38)$$

With the drag known, the thrust required is also known and from this, the required fuel can be calculated. The engine weight was estimated using the method described in Chapter 3, with the engine thrust specific fuel consumption used in Equation (4.39) to calculate the required fuel mass:

$$m_{fuel} = SFC \cdot D \cdot \frac{R}{V_{cruise}} \quad (4.39)$$

This formula can also be used to calculate the achievable range with the amount of mass that is left for fuel without breaking the MTOM requirement.

#### 4.4.4. Results

With the formulas complete, several results can be obtained before deciding whether to move on with further analysis into stability & control, and performance characteristics. The airship has been optimized to have a mass of 2700 kg in total, as prescribed by the mass budget with contingency. In this MTOM, 720 kg will be the effective payload mass, meaning that in this mass everything other than the mass of the skin encapsulating the hydrogen volume will be incorporated. Taking into account that 350 kg of payload mass will be allocated to the 2 astronauts being transported, only 370 kg is left for systems such as structures, propulsion, and fuel. The mass of the fuselage is estimated via the same estimation methods prescribed in Section 4.1.2. This leaves 110 kg for control surfaces, the propulsion system, fuel, and other miscellaneous mass.

When flying at 400 km/h, it was found that the drag of the airship was 2298 N, from which it followed that the propulsion system mass would be 231 kg. Naturally, this is too much mass already for the available amount and thus renders this configuration infeasible. It was therefore decided to find a combination of speed and, eventually, range that would render achievable. Naturally, the more the speed decreased, the more the drag decreased and the more the fuel mass could increase, due to a lighter propulsion system. However, to achieve the range of 1000 km, as determined by the requirements, the speed would have to decrease by 90%. A compromise was found at 50% of the range requirement, thus 500 km, and 25% of the speed, thus 100 km/h. This speed is significantly faster than current-day rovers and has far more range, thus still providing plenty of advantages. It does mean that certain requirements are not met and that will be reflected in the trade-off, which will be performed after the Verification & Validation (Chapter 5) in Chapter 7.

# Verification and Validation of Design Concepts

This chapter will present the verification and validation of each design concept. The methods used to obtain design parameters need to be verified and validated to perform a trade-off based on the design concepts. Each design is based on a set of parameters obtained through numerical calculations, which were carried out using software developed internally. To verify the programs, first unit testing will be performed on individual formulas, after which a global verification procedure occurs. To validate the programs, existing aircraft will be used: the inputs to the program shall resemble an existing aircraft, and the program's outputs will be compared to the parameters of those aircraft.

## 5.1. Fixed-Wing Aircraft: Flying Wing & Biplane

*By Adrian Beño, Joachim Bron, Timo de Kemp*

Verification refers to checking whether the equations solved during the design process were solved correctly. In order to perform verification, two different verification methodologies were used: code testing, composed of unit tests and global tests, and verifying whether the numerical solvers produce results compatible with analytical solutions of arbitrary, simple problems.

### 5.1.1. Code test

The numerical tools for the design of the fixed-wing aircraft consist of a combination of Microsoft Excel files. These were tested using unit tests, where the outputs to a particular combination of inputs are known. The input-output for cells with formulas was then compared to the expected output to detect mistakes in the tools and calculations. Once the Excel files were fully unit tested, the tools were used to design the two fixed-wing aircraft. A detailed description of the unit tests is omitted since these were directly implemented into the Excel files, and each calculation was in a bottom-up fashion, instead of testing in a separate phase.

### 5.1.2. Comparison with analytical solutions

Two comparisons of numerical simulation with analytical solutions are presented. Firstly, the  $C_l - \alpha$  curve, as predicted analytically by inviscid thin airfoil theory, is compared to the  $C_l - \alpha$  of the NACA0006 airfoil at  $Re = 10^8$ . At this relatively low Reynold's number, the flow can be assumed to be dominantly governed by inertial effects rather than viscous effects. Furthermore, the thickness of the airfoil can also be assumed to approach an infinitely thin airfoil. This comparison is shown in Figure 5.1, where an extremely close match is visible and the thin airfoil theory prediction of  $\frac{dC_l}{d\alpha} = 2\pi \text{ rad}^{-1}$  is met. Also, the airfoil is symmetric, which is reflected in the  $C_l - \alpha$  having an intersection with the origin.

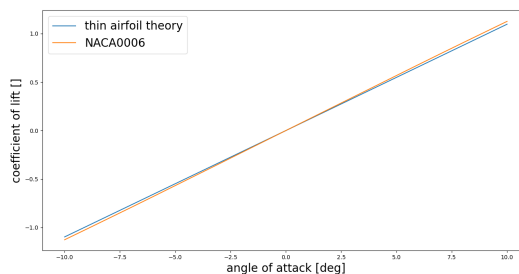


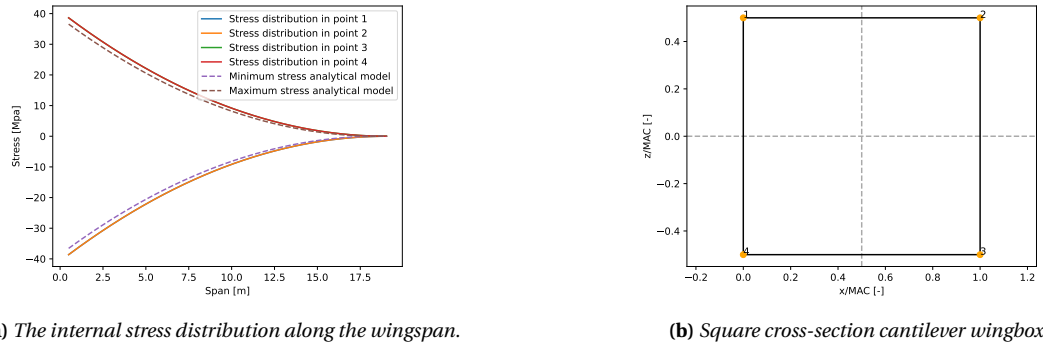
**Figure 5.1:** Comparison of  $C_l - \alpha$  curves, as predicted by thin airfoil theory and as computed with XFLR5 for a NACA0006 airfoil at  $Re = 10^8$ .

Secondly, a cantilever beam's analytical and numerical stress distributions under a constantly distributed

load are presented. The analytical solution is given by Equation (5.1):

$$\sigma_y = \frac{\left(\frac{b}{2} - y\right)^2 w z}{2I} \quad (5.1)$$

Where  $y$  [m] is the spanwise wing position, starting at the root,  $z$  [m] is the vertical position along the wing,  $w$  [N/m] is the load distribution, and  $I$  [ $m^4$ ] is the area moment of inertia. For this verification simulation, a rectangular wing box is assumed; hence the maximum and minimum vertical position distributions are provided. The comparison of our numerical solver with the analytical solution is provided in Figure 5.2a. A close match is visible, adding to the confidence in the model.



(a) The internal stress distribution along the wingspan.

(b) Square cross-section cantilever wingbox

**Figure 5.2:** Comparison of numerical simulation prediction to the analytical solution.

Validation refers to checking whether the equations chosen to be solved during the design process represent the governing physical phenomena of the real world. In order to perform validation, two different validation methodologies were used, as listed below.

- Most papers published on low Reynold's number high lift airfoils are conducted in wind tunnels on small models. The scalability of these results to our design must be validated.
- Most weight estimation calculations use weight estimation formulas from [7]. These formulas are based on statistical relationships of Earth-based aircraft. Hence, validation must be performed for their validity in the Mars atmosphere.

### 5.1.3. Simulation scalability

A comparison between low Reynold's number lift curve characteristics of high lift low Reynold's number airfoil S1223, as predicted by XFLR5 simulation and experimentally measured by Ma et al. [26] is presented. This is given in Figure 5.3. The maximum lift coefficient is predicted to desired accuracy. The overall shape of the curve is also following expectations. The only source of lowered confidence in the model stems from the curve being slightly shifted to the left, by around 4°. This results in the maximum relative error in any  $C_l$  prediction of 11 %. Because verifying the non-viscous case yielded a perfect match, we conclude that this 11 % error stems exclusively from the viscous effects, which XFLR5 superimposes on the otherwise linear non-viscous model. Since the correct angle of attack is not attractive to the design, high confidence in the model's validity is achieved. However, future design calculations shall be carried out with an 11 % uncertainty margin in the theoretically predicted lift coefficient. The scalability and extrapolability of simulation results are valid if all non-dimensional flow numbers, such as Reynold's number, are kept constant across the extrapolation.

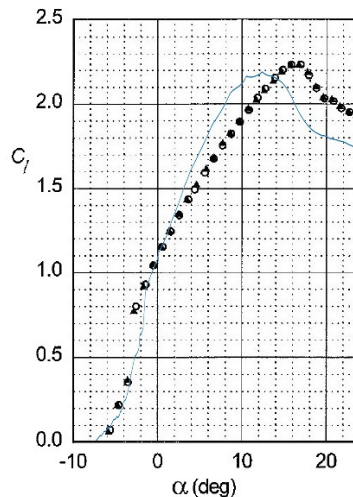


**Figure 5.3:** Comparison of lift curves of airfoil S1223. The blue line corresponds to XFLR5 numerical simulation. Black dots correspond to experimentally produced data by [26].

#### 5.1.4. Weight estimation validation

Secondly, weight estimation formulas from Torenbeek [7] are based on statistical aircraft relationships of Earth-based aircraft. Unfortunately, a statistical analysis of how much these differ concerning Mars-based aircraft cannot be conducted, as there are no examples available for Mars. At the same time, some assumptions about their validity can be concluded. For example, the gravity on Mars is about three times as low as Earth's. Hence aircraft structures on Earth have to withstand about three times as high loads. Hence predictions by Torenbeek [7] are conservative and may be reduced by around 50 %.

## 5.2. Tiltrotor

By Sebastian Harris, Javier Alonso Garcia, Thomas van de Pavoordt

Verification of the tiltrotor is done in two parts: Section 5.2.1 starts with verifying individual functions in the code used to determine all parameters related to the tiltrotor. Section 5.2.2 tests the system as a whole through sensitivity analyses. After verification, Section 5.2.3 will explain the validation done for the tiltrotor analysis.

### 5.2.1. Unit test verification

By Javier Alonso Garcia, Thomas van de Pavoordt

Unit testing of the tiltrotor is focused on code verification of the different functions calculating performance. The way code verification is set up is that every function has correlations between inputs and outputs that can be derived by engineering instinct. Using Python's library `unittest`, it was tested whether a variation in a specific input resulted in the corresponding correlation in output, i.e., the positive correlation should test `TRUE` when an increase in input results in an increase in output. The functions tested and the expected correlation between input and output are given in Table 5.1. All functions passed their unit tests and can, in that sense, be considered successfully verified.

**Table 5.1:** Functions undergoing unit testing and their expected correlation between input and output

Function	Input	Output	Correlation
RadiusMassElementMomentum	Mass	Thrust	Positive
	Mass	Radius	Positive
	Mass	Rotor Mass	Positive
	# of rotors	Thrust	Negative
	Density	Radius	Negative
	Gravity	Thrust	Positive
Area	C_L	Area	Negative
	Mass	Wing area	Positive
	Dynamic pressure	Wing area	Negative
	Gravity	Wing area	Positive
DragEstimation	Fuselage size	C_d_0	Positive
Size_power_subsystem	T_0 Thrust	Battery mass	Positive
	Cruise time	Battery mass	Positive
	Take-off time	Battery mass	Positive
Class2Weight	Rotor radius	Tail weight	Negative
	Fuselage size	Body weight	Positive
	Braced Wing	Wing weight	Negative
	Ultimate load	Tail weight	Positive
AircraftClimbPerf	Battery mass	ROC	Positive
	Power density	ROC	Positive
	Mass	ROC	Negative
RotorClimbPerf	Mass	ROC	Positive
	Rotor radius	ROC	Negative
	# of rotors	ROC	Positive

### **5.2.2. System test verification**

*By Javier Alonso García*

In order to test the system as a whole, two different sensitivity analyses were performed. The first was a typical sensitivity analysis using Python's *SALib* library, which tested the correlation between a set of inputs and outputs of the design function. The Sobol indices for this study can be seen in Table 5.2.

**Table 5.2:** Sensitivity analysis between function inputs and outputs

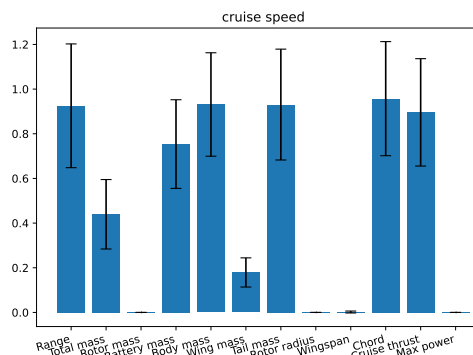
**(a) Sensitivity of the design to prescribed inputs from the customer**

Inputs / Outputs	Range	Total mass	Rotor mass	Battery mass	Body mass	Wing mass	Tail mass	Rotor radius	Wing-span	Chord	Cruise thrust	Max power
payload mass	0.06	0.12	0.00	0.04	0.03	0.05	0.03	0.00	0.00	0.02	0.05	0.00
design range	0.03	0.02	0.00	0.09	0.01	0.01	0.01	0.00	0.00	0.00	0.01	0.00
cruise speed	0.93	0.44	0.00	0.75	0.93	0.18	0.93	0.00	0.00	0.96	0.90	0.00
maximum mass	0.02	0.41	1.02	0.11	0.01	0.76	0.01	1.02	1.01	0.01	0.02	1.02

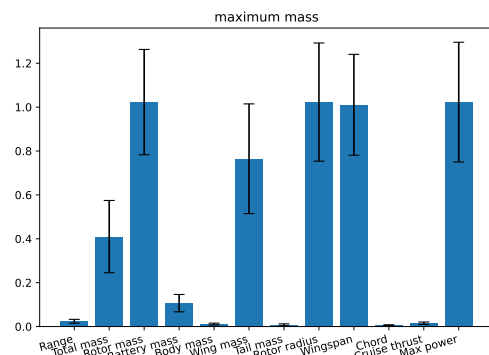
**(b) Sensitivity of the design to calculated values**

(c) Sensitivity of the design to assumed values

Inputs / Outputs	Range	Total mass	Rotor mass	Battery mass	Body mass	Wing mass	Tail mass	Rotor radius	Wing-span	Chord	Cruise thrust	Max power
$C_l$	0.13	0.43	0.42	0.19	0.76	0.31	0.61	1.01	1.01	0.76	0.51	1.05
Power density	0.25	0.04	0.00	0.82	0.02	0.00	0.01	0.00	0.00	0.02	0.02	0.00
Energy density	0.68	0.00	0.00	0.00	0.00	0.00	0.00	0.00	0.00	0.00	0.00	0.00
Blade density	0.00	0.20	0.23	0.00	0.09	0.02	0.07	0.00	0.00	0.09	0.11	0.00
Fill factor	0.01	0.31	0.35	0.00	0.14	0.04	0.11	0.00	0.00	0.14	0.18	0.00
Ultimate load	0.00	0.01	0.00	0.00	0.01	0.62	0.23	0.00	0.00	0.01	0.01	0.00
Take-off time	0.01	0.00	0.00	0.00	0.00	0.00	0.00	0.00	0.00	0.00	0.20	0.00



(a) Sensitivity of the design to the cruise speed

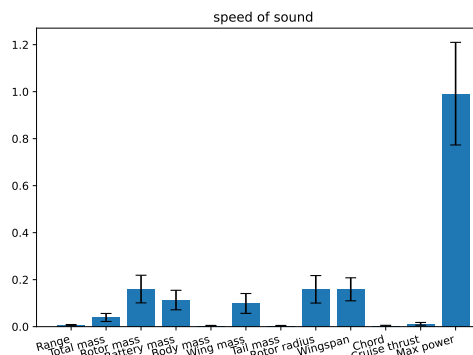


(b) Sensitivity of the design to the MTOM

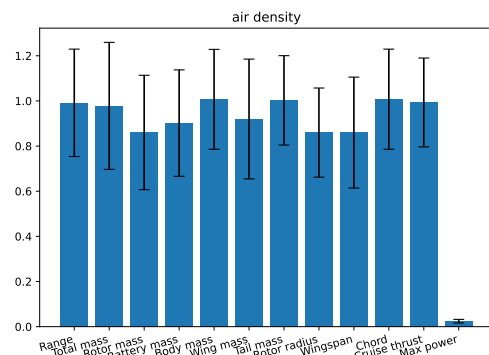
**Figure 5.4:** Sensitivity of the design to prescribed inputs from the customer with a 95% confidence interval

Firstly, as seen in Table 5.2a, cruise speed and the maximum allowed mass have a significant effect on many of the outputs, in some cases having a score greater than 1, implying that variations in this input will have effects on other inputs, leading to significant variability in the final output. These effects can be better visualized in Figure 5.4.

Similarly, from Table 5.2b it can be seen that the air viscosity at cruise speed and gravity have mostly no significant effects on the design output for the expected ranges. On the other hand, the speed of sound slightly affected several output parameters, and the air density significantly affected all outputs except for the maximum power (see Figure 5.5 for a more precise visualization). These results are especially significant since these two values vary with temperature and are not constant throughout the planet.



(a) Sensitivity of the design to the speed of sound



(b) Sensitivity of the design to the air density

**Figure 5.5:** Sensitivity of the design to calculated inputs from the environment with a 95% confidence interval

Finally, some aspects of the design, such as the lift coefficient or the power density of the batteries, were extracted from literature. However, it is still possible that the system's overall performance, once assembled, differs from the values used in the simulation. For this reason, Table 5.2c showcases these values' impact on the design. The results showed that the most critical parameter is  $C_l$ , which impacts all aspects of the design, followed by the battery power density, which had a substantial impact on the battery mass, and the battery energy density, which significantly impacted the aircraft's range.

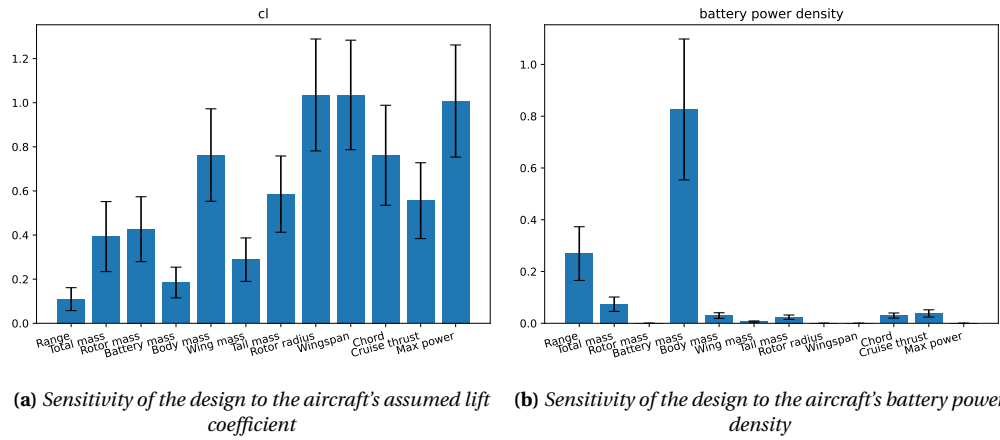


**Figure 5.6:** Sensitivity of the design to assumed performances with a 95% confidence interval

As a second system test, the influence of upstream functions' outputs on the simulation outputs was tested. This offered insight into determining which functions were more critical, which was helpful when deciding which margins were appropriate for the validation. This was done by adding 10% to the outputs of each function one at a time and comparing the result with the data obtained without perturbances. The result of this test can be seen in Table 5.3.

**Table 5.3:** Change in output value due to a 10% change in a function's output

Output/Function	Rotor sizing	Wing sizing	Drag	Power sizing	Class2Weight
Range	7.63%	-7.86%	-0.11%	3.81%	12.44%
Total mass	-0.39%	8.52%	0.07%	8.84%	3.77%
Rotor mass	10.00%	0.00%	0.00%	0.00%	0.00%
Battery mass	-11.47%	19.64%	0.19%	23.06%	4.34%
Body mass	-3.15%	3.29%	0.02%	3.42%	11.42%
Wing mass	4.02%	13.51%	0.07%	10.75%	14.39%
Tail mass	-18.50%	36.27%	0.12%	18.91%	17.56%
Rotor radius	10.00%	0.00%	0.00%	0.00%	0.00%
Wingspan	3.42%	3.77%	0.03%	3.92%	1.49%
Chord	-3.66%	3.77%	0.03%	3.92%	1.49%
Cruise thrust	-17.71%	27.13%	0.26%	16.40%	5.99%
Max power	10.00%	0.00%	0.00%	0.00%	0.00%

### 5.2.3. Validation

By Sebastian Harris

The validation procedure for the design process of the tiltrotor is doubly complex, first in the aspect that tiltrotors are unique and few designs were developed into finished products. Next, using rotorcraft on Mars has only recently become a possibility, thus further reducing the available validation data. However, the process of sizing rotors should be comparable with rotorcraft on Earth in the same conditions. As

such, the validation procedure was run by modifying the design environment to match Earth's. The two main outputs of the function are the rotor size and the rotor power. The following data was collected and used as an input:

**Table 5.4:** Available data from various tiltrotor aircraft [27]

Name	Rotor Radius [m]	Take-off Mass [kg]	Power[kW]	Rotors	Blades	Tip Mach
V-22	5.8	23859	5498	2	3	0.9
V-280	5.35	17200	4470	2	3	0.75
AW609	3.96	7620	1446	2	3	0.7

After importing this data into the function, the output is compared to the true values. The results are tabulated below:

**Table 5.5:** Differences between calculated and real data for various tiltrotors

	V-22		V-280		Aw609	
	Radius	Power	Radius	Power	Radius	Power
Calculated	5.4	5428	5.5	3259	4	1401
Data	5.8	5498	5.35	4470	3.96	1446
Difference	6.9%	1.26%	-2.8%	27.1%	-1%	3.12%

The significant variation in power related to the V-280 is mainly due to the lack of information regarding the vehicle. As it is relatively recent and under development, the values found are most likely outdated and, as such, need to be validated. Other validation procedures are unavailable, as the lack of information on other tiltrotor aircraft leads to a lack of validation that can be performed on this preemptive study. However, more in-depth validation procedures will be possible for the following steps of the Design Synthesis Exercise by performing wind-tunnel validation, testing with scale models, and otherwise ensuring the design performance follows that of the models.

## 5.3. Multicopter

By Patrick Kostelac

The verification of the multicopter is done in two parts; first unit verification on formulas, and second function testing verification. The sensitivity analysis is done by varying the inputs. The validation is done by performing a local validation of assumptions and formulas and a global validation.

### 5.3.1. Unit testing verification

The first step of the unit verification is making sure that the inputs to the program have the correct values. The values should be presented in SI units. This was done by comparing the values used in the program to the values obtained in Haberle et al. [28]. The values on the Martian atmospheric conditions such as the density, speed of sound, and the gravitational acceleration were found to be within 10% of the literature, thus the test passed and they were verified.

The second step of unit verification is the verification of the individual formulas used in the program. The code used for the parameter estimation can be divided into two parts, a part used for aerodynamic modeling and a part used for mass estimation. The aerodynamic modeling was verified by first confirming that the units of the formulas are equal on both sides. Then by comparing the formula to Kaya and Kutay [1]. After comparison, the output value of the program is compared to a hand-calculated value and the values obtained in the paper. The paper has validated the formulas with an experiment and they are thus considered correct and verified. The mass estimation is performed on a combination of statistical

relations and geometric relations. The mass estimation is a combination of well-known geometric relations which are verified and the statistical relations from the book Prouty [2] and was thus considered validated. The verification procedures are the same as in the aerodynamic modeling.

### 5.3.2. Function testing verification

The first output to be verified is the plot showing the maximum allowable radius at each rpm. First the inputs are verified. Then the maximum tip Mach number is verified using data attained by NASA<sup>1</sup>. The output of the graph was first verified by visual inspection. At the same blade radius, the higher RPM should produce more lift, similarly for the same RPM, a larger blade radius increases lift. Lastly, it is expected that the larger blades will produce more lift at the tip Mach number of 0.85. The plot has passed the visual inspection test. After the visual inspection tests, the maximum radius for each RPM in accordance with the Mach number constraints was independently calculated and compared to the graph values. The values matched and thus the graph was verified.

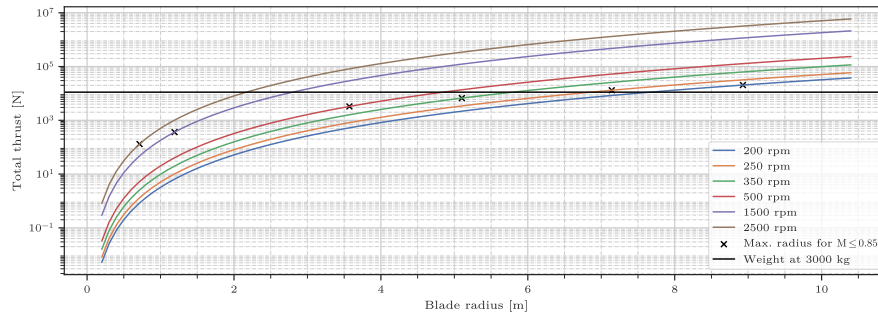


**Figure 5.7:** Radius–rotation speed combinations for six blades and four coaxial rotors.

The next step was verifying the lift, torque, and drag calculations. The lift and torque calculations use the formulas from Kaya and Kutay [1] thus it is only necessary to verify the inputs. Most of the inputs are design parameters so the only verification measure was checking that the correct inputs are taken. However, one of the inputs is the induced velocity. The induced velocity uses thrust as input and thus a loop is created. In order to ensure that the correct values are used, `scipy.optimize.least squares` was used until the change in thrust and induced velocity was below 1 %. The `scipy` function is considered to be already verified. The drag function takes only the design parameters, cruise and take-off speed, and density as input. Thus only the use of correct values was verified.

### 5.3.3. Local validation

The validation of the program is performed by making sure that the formulas used in the program are valid and that the assumptions used in these formulas hold for the use case of a large Martian multicopter. In order to validate the formulas used in the program, the assumptions used in the formulas presented by Kaya and Kutay [1] need to be valid in the low Reynolds number environment. Only the airfoil aerodynamic characteristics are affected by the atmosphere and thus to confirm that the assumptions are valid on Mars, the airfoil data for low Reynolds number and low density is used.

Firstly it is assumed that the blades of the rotors are rigid with a constant chord. In the multicopter design, the blades do indeed have a constant chord making that part of the assumption valid. To validate the rigidity the blades were assumed to be cantilever beams mounted at the rotor hub. To account for the worst-case scenario the lift is assumed to act on the blade tip. With that assumption, the deflection of a seven meter blade is half a millimeter which is several orders of magnitude smaller, and thus this assumption is valid. Secondly, it was assumed that the lift coefficient of the airfoil varies linearly with angle of attack. This is validated as shown by Koning [29] since it shows that the slope of the  $C_l - \alpha$  curve remains linear within the operation angle of attack range ( $2^\circ$ - $15^\circ$ , which makes the assumption valid. The next assumption states that the pitch angle of the blade changes linearly with the radial position.

<sup>1</sup>URL: <https://mars.nasa.gov/technology/helicopter/> [cited 2023-05-16]

This assumption is valid for the design. The next assumption stated that lift acting on the blade has a greater magnitude than drag. According to Koning [29] the  $C_l/C_d$  varies between eight and twenty meaning that the assumption is valid. The next assumption stated that the blades are identical which is true for the design thus the assumption is valid. Lastly, it is assumed that lift and drag are the only aerodynamic forces acting on the blade, this is true for the design and thus the assumption is valid. An additional assumption made for the program states that the coaxial rotors are 88 % as efficient as two separate non coaxial rotors, which is confirmed by Coleman [19]. This validates all of the assumptions concerning the rotor blade properties, meaning that the formulas are validated and can thus be used for the program.

To validate the working of the aerodynamic side as a whole, the value of  $ct/\sigma$  is calculated. This represents the thrust coefficient divided by the solidity ratio and it is the main descriptor of helicopter performance. Standard values for this parameter range from 0.12 to 0.30. The calculate multicopter value is  $ct/\sigma = 0.306$ . This is on the high end but because of the large number of rotors, this value is acceptable and thus validated. To validate the mass calculations, first the blade mass is validated, the blades were assumed to be of triangular shape, this needs to be validated. In Figure 5.8 the maximum thickness over chord ratio of the clf5605 is 0,05 which decreases to 0 at the trailing edge. This area of this is thus approximately equal to the triangle area and this assumption is thus valid for the mass calculation only. Thus we can assume that the area of the airfoil is approximately the area of a triangle with the base equal to the chord times the maximum thickness over chord ratio and the height being the chord length.

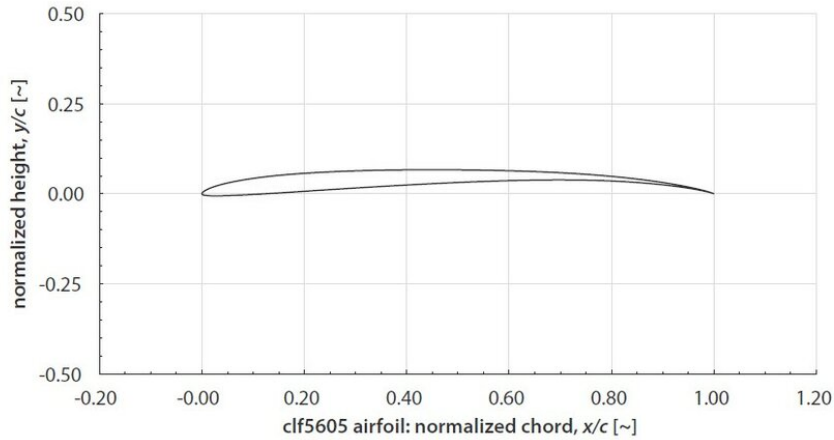


**Figure 5.8:** Cross section area of the clf5605 airfoil

The next step in the mass estimation validation is the validation of the load-carrying components. Since the load-carrying components were designed from scratch using well-known formulas, in order to validate their mass, the use of the assumptions in the formulas needs to be validated. The first assumption made is that the cylindrical spars are thin-walled. The spars have a length of 8.4 m and diameters of 0.16 m, while their thickness is only 2 mm. This is a two orders of magnitude difference meaning that the thin-walled assumption is valid. The functions used to determine the diameter are considered to be valid as they are well-known and used functions. Thus the mass calculation of spars is validated.

The last step in the mass validation is the validation of the sizing methods used in the book Prouty [2]. The methods in the book are made for Earth helicopters before 1990 which greatly differs from the Martian multicopter. The hub sizing is based on centrifugal forces, which are independent of the environment. However, our design does not use swashplates and benefits from more than 30 years of innovation thus the expected mass of the hubs is 20 % of the estimated value. However, this value can not be validated, thus a safety factor for the mass of the hubs of  $\pm 50\%$  is used to account for uncertainty. The fuselage mass estimation is more accurate since we assume a helicopter fuselage. The mass is based only on the wetted area which for the current design is  $5 \times 3 \times 2$  m. In this case, the error is smaller than for the hubs, however, the fact that the book is based on helicopters older than 30 years still introduces uncertainties, which should be accounted for with at least  $\pm 25\%$  in the sensitivity analysis.

### 5.3.4. Sensitivity analysis

The sensitivity analysis is split into two parts. First, the variation of aerodynamic parameters, which affects the thrust and the torque of the design. The second part of the sensitivity analysis covers the mass estimation. Here the input parameters as well as the outputs of the statistical relations will be varied in order to determine their effect on the final mass.

**Table 5.6:** Sensitivity analysis on aerodynamic input parameters

Input parameter	Change	Effect
<b>Density</b>	The Martian atmosphere density varies between 0.01 and 0.02 $kg/m^3$ during the year, thus this effect should be explored	Thrust and torque vary proportionally with density
<b>Temperature</b>	The Martian atmosphere temperature varies between 150 and 275 K which changes the speed of sound from 191 to 259 m/s	Increasing the temperature increases the torque and thrust
<b>M_max</b>	The maximum allowable Mach number is a design choice, and shall thus be varied from 0.5 to 0.9 to observe its impact	Thrust and torque vary quadratically with maximum Mach number
<b>c to R ratio</b>	The c to R ratio is a design choice and is varied from 10 to 30 to observe its impact	Increasing the twist increases both thrust and torque
<b>Twist</b>	Twist is a design choice and shall thus be varied to observe its impact	The twist is directly connected to the thrust and the torque produced
<b>Number of rotors</b>	The number of rotors is a design choice and shall thus be varied to observe its impact	The number of rotors is proportional to the thrust and torque produced
<b>Number of blades</b>	The number of blades is a design choice and shall thus be varied to observe its impact	The number of blades is proportional to the thrust and torque produced

The impact of density on thrust and torque is validated as the density is proportional to aerodynamic loads. The impact of temperature is correlated to the speed of sound through  $V_{sound} = \sqrt{\gamma \cdot R \cdot T / M}$ . The speed of sound influences the rotational velocity through tip mach number restrictions, smaller temperature gives smaller torque and thrust thus it is validated. The maximum tip mach number influences the torque and thrust as explained in the sentence before. The chord-to-radius ratio varies the chord of the blades, and thus varies the solidity ratio which is directly correlated to thrust and torque. The twist is a parameter in both the torque and thrust formulas which makes it valid. Lastly, both the number of rotors and blades increase both the torque and thrust which is valid as increasing the area will increase the aerodynamic forces.

The sensitivity analysis for the mass estimation deals both with the input parameters and the outputs of statistical relations. Input parameters such as the blade airfoil infill percentage and fuel consumption will be varied in order to find their minimum and maximum masses. Additionally, the statistical relations based set by Coleman [19] will be varied according to the values stated in Section 5.3.3 in order to get a more accurate idea of the mass estimation.

**Table 5.7:** Sensitivity analysis on mass parameters

Parameter	Change	Effect
<b>Infill percentage</b>	The infill percentage varies between 8% and 100%	Mass varies between 144 kg and 1800 kg
<b>Fuel consumption</b>	The fuel consumption shall be varied by $\pm 25\%$	Mass varies between 328 kg and 546 kg
<b>Hub sizing</b>	The hub sizing output shall be varied by $\pm 50\%$	Mass varies between 101 kg and 304 kg
<b>Fuselage sizing</b>	The fuselage sizing output shall be varied by $\pm 25\%$	Mass varies between 64 kg and 106 kg
<b>Engine sizing</b>	The engine sizing output shall be varied according to Pratt and Whitney estimations	Mass varies between 41 kg and 81 kg

Before it is assumed that the total mass is 2700 kg from which the fuel mass is allocated, the extra fuel is added for emergencies or avoidance maneuvers. However, the actual nominal mass with enough fuel for

a 1000 km trip is 2534 kg. By performing the mass sensitivity analysis it was discovered that the minimum possible mass is 1707.5 kg while the maximum possible mass is 3856.6 kg. This range gives an idea of the code accuracy and with that the current mass estimation accuracy.

### 5.3.5. Global validation

In order to perform the global validation of the system, the question arises of what the key information output by the model is. The answer to that question is the thrust, torque, and mass of the multicopter. According to those values, the rest of the design will follow. In order to validate the program as a whole, the output of the program will be compared to the performance of a standard helicopter. If the program output values are within 20 % of the existing helicopter values, the program would be considered validated. The helicopter used for comparison will be the Hughes TH-55 Osage whose parameters<sup>2</sup> can be seen in Table 5.8 . Using this set of inputs in the program used for calculating the multicopter parameters, the results in Table 5.9 were obtained.

**Table 5.8: Hughes TH-55 Osage parameters**

Airfoil	NACA0015, $CL\alpha = 0.1/\text{deg} = 5.729/\text{rad}$
Rotor radius	3.8545 m
Empty weight	406k g, 3923 N
Loaded weight	703 kg, 6896 N
Twist root	$2^\circ = 0.0349 \text{ rad}$
Twist tip	$8^\circ = 0.1395 \text{ rad}$
Omega	(400-530)rpm = (41.9-55.5) rad/s
Chord to radius	1/20
Blades	3
Rotors	1

**Table 5.9: Program aerodynamic results**

Variable	Low rpm take-off	High rpm take-off	Low rpm cruise	High rpm cruise
Thrust	3400 N	7600 N	6100 N	10300 N
Torque	3800 Nm	6600 Nm	3200 Nm	6700 Nm

Comparing these values to the empty weight and the loaded weight of the Hughes, it can be seen that at high rpm, the thrust produced during take-off is slightly higher than the total weight of the aircraft. It is safe to assume that the thrust produced by the aircraft during take-off would be higher than its weight. Thus it is safe to assume that the thrust equation at take-off is validated. During cruise, the thrust produced is increased and the thrust is significantly higher than the weight, however, these values were computed with zero elevation density and it can be assumed that the helicopter would cruise at higher altitudes which would reduce the total thrust making it closer to the aircraft weight. Thus we can also validate the thrust equation during cruise. The fact that the thrust values are 11 % higher than the weight indicates that the thrust might have been slightly over-predicted when compared to the real case, meaning that the real thrust is probably slightly lower than what the program outputs which should be noted. There are no available values for the torque of the rotor during cruise and take-off thus those values could not be validated. Lastly, the mass calculation was validated. The mass calculation predicted the helicopter empty mass to be 369 kg. This is within the 10 % of the actual value, this is considered enough to validate the mass of the multicopter. However, it is important to note that the mass is underestimated and it is possible that the mass would exceed the 3000 kg target. To conclude the model over-predicts the thrust produced by 11 % while under-predicting the mass by 10 % which should be taken into account for the design. However, both of those are within the aforementioned 20 % meaning that the program is validated.

<sup>2</sup>URL: [http://www.flugzeuginfo.net/acdata\\_php/acdata\\_269\\_en.php](http://www.flugzeuginfo.net/acdata_php/acdata_269_en.php) [cited 2023-05-22]

# Verification and Validation Plan

## Preliminary Design

This chapter details the Verification and Validation plan and who is accountable for each section of the Verification and Validation. Section 6.1 details who is responsible for the verification. Section 6.2 dives into several verification and validation methods. Section 6.3 applies several Verification and Validation methods to the model. Section 6.4 proposes a plan for verification and validation for the report's future, from preliminary design to detailed design and the final product.

### 6.1. Responsibilities

*By Timo de Kemp*

Every engineer is responsible for creating unit tests for their code before the functions have been created. This will ensure that the engineers are not biased in creating the unit tests after their functions have been written. When multiple functions from the engineer work together, the engineer will design tests to show that the functions have the correct inputs and outputs. The systems and integration engineers are responsible for making sure that the functions of different departments/engineers can be appropriately integrated into the primary function. This includes designing tests and ensuring the engineers create functions that work together.

### 6.2. Verification and Validation methods

*By Timo de Kemp, Freek Braspenning*

The methods to do verification and validation are analysis, inspection, demonstration, and testing. What these terms mean will be explained in the next paragraphs [30].

- **Analysis:** The use of mathematical modeling and analytical techniques to determine the compliance of the design with its requirements or the code with its expected value based on calculated data.
- **Inspection:** Determination of requirement compliance by visual inspection, often used to verify physical design features.
- **Demonstration:** Show that the end product achieves a requirement(verification) or customer expectation(validation). It differentiates from testing by the lack of detailed data collection.
- **Testing:** A realized end product, with detailed data collection, is used to verify or validate its performance.

### 6.3. Model Verification and Validation

*By Timo de Kemp*

This section implements and applies some of the previously discussed Verification and Validation methods to the model.

#### 6.3.1. Model verification

**Unit tests** Unit tests will be done for the functions created. These unit tests will include tests for the order of magnitude expected, a range of expected numbers, and extreme values.

**Module tests** The connection between other functions is tested in module testing. The module is a collection of related functions that collectively provide input to the subsystem. Testing of these modules can be done in various ways. In this project's scope, the module tests that will be performed are extreme value testing, sensitivity analysis, and integration testing.

**Subsystem tests** A subsystem consists of multiple modules, and the interaction between these modules is tested with subsystem tests. These tests include but are not limited to integrated tests and acceptance tests.

**System tests** The system is the collection of all subsystems. The system is tested for the integration of the subsystems. These tests include methods, as discussed in module tests and subsystem tests.

### 6.3.2. Model validation

*By Freek Braspenning*

Once the model is verified, its validity is tested with respect to experimental data. This ensures that the suitable model has been solved to represent reality accurately. The model will be inputted with the same conditions for the experimental setup. Martian conditions should be approximated to the best of your abilities when testing on Earth. Another method to validate the model is to run the model using Earth parameters and compare the results to experimental data.

Experiments such as wind tunnel tests, scaled models, and prototype test flights will validate the model data. In addition, the scaled models can be validated for aerodynamics, structures, and transportation. Finally, prototypes can be flown on Earth or Mars to simulate relevant flow characteristics.

## 6.4. Product Verification and Validation

After the conceptual design phase, the team will present a product that should meet all requirements. This product will be verified and validated in various ways. During the conceptual design phase, it can be verified using simulations and analysis of the model, but also limited testing such as wind tunnel tests.

Verification and validation processes are continued throughout the future of the project. With further development of the design concept, more thorough verification and validation methods are used. These methods include testing on prototypes, demonstration of working concepts, and inspections of the final product.

Throughout the project, the design is validated with respect to the requirements. The methods of validation change as the design takes shape. At the start, most of the validation tests would be analyzed, while later on, prototypes could be tested to validate the design.

Testing methods for validating are proposed in Table 6.1 for a select number of requirements.

**Table 6.1: Driving requirements**

Identifier	Description	Verification method
REQ-ASTR-SAFE-01	The system shall not produce more than <TBD>positive gs in any direction.	Testing
REQ-SAG-REUS-03	The system's assembly process shall be repeatable.	Demonstration
REQ-GOPS-ACT-ASS-01	The system shall be able to be assembled by 2 astronauts.	Demonstration
REQ-AERO-LFT-02	The aerodynamic system shall have a maximum lift coefficient of <TBD>.	Testing
REQ-AERO-LFT-04	The aerodynamic system shall have a stall angle of <TBD>degrees.	Testing
REQ-STG-PAY-02	The system shall be able to hold 100 kg of payload.	Demonstration
REQ-PWR-ELEC-01	There shall be <TBD>Watts of power available to power all essential systems.	Analysis
REQ-ETHC-02	The system shall not pollute the Martian environment.	Analysis
REQ-CLMB-01	The climb rate at take-off altitude shall be at least <TBD>m/s.	Testing
<b>Key requirements</b>		
REQ-SAG-LF-03	The system shall obtain power from sources available on Mars.	Analysis
REQ-LCD-LVEH-SIZE-01	The system shall have a volume of less than <TBD>[m <sup>3</sup> ].	Inspection
REQ-LFSP-AIR-01	The system shall provide breathable air to the astronauts.	Testing
REQ-CRUS-05	The nominal cruise speed shall be 111 m/s.	Demonstration

# Trade-Off

By Dominik Stiller

A trade-off is performed among the five options to find the optimal design for our mission. Finally, the results are checked for robustness through a sensitivity analysis. This chapter details the methodology in Section 7.1 and the results of the trade-off in Section 7.2.

## 7.1. Methodology

We used a traditional numerical trade-off. This method requires weighted criteria, assigning a score per design option. The steps to choose the optimal design were as follows:

1. Decide on criteria candidates.
2. Determine weights for all criteria candidates.
3. Decide on scoring categories and their numerical value.
4. Determine scoring category assignment for each criterion.
5. Perform preliminary sizing for all design options to estimate criteria values (Chapter 4).
6. Select significant criteria from candidates.
7. Determine optimal option from total weighted scores.
8. Check the robustness of results using sensitivity analysis.

Infeasible options were already eliminated in the baseline phase. This means that all effort for preliminary sizing was focused on promising concepts.

Determining a total score for something as complex as an aircraft design is challenging: disparate criteria such as range and sustainability must be combined, and qualitative criteria such as feasibility must be quantified. These challenges were considered throughout the process to achieve an unbiased and representative result. Note that the actual process was less linear than presented here, and some internal iterations were necessary.

### 7.1.1. Selection of criteria

Before starting the preliminary sizing, our group agreed on a range of criteria candidates that may be relevant for the trade-off. These criteria came from the requirements and consideration of differences between the designs. Both qualitative and quantitative aspects were considered. The quantitative candidates were:

- **Range at 350 kg payload:** The range at the design payload of 350 kg (250 kg for two suited astronauts + 100 kg for cargo) should be maximized. This would reduce the need for refueling.
- **Max. payload at 1000 km range:** The maximum payload at the design range of 1000 km should be maximized. This may allow the transportation of another astronaut or more cargo.
- **Cruise speed:** The cruise speed should be maximized (within Mach limits). This reduces travel time.
- **MTOM:** The MTOM should be minimized.
- **Landing/take-off distance:** The landing/take-off distance should be minimized, VTOL (zero distance) would be optimal. A longer distance would restrict landing sites due to craters and rocks.
- **Availability:** The availability depending on diurnal, seasonal, and weather-related conditions should be maximized. For example, a solar-powered design may be limited to daytime flight.
- **Packed volume:** The volume of the aircraft disassembled for transport from Earth to Mars should be minimized. This allows greater flexibility with launchers or shipment of multiple aircraft to Mars at once.
- **Number of disassembled parts:** The number of parts into which the aircraft is disassembled for transport from Earth to Mars should be minimized. This facilitates assembly at the destination.

The qualitative candidates were:

- **Feasibility:** The feasibility should be maximized. While crewed flight on Mars has yet to be attempted, technologies that are flight-proven in Earth conditions should be preferred. Also, critical assumptions with large uncertainties reduce feasibility.
- **Sustainability:** The sustainability should be maximized. The aircraft should limit the negative impact on the future populations of Earth and Mars. Important aspects are in-situ resource utilization (ISRU), pollution, and recyclability.
- **Assembly complexity:** The assembly complexity should be minimized. There is little infrastructure and personnel on Mars to help with assembly. Ideally, the aircraft can be assembled with just two astronauts and no tools.
- **Safety:** The safety should be maximized. High safety standards apply to crewed flights.

We aimed to select four to six criteria for the trade-off since more would dilute the relevant differences between designs. The selection was based on (1) the importance due to customer requirements and group discussion, (2) the spread between design options, and (3) whether the values can be determined through preliminary sizing.

The selected criteria and justifications are in Table 7.1. Four criteria were chosen: "range at 350 kg payload", "landing/take-off distance," "feasibility," and "sustainability."

**Table 7.1:** Candidate criteria and why they were (or were not) selected. Four are selected (marked by ✓), and seven are either not distinguishing enough or hard to quantify with only preliminary sizing.

Criterion	Justification
✓ <b>Range at 350 kg payload</b>	Important due to user requirements
✓ <b>Landing/take-off distance</b>	Large differences between VTOL/HTOL designs; important for possible landing sites
✓ <b>Feasibility</b>	Design feasibility impacts the development time and subsequent cost required to develop the design as well as how realistic it is to build
✓ <b>Sustainability</b>	Sustainability is crucial as the design should limit its impact on the Martian environment as well as that on the Earth environment
Assembly Complexity	Important due to the limited infrastructure available, but also all designs could be designed for simplified assembly
Max. payload at 1000 km range	Important due to user requirements, but high correlation with "range at 350 km payload"
Cruise speed	All designs have a similar cruise speed of 400 km/h
MTOM	All designs have a design MTOM of 2700 kg; if below, the difference is filled with fuel, which makes designs more comparable under "range at 350 km payload"
Availability	All designs have an availability greater than 90 %
Packed volume	All designs easily fit into payload fairings of possible launchers
Safety	Safety highly depends on detailed design (e.g., cockpit structure); all designs have similar safety aspects

### 7.1.2. Weighting of criteria

More weight should be given to essential criteria. To prevent bias towards one particular design, we initially determined weights democratically. Each group member assigned a weight to each criterion, then the average per criterion was taken and rounded to the nearest integer. However, the group and the customer considered the resulting weights imbalanced. Therefore, we decided to weigh all criteria equally but analyze the sensitivities to halved or doubled weighting.

### 7.1.3. Scoring of criteria values

To compare values of disparate criteria, we scored them among five categories ranging from "unacceptable" to "exceptional." For the quantitative criteria, we defined numerical intervals for each category. For qualitative criteria, the category was determined based on multiple sub-criteria.

The scoring categories are shown in Table 7.2. The categories were assigned as follows:

- **Range at 350 km payload:** The nominal range from the user requirements is 1000 km. The range is "good" if it is within 10 % of 1000 km. The performance is "exceptional" if the range is more than twice the requirement and "unacceptable" if below 700 km.
- **Landing/take-off distance:** A longer distance increases the risk of collision with rocks or interference from craters. VTOL (i.e., a distance of 0 m) circumvents these risks. However, the two fixed-wing aircraft are the only options that require a non-zero distance of 2000 m. Therefore, this criterion is essentially binary and may be sensitive to the interval boundary. While statistical analyses of rock and crater distributions to find physically meaningful boundaries were considered, they proved too complex for this trade-off. Therefore, we used a more pragmatic approach: the 2000 m are not "unacceptable" (we could design a robust landing gear or target flat, explicit landing sites) but are also not "good" (the landing sites will likely be somewhat limited). Therefore, the 2000 m distance is considered "acceptable." The effect of this choice was checked in the sensitivity analysis.
- **Sustainability:** The sustainability aspect of the trade-off is broken down into four criteria. (1) The power or propulsion system should prevent emitting foreign molecules into the atmosphere (e.g., violated by a magnesium-powered engine emitting solid carbon). For all systems, the existence of power generation emissions negatively impacts the sustainability of the design. (2) Emissions due to the lifting system should be prevented (e.g., violated by leaking hydrogen of the airship). (3) Recyclability of the aircraft structures improves sustainability, as the aircraft's end-of-life is crucial. Metals and thermoplastics are preferable to CFRP. (4) The use of batteries on the aircraft positively affects the sustainability of the system, as the technologies will be compatible with Earth technologies (batteries are a cornerstone for sustainable energy for Earth and thus heavily researched), source its power from renewable sources, and allow for re-using of the batteries as static energy storage for future missions.
- **Feasibility:** The feasibility of the design is primarily based on the Technology Readiness Level (TRL)<sup>1</sup> of the power generation, thrust generation, and control system. The score is assigned as these three systems' lowest TRL. In the event of a draw, the number of similar existing designs is used to distinguish the remaining designs (e.g., there is more precedent for fixed-wing aircraft than tiltrotors as more designs exist and have been flight-proven).

The trade-off results were based on the expected value for each criterion. However, we also derived best-case and worst-case values. This was useful for checking the significance of trade-off results, the effect of sizing uncertainties, and sensitivity analysis for weighting. Different assumptions were used for best-case/worst-case values (e.g., propulsive efficiency and atmospheric density) for the quantitative criteria. For the qualitative criteria, the score category was shifted up/down (e.g., "great" becomes "good" / "exceptional").

<sup>1</sup>Multiple definitions of TRLs exist. We use the following relevant for our subsystems: 4 = technology validated in a laboratory, 5 = technology validated in the Earth environment, 6 = technology demonstrated in the Earth environment, and 9 = technology validated in the Mars environment. For example, the Mg/CO<sub>2</sub> engine has TRL 4, while electric rotor propulsion has TRL 9.

Each scoring category was then assigned a numerical score between zero and four. No points were gained for an "unacceptable" design, while four were given to "exceptional" designs. The categories in between used consecutive integers, i.e., a linear scale.

The total weighted score was then calculated based on each criterion's weights and the numerical scores of the assigned category. The minimum possible total score is 0, and the maximum possible total score is 16 (if all criteria are "exceptional"). The scale for the total weighted score was then linearly stretched out to 0–100. This is the score that is discussed subsequently in the trade-off results.

The total weighted score can be interpreted as follows:

- **0:** all criteria are "unacceptable"
- **0–25:** on average, the criteria are between "unacceptable" and "acceptable"
- **25–50:** on average, the criteria are between "acceptable" and "good"
- **50–75:** on average, the criteria are between "good" and "great"
- **75–100:** on average, the criteria are between "great" and "exceptional"
- **100:** all criteria are "exceptional"

## 7.2. Results

The trade-off results are shown visually in Figure 7.1 and summarized with criteria values in Table 7.3. For the expected values of each criterion, the tiltrotor wins with a score of 81, followed by the multicopter with a score of 62. The airship scores the lowest at 38 points. The fixed-wing aircraft rank between the airship and the multicopter.

The tiltrotor has the lowest spread between the best case and worst case (69–94), which indicates that the final design is more likely to be in the range of the preliminary sizing. In the best case, the multicopter is on par with the expected case of the tiltrotor. However, despite some overlap, the tiltrotor range is significantly above the multicopter range. The best-case scores for the blended wing and biplane aircraft are around the expected score for the multicopter, while the airship scores only 38, even in the best case.

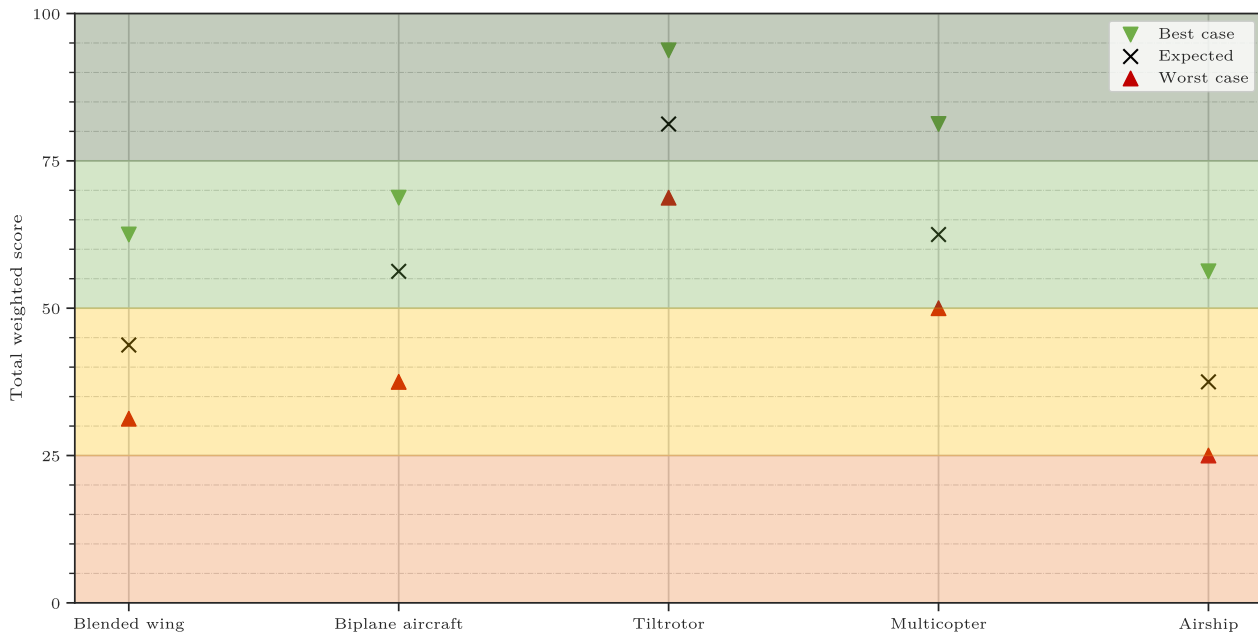


**Figure 7.1:** Results of the trade-off. The tiltrotor wins for the expected case, par with the multicopter's best case.

The robustness of the results was analyzed through a sensitivity analysis. The trade-off was performed

again with the expected values, but the initially equal weights of each criterion were perturbed 1000 times. This was done by uniformly sampling factors between 0.5 and 2 (such that there is an equal chance of obtaining a factor greater or lower than 1), by which the weights are multiplied. This means that a criterion can be halved or doubled in importance. The robustness is then measured by the inter-quartile range (IQR) of the resulting total weighted scores (corresponds to box height in box plots; smaller IQR = more robust). Note that we do not perturb the actual criterion values (e.g., the range for the multicopter) since the best-case and worst-case scenarios cover this more physically.

The sensitivity analysis results are shown in Figure 7.2. The relative ranking is very similar to the results from Figure 7.1. In general, the better designs are also more robust to perturbations. The airship score is the most sensitive (IQR = 13). The tiltrotor is the most robust design (IQR = 4). Even more importantly, the whiskers of the tiltrotor box do not overlap with any other box, which means that the tiltrotor is statistically significantly better.

We also performed a targeted sensitivity analysis for the "landing/take-off distance" criterion since the two fixed-wing design scores may be sensitive to the boundary (see Section 7.1.3). Regularly, the landing distance of 2000 m is considered "acceptable." If considered "good," the biplane aircraft would be on par with the multicopter in the expected cases, while it would be better than the biplane if 2000 m were considered "great." However, the tiltrotor is the best option in any case.

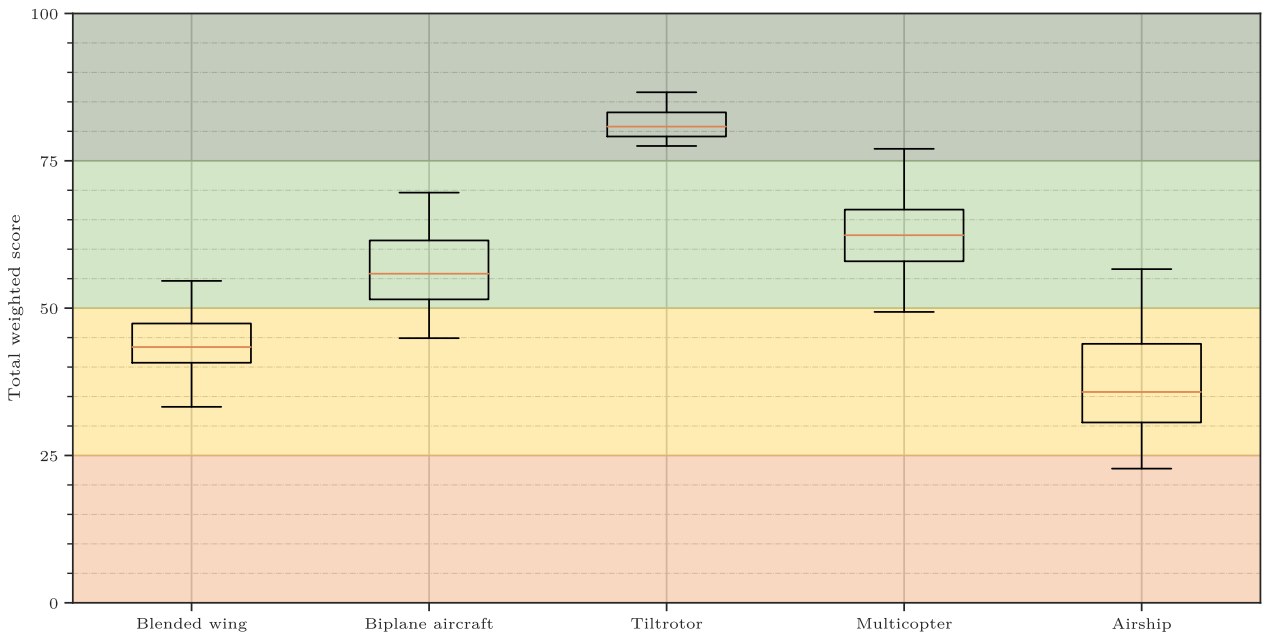


**Figure 7.2:** Sensitivity analysis for the trade-off. The boxes denote the IQR, while the whiskers extend from  $Q1 - 1.5IQR$  to  $Q3 + 1.5IQR$ . The criteria weights are perturbed by uniformly sampled factors between 0.5 and 2. The outcome of the trade-off is robust to these perturbations. Better designs are less sensitive.

From these results, the tiltrotor is the optimal option under the chosen criteria and will be designed in more detail going forward. This choice is robust under perturbed weights and different assumptions. The multi-copter is the second-best option, but possibly matched by the fixed-wing aircraft HTOL is penalized less. The airship is the worst due to its unacceptable range. Among the fixed-wing aircraft, the biplane aircraft performs better than the flying wing.

**Table 7.2:** Score assignment for each criterion. Intervals are given for quantitative criteria.

<i>Score value</i>	<b>Unacceptable</b> <b>0</b>	<b>Acceptable</b> <b>1</b>	<b>Good</b> <b>2</b>	<b>Great</b> <b>3</b>	<b>Exceptional</b> <b>4</b>
<b>Range at 350 kg payload [km]</b>	< 700	[700, 900)	[900, 1100)	[1100, 2000)	$\geq 2000$
<b>Landing/take-off distance [m]</b>	>5000	[5000, 1500)	[1500, 500)	[500, 1)	0 (VTOL)
<b>Feasibility</b>	Min. TRL $\in [1, 4)$	Min. TRL $\in [4, 6)$ and <1000 existing designs	Min. TRL $\in [4, 6)$ and >1000 existing designs	Min. TRL $\in [6, 9)$	All TRL = 9
<b>Sustainability</b>	No criteria fulfilled	1 criterion fulfilled	2 criteria fulfilled	3 criteria fulfilled	All 4 criteria fulfilled

**Table 7.3:** Trade-off summary including criteria values and scores. The total weighted score in the last column indicates the overall goodness of the design. The tiltrotor design has the highest score, which is robust to perturbations and is selected.

	<b>Range at 350 kg payload [km]</b>	<b>Landing/take-off distance [m]</b>	<b>Feasibility</b>	<b>Sustainability</b>	<b>Score</b>
<i>Weight</i>	1	1	1	1	
<b>Blended wing</b>	1779	2000	Min. TRL of 4 (Power) and <1000 existing designs	Emits carbon, and the energy source is not renewable	44
<b>Biplane aircraft</b>	2157	2000	Min. TRL of 4 (Power) and >1000 existing designs	Emits carbon, and the energy source is not renewable	56
✓ <b>Tiltrotor</b>	1885	0	Min. TRL of 6 (Control)	Rotor blades are not recyclable	81
<b>Multicopter</b>	1270	0	Min. TRL of 4 (Power) and <1000 existing designs	The energy source is not renewable, and rotor blades are not recyclable	62
<b>Airship</b>	480	0	Min. TRL of 4 (Power) and <1000 existing designs	Emits carbon and hydrogen, and the energy source is not renewable	38

# Technical Risk Assessment

By Sebastian Harris, Freek Braspenning

The Technical Risk Assessment can be conducted once more on the final design. This follows a set methodology, described in Section 8.1. Next, the risks from previous reports are summarized in Section 8.2. Finally, the risks stemming from this design phase are researched and assessed in Section 8.3.

## 8.1. Methodology

Within the Risk Assessment process, various methods are available to both size risks and their impact. In the context of this report, the scale in Table 8.1 is used.

**Table 8.1:** Score associated with probabilities and impacts of the risks

Scale	Probability	Impact
5	Very High ( $p > 95\%$ )	Catastrophic (Complete Mission Failure)
4	High( $60\% < p < 95\%$ )	Partial Mission Failure
3	Medium ( $30\% < p < 60\%$ )	Moderate performance reduction
2	Low ( $1\% < p < 30\%$ )	Small performance reduction
1	Very Low ( $p < 1\%$ )	Negligible

After recalling the risks identified and assessed in the previous reports, additional risks can be identified as the chosen design is known.

## 8.2. Risks from previous reports

For the sake of conciseness, the risks listed in previous reports will only be mentioned when their original risk was unacceptable. The risks in Table 8.2 were identified.

**Table 8.2:** List of Risks from previous reports

Risk ID	Description	Risk ID	Description
R-PREP-01	Imperfections in manufacturing	R-OP-06	Improper Maintenance
R-PREP-02	Damage during transport	R-TO-03	Dust clogs any air intake
R-PREP-03	Errors in Assembly	R-TO-06	Insufficient runway length
R-PREP-04	Missing items in package	R-TO-07	Insufficient lift produced
R-PREP-05	Launcher failure	R-CR-01	Engine Failure
R-STAT-01	Dust Storm leading to aircraft damage	R-CR-02	Dust clogs any air intake
R-STAT-02	Damage due to strong winds	R-CR-03	Control surface failure
R-STAT-03	Damage due to radiation	R-CR-04	Corrupted on-board computer
R-STAT-04	Incident when refueling/recharging	R-CR-05	Structural failure
R-STAT-05	Pre-flight procedures fail	R-LD-01	Engine failure
R-STAT-06	Unable to refill energy storage	R-LD-02	Dust clogs any air intake
R-STAT-07	Failure to assemble on site	R-LD-03	Control surface failure
R-OP-01	Life support failure	R-LD-04	Non-functional landing gear
R-OP-03	Compromised thermal insulation	R-LD-08	Landing site is too small
R-OP-04	Astronauts unable to operate the aircraft	R-LD-09	Landing gear failure
R-OP-05	Power system failure		

### 8.3. Additional risks

With the final design settled additional concept-specific risks arise. These risks are listed in Table 8.3.

**Table 8.3: Additional Risks**

Risk ID	Description	Probability (1-5)	Impact (1-5)
R-AR-01	Faulty batteries	1	5
R-AR-02	Transmission failure	1	4
R-AR-03	Gearbox Failure	1	4
R-AR-04	Hydraulic failure	1	4
R-AR-05	Avionics failure	1	3
R-AR-06	Brownout	4	3
R-AR-07	Short-circuiting of electrical components	1	4
R-AR-08	Rotor failure	1	4
R-AR-09	Autopilot failure	1	2
R-AR-10	Instrument failure	1	3
R-AR-11	Temperature control failure	1	3
R-AR-12	Astronauts unresponsive	1	5
R-AR-13	Battery Ageing	5	3
R-AR-14	Vortex Ring State	3	3
R-AR-15	Center of gravity shift	2	5

To facilitate understanding, both Brownouts and Vortex Ring States will be further explained. A brownout consists of the dust thrown up by the rotors to cloud the pilot's vision, resulting in a total lack of visibility. This lack of vision can lead to crashes and errors in piloting. Considering the decreased gravity on Mars, these brownouts could last much longer as the particles will not settle. Separately, the vortex ring state consists of a situation in descent where the wake of the rotor causes the airflow to rotate over and re-enter the flow of the rotor. This leads to a large decrease in thrust, which is not always done symmetrically, potentially rolling the aircraft. On Mars, the decreased viscosity should decrease the strength of the vortices and thus limit the occurrence of this state. Nonetheless, the risk is non-zero, and it must be assessed. From the data present in Table 8.3, the design risk matrix can be created in Table 8.4

**Table 8.4: Additional Design risk matrix**

		Probability				
		Very Low (1)	Low (2)	Moderate (3)	High (4)	Very High (5)
Impact	Catastrophic (5)	R-AR-01, R-AR-12	R-AR-15			
	Critical (4)	R-AR-02, R-AR-03, R-AR-04, R-AR-07, R-AR-08				
	Moderate (3)	R-AR-05, R-AR-10, R-AR-11		R-AR-14	R-AR-06	R-AR-13
	Marginal (2)	R-AR-09				
	Negligible (1)					

**Table 8.5: Mitigation of Additional Risks**

Risk ID	Mitigation	Probability (1-5)	Impact (1-5)
R-AR-01	Isolate battery storage and regularly inspect	1	3 (-2)
R-AR-02	Redundant transmission	1	1 (-3)
R-AR-03	Redundant gearbox	1	2 (-2)
R-AR-04	Redundancy in the hydraulic	1	1(-3)
R-AR-05	Redundant Avionics	1	1 (-2)
R-AR-06	Use Infrared Imaging	4	1 (-2)
R-AR-07	Use fuses	1	3 (-1)
R-AR-08	Ensure Rotor and Cockpit are not aligned	1	2 (-2)
R-AR-09	Install alert system and manual override	1	1(-1)
R-AR-10	Redundancy in instruments	1	1(-2)
R-AR-11	Redundancy in temperature control failure	1	3 (-2)
R-AR-12	Automatically engage autopilot when crew is unresponsive	1	3 (-2)
R-AR-13	Monitor battery health and performance	5	1 (-2)
R-AR-14	Set limit on descent speed and train crew in Vuichard Correcting Technique	2 (-1)	1 (-2)
R-AR-15	Calculate the center of gravity when loading payload and alert astronauts if too close to the neutral point	1(-1)	5

With the data present in Table 8.5, the new mitigated design risk matrix can be created, as seen in Table 8.6. Compared to Table 8.4 the risks have shifted to the bottom left, reducing their probability and consequence.

**Table 8.6: Design risk matrix**

		Probability				
		Very Low (1)	Low (2)	Moderate (3)	High (4)	Very High (5)
Impact	Catastrophic (5)	R-AR-13, R-AR-15				
	Critical (4)					
	Moderate (3)	R-AR-01, R-AR-07, R-AR-11, R-AR-12				
	Marginal (2)	R-AR-03, R-AR-08				
	Negligible (1)	R-AR-02, R-AR-04, R-AR-05, R-AR-09, R-AR-10	R-AR-14		R-AR-06	

As visible, all risks determined in this phase have been mitigated. In the following stage of the design process, these risk mitigation steps will be implemented in the final design.

# Sustainable Development Strategy

*By Thomas van de Pavoordt*

To design for sustainability, firstly, a definition of sustainability was agreed upon. We define sustainability after Brundtland [31]:

"Meeting the needs of the present without compromising the ability of future generations to meet their own needs."

Since the future of humanity may be multi-planetary, we need to consider the needs of future generations on both Earth and Mars. This means that both the development, design, and manufacturing of the system on Earth and the operations of the system on Mars should be sustainable.

During this preliminary design phase of all the different options, sustainability is becoming increasingly integrated. Each design concept was created with the goal of sustainability in mind, especially given the fact that it is a customer requirement to only utilize in-situ available resources. Moreover, from the sustainability definition, requirements were derived concerning manufacturing on Earth, pollution on Mars, and the use of recyclable materials. As seen in the baseline report. These requirements will have to be met and are therefore integral to our design. Additionally, in the trade-off process, sustainability was considered as a trade-off criterion. This ensured that all designs aimed towards scoring as high as possible in this category. The tiltrotor design concept was equipped with batteries and a propulsion system powered by electrical (solar) energy, while the jet engine designs use magnesium and carbon dioxide, both of which are available on Mars. This ensured that the in situ resource use requirement was met. Sustainability was one of the stand out criteria for the tiltrotor and contributed to the final design choice as can be seen in Table 7.1 in Chapter 7. The tiltrotor design uses completely renewable energy and ensures no pollution of the Martian atmosphere, thus contributing to the sustainable development strategy.

Only in the detailed conceptual design phase of the report it is possible to dive deeper into the effects of the design on the sustainability goals. This means, but is not limited to, assessment of the materials used, how these materials are manufactured, what their recyclability is, and their end-of-life plan. It will have to be assessed what footprint the design will leave on Mars and whether this can be considered polluting. The assembly as well as the transportation from Earth to Mars will have to be assessed and their impact to the Earth's atmosphere will be evaluated. The life span of the aircraft will have to be considered along with the re-usability of the system. All these aspects, and more, are inherent to the detailed conceptual design and thus, the sustainability manager will prepare to enforce these during the final phase.

Summarizing, the following new sustainability goals have been set:

- Use in-situ, renewable fuels
- Use non-toxic, abundant, recyclable materials
- Evaluate manufacturing processes and their impact on Earth
- Evaluate assembly process and its impact on both Earth and Mars
- Evaluate the impact of transportation on Earth atmosphere
- Evaluate the impact of pollution on the Martian atmosphere and potential life on Mars
- Evaluate re-usability of system
- Evaluate end-of-life plan

These goals will, as said above, be enforced by the sustainability manager in weekly inspections on the progress of each subsystem design and their interfaces for the final design concept.

# Project Logic

This chapter describes the logistics of the product development, as well as the agenda for the final report. Section 10.1 shows the development of the chosen design after the preliminary design phase. The operational and logistic flow of the product is provided by Section 10.2. Section 10.3 explores the iteration phase of the preliminary design. Section 10.5, Section 10.4 and Section 10.6 provide the updated Work Flow Diagram, Work Breakdown Structure, and Gantt Chart, respectively, for the final phase of the design.

## 10.1. Project description & development logic

*By Timo de Kemp*

The Project Description & Development Logic (PD&DL) diagram describes the stages of the product production and operation which take place after the preliminary design has been finalized. The first step is to finalize the design in the detailed design phase after which it will be produced and tested. Once testing is complete the the design and the crew are prepared for operation. The final stage of the project is the operation on Mars, which ends with the End of Life operations.

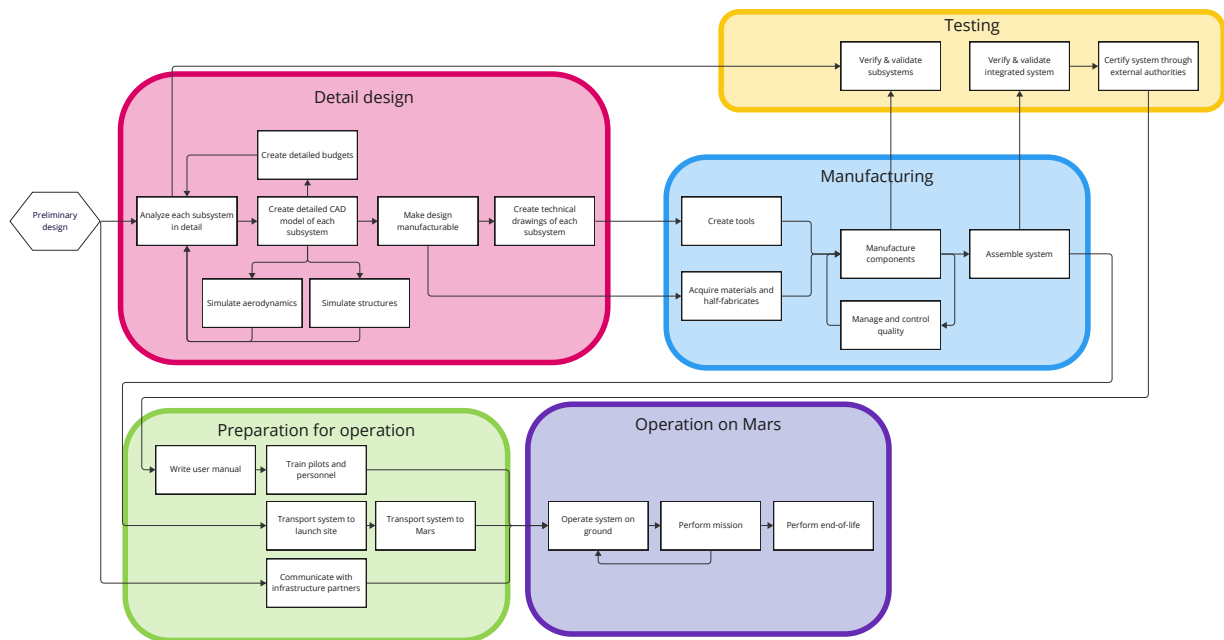


**Figure 10.1:** Project Design & Development Logic for post preliminary sizing phase

## 10.2. Operations and logistics description

*By Timo de Kemp*

In this chapter the operations and logistic concept for the production and operation phase of the aircraft will be discussed. As can be seen in Figure 10.2 the flowchart starts from raw materials, which have to be transported and manufactured into the sub-assemblies that have to be transported to Mars. As multiple sub-assemblies will have to be transported to Mars, the three dots in Figure 10.2 indicate that the amount of sub-assemblies to be transported has not yet been determined.

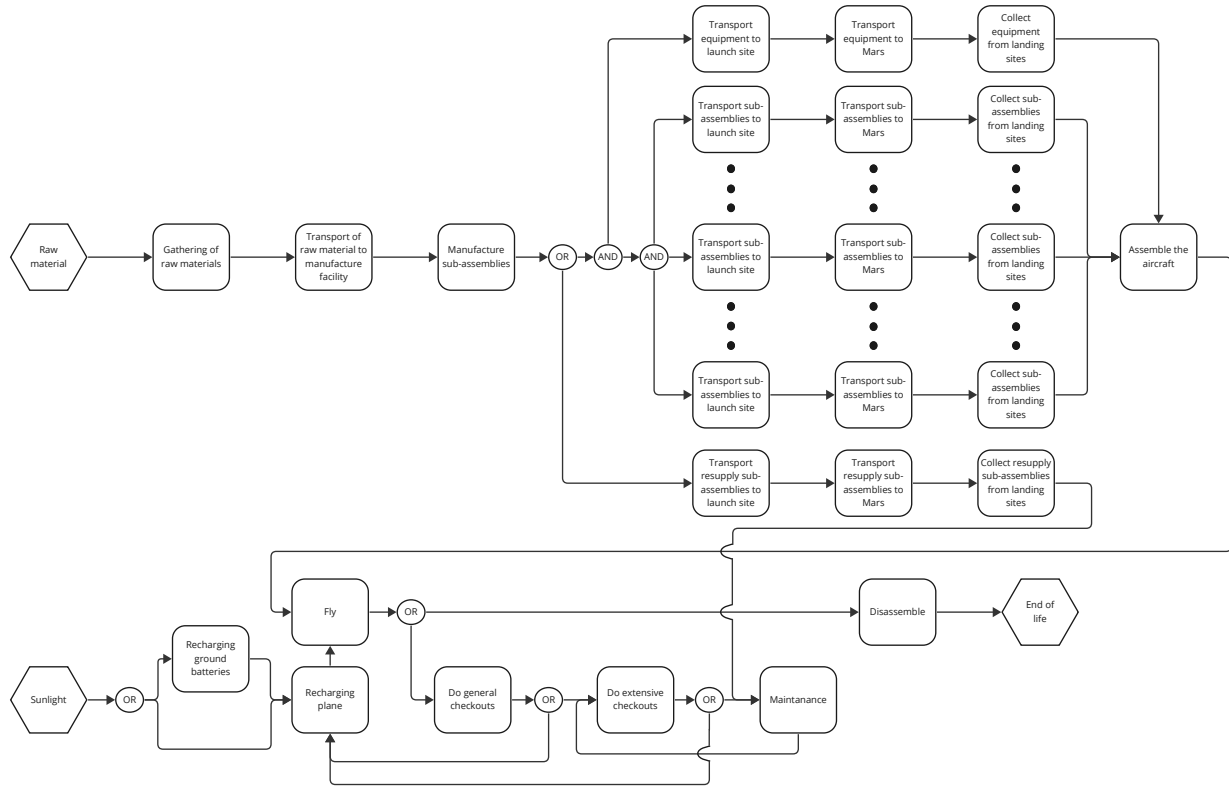


**Figure 10.2:** Flow chart which describes the operations and logistics for the production and operation phase.

Since the assembly is performed on Mars, additional equipment needs to be transported. The same equipment can be used for the assembly as well as maintenance if necessary. The equipment for assembly will consist, but is not limited to, assembly jigs, fasteners, fastener tools, and heavy duty machines. Additionally, the sub-assemblies that are transported from Earth need to be checked for possible damage due to transportation.

There is no infrastructure necessary for the flight itself. However the turnaround time can take up to 10 hours of sunlight as the solar panels are used for recharging. In order to decrease the turnaround time an additional charging system can be implemented.

### 10.3. N2 charts

By Patrick Kostelac, Javier Alonso

The  $N^2$  chart is a diagram in the shape of a matrix, representing the functional and physical interfaces between system elements. In the design phase, the  $N^2$  chart is used to determine the inter dependencies of each system. The outputs of each system are presented on the horizontal axis and the inputs of each system are presented on the vertical axis. This way the key subsystems can be identified as those which influence multiple other subsystems. For the current design, the propulsion system can be clearly identified as a key subsystem. Subsequently, the chart can be used to identify further risks. Some subsystems are dependent on many other subsystems and thus their design can be significantly constrained. In this case those would be the propulsion and structures subsystems. The  $N^2$  chart also shows possible iterations within the subsystems. Two subsystems which are dependent on each other will be iterated according to the  $N^2$  chart until the output changes by less than 1% when the values for the final design are reached.

Mass estimation	-Mass budget	-Mass budget	-Mass budget	-Mass budget	-Mass budget	-Mass budget	-Mass budget	-Mass budget	-Mass budget
Sensor's mass	Sensing and communication		-Power consumption of instruments		-Attitude determination	-Astronaut vitals information -Surrounding environment information		-must allow electromagnetic waves through	
		Propulsion	-Power for propulsion -Energy for cruise -Torque required	-Propeller-wing interaction -Rotor radius	-Thrust location and direction -Engine failure stability		-Vibrational loads -Lifting loads -Thrust loads -Blade loads		
-Battery mass -Engine mass -Assembly mass -Solar panel mass	-Power budget	-Power budget	Power and energy		-power budget	-Power budget -Operative temperature of the batteries	-Solar panel size		-Power budget
		-Drag	-Wing planform area	Aerodynamics	-Stability derivatives -Wing and tail loads		-Wing loads -Tail loads -Wing dimensions		
-control surfaces mass		-Maneuvering capabilities -autopilot data	-power needed for control surfaces movement	-Control surfaces -Tail volume	Stability and control		-Tail loads -Ultimate load		
-Life support mass	-Astronaut vitals information -Oxygen storage information		-Thermal control power consumption			Life support	-oxygen storage -crash worthiness	-Emissivity and absorptivity -Radiation shielding -Damage tolerant materials	
				-Body shape	-Cg location	-crew/cabin protection and location	Structures	-General geometry -Loads	-Payload bay volume
-Wing mass -Tail mass -Body mass -Landing gear mass -Rotor mass				-Skin friction		-Insulation capabilities	-Minimum allowable thicknesses -Allowable stresses	Material	
-Payload mass	-Telemetry data -Avionics data	-Maximum acceleration	-Required power	-			-payload bay location and protection	-insulation -protection	Payload

**Figure 10.3:**  $N^2$  chart of the system

## 10.4. Work Breakdown Structure

By Freek Braspenning, Patrick Kostelac

The Work Breakdown Structure (WBS) for the final report is set up as can be seen in Figure 10.4. The WBS for the final report goes into the lower-level tasks. The WBS is built up from the Work Flow Diagram (WFD) as it takes the same higher-level tasks. These higher-level tasks form the work packages which are further divided into sub-tasks. The workload for each task is then estimated and a team member is assigned. The initials of the group members responsible for each task are presented alongside the total estimated task duration (in man work hours). In case the entire group is responsible for the task, Group is written instead of the mentioning every name. The final output of the DSE is the final symposium presentation.

## 10.5. Work Flow Diagram

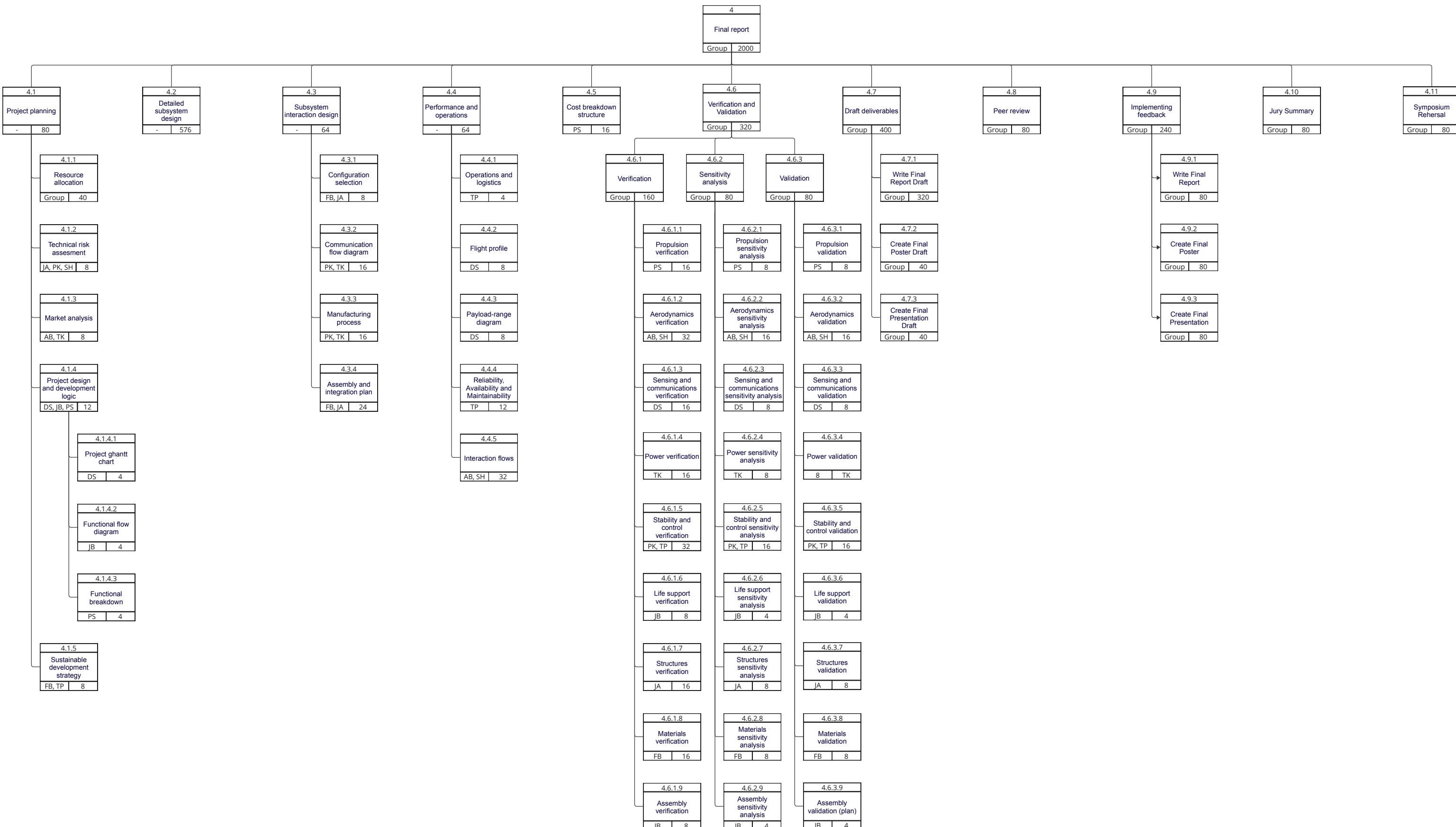
By Freek Braspenning, Patrick Kostelac

A detailed WFD for the final phase of the project was created and can be seen in Figure 10.5. The midterm report serves as a starting point for the final phase of the report. The WFD shows the tasks up to the second order of precision. The tasks which can be done simultaneously are presented in parallel and the tasks which need to be performed sequentially are presented in series.

## 10.6. Gantt chart

By Javier Alonso

The Gantt chart in Figure 10.6 will show how the tasks from the WBS in time. This will prove very useful for project management reasons. The Gantt chart shows a detailed work distribution for each day. This reduces the amount of non useful work done as well as increases the overall productivity of the team. The Gantt chart is designed to have tasks that are no smaller than 4 hours.



Name	Initials
Dominik Stiller	DS
Sebastian Harris	SH
Freek Braspenning	FB
Joachim Bron	JB
Javier Alonso Garcia	JA
Pedro Coimra Dos Santos	PS
Adrian Beho	AB
Patrick Kostelac	PK
Timo de Kemp	TK
Thomas van de Pavoordt	TP

Figure 10.4a: Work breakdown structure for the final phase

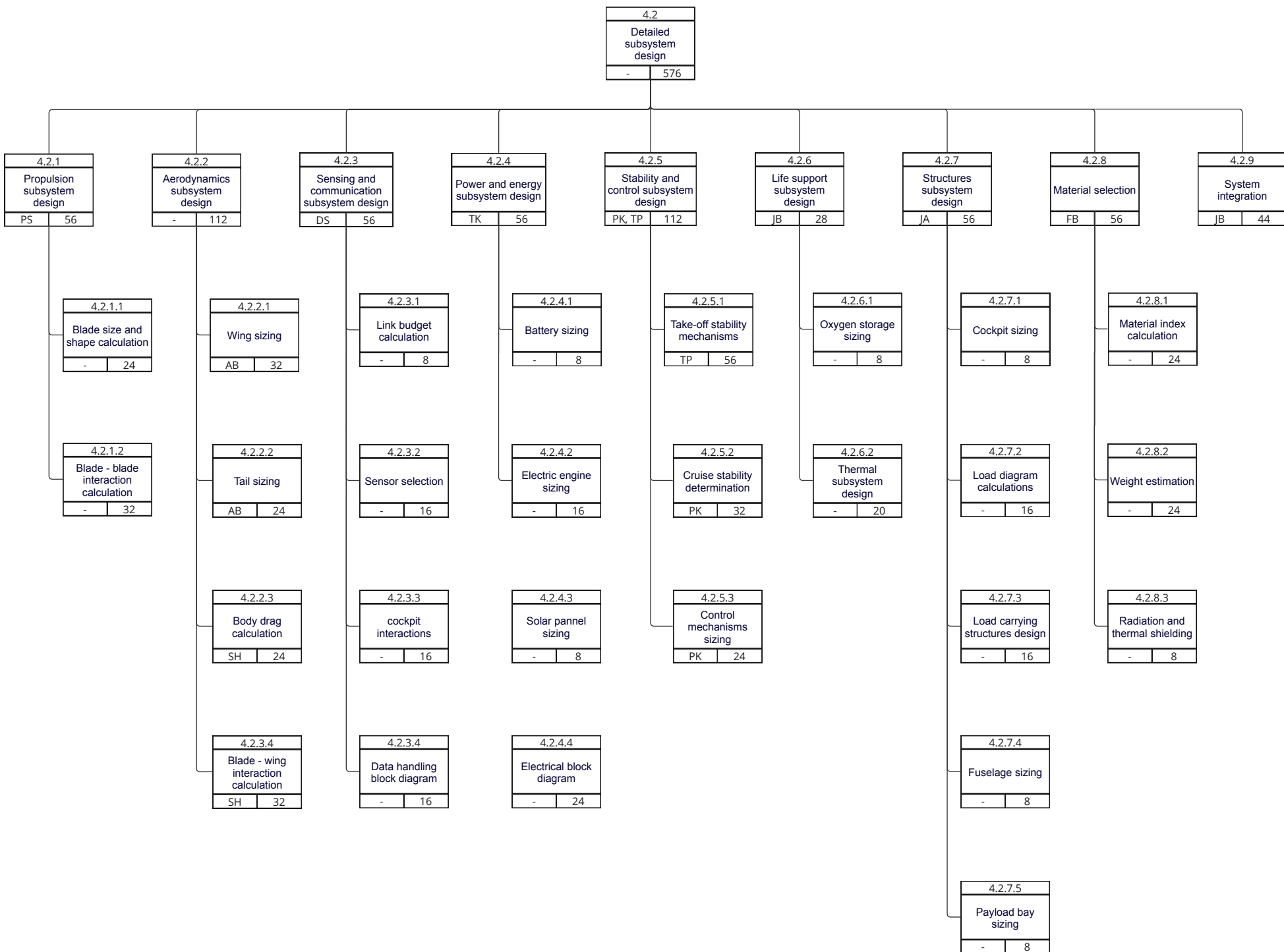


**Figure 10.4b:** Sub-work breakdown structure for the detailed subsystem design

Name	Initials
Dominik Stiller	DS
Sebastian Harris	SH
Freek Braspenning	FB
Joachim Bron	JB
Javier Alonso Garcia	JA
Pedro Coimra Dos Santos	PS
Adrian Beho	AB
Patrick Kostelac	PK
Timo de Kemp	TK
Thomas van de Pavoordt	TP

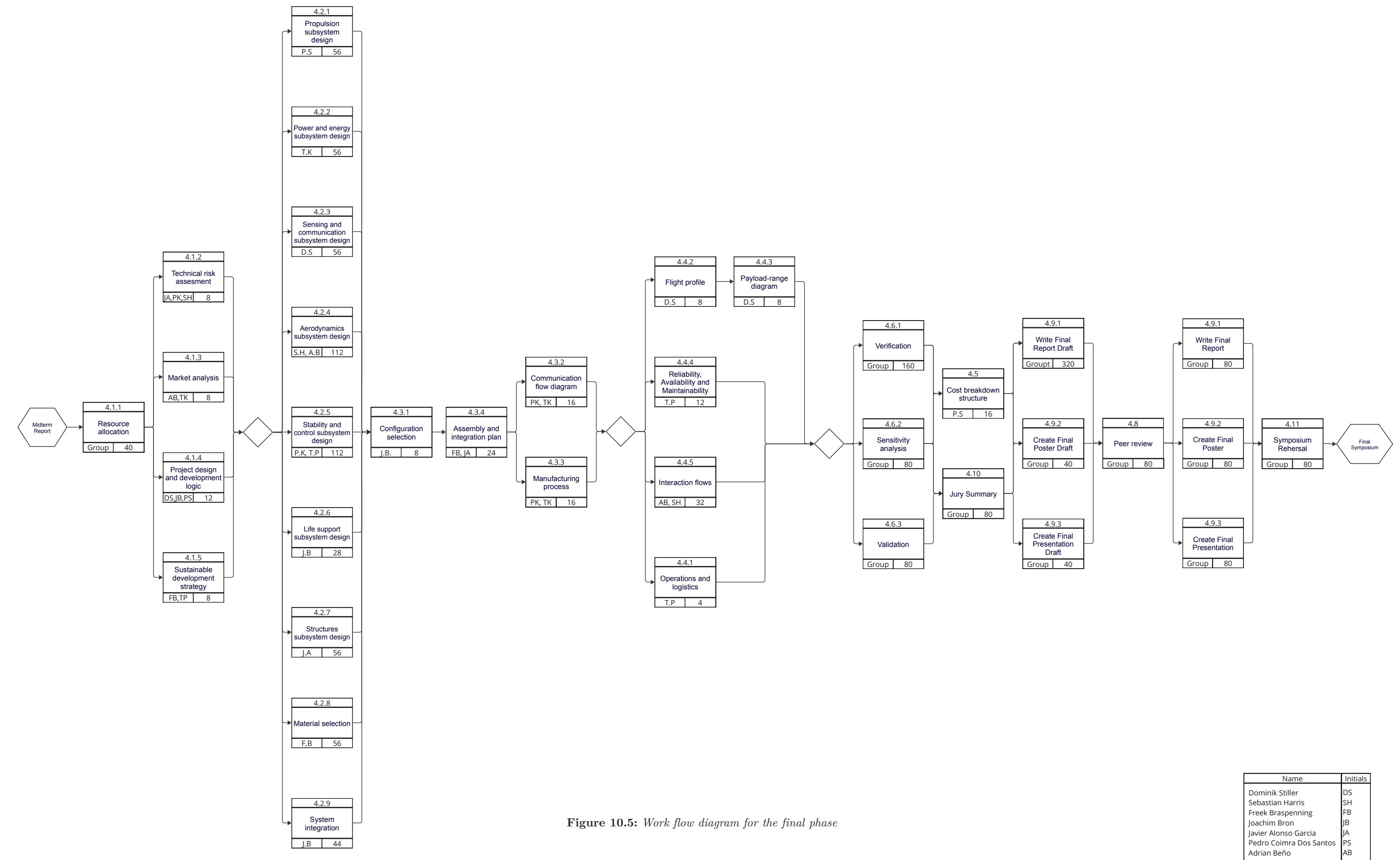
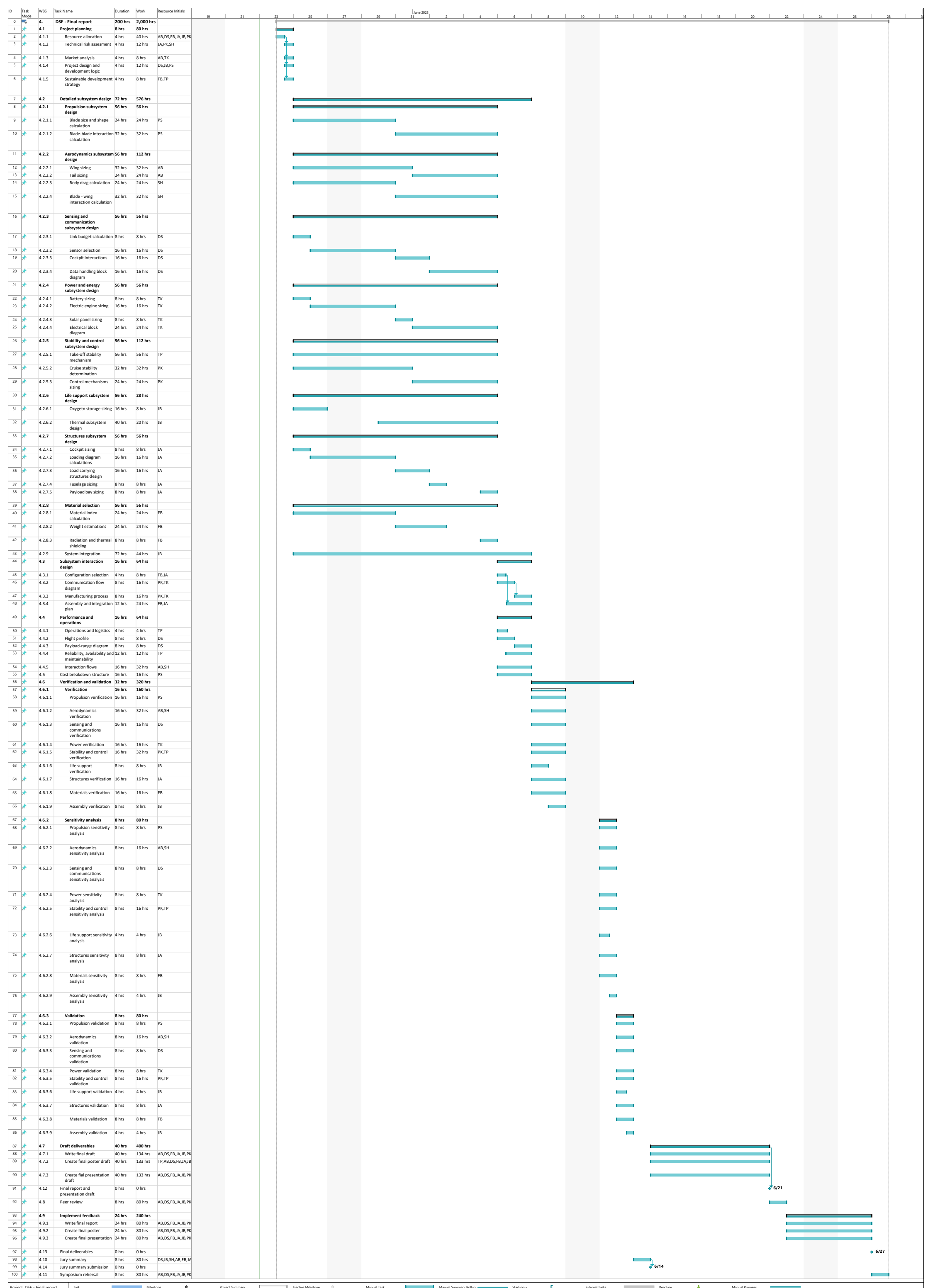


Figure 10.5: Work flow diagram for the final phase



# Bibliography

- [1] Kaya, D., and Kutay, A., "Aerodynamic Modeling and Parameter Estimation of a Quadcopter Helicopter," *AIAA Atmospheric Flight Mechanics Conference*, 2014, p. 28.
- [2] Prouty, R. W., *Helicopter performance, stability, and control*, R.E. Krieger Pub. Co, Malabar, Fla, 1990.
- [3] Yuasa, S., and Isoda, H., "Carbon dioxide breathing propulsion for a Mars airplane," *25th Joint Propulsion Conference*, American Institute of Aeronautics and Astronautics, Monterey, CA, U.S.A., 1989. doi:10.2514/6.1989-2863.
- [4] Wickman, J., "In-Situ Mars Rocket and Jet Engines Burning Carbon Dioxide," *AIAA*, Vol. 99, No. 2409, 1999. doi:10.2514/6.1999-2409.
- [5] Pratt & Whitney, "F135-PW-600 - The World's Most Advanced Fighter Engine," , 2022.
- [6] Svoboda, C., "Turbofan engine database as a preliminary design tool," *Elsevier Science Ltd.*, 2004.
- [7] Torenbeek, E., *Synthesis of subsonic airplane design: an introduction to the preliminary design, of subsonic general aviation and transport aircraft, with emphasis on layout, aerodynamic design, propulsion, and performance*, Delft University Press ; Nijhoff ; Sold and distributed in the U.S. and Canada by Kluwer Boston, Delft : The Hague : Hingham, MA, 1982.
- [8] Selig, M. S., and Guglielmo, J. J., "High-Lift Low Reynolds Number Airfoil Design," *Journal of Aircraft*, Vol. 34, No. 1, 1997, pp. 72–79. doi:10.2514/2.2137.
- [9] Seshagiri, A., Cooper, E., and Traub, L. W., "Effects of Vortex Generators on an Airfoil at Low Reynolds Numbers," *JOURNAL OF AIRCRAFT*, Vol. 46, No. 1, 2009. doi:10.2514/1.36241.
- [10] Traub, L. W., "Aerodynamic Impact of Aspect Ratio at Low Reynolds Number," *JOURNAL OF AIRCRAFT*, Vol. 50, No. 2, 2013. doi:10.2514/1.C031980.
- [11] Gross, J., and Traub, L. W., "Experimental and Theoretical Investigation of Ground Effect at Low Reynolds Numbers," *JOURNAL OF AIRCRAFT*, Vol. 49, No. 2, 2012. doi:10.2514/1.C031595.
- [12] Somerville, A., Marino, M., Baxter, G., and Wild, G., "Understanding box wing aircraft: essential technology to improve sustainability in the aviation industry," *Aviation*, Vol. 20, No. 3, 2016. doi:10.3846/16487788.2016.1195076.
- [13] Vos, R., "Lecture Notes AE1222-II – A/C preliminary sizing(class I weight estimation method)," , Feb. 2021.
- [14] Raymer, D. P., French, J., Finger, D. F., Gomez, A., Singh, J., Pillai, R. G., Monjon, M. M., Marcos De Souza, J., and Levy, A., "The Raymer Manned Mars Airplane: A Conceptual Design and Feasibility Study," *AIAA Scitech 2021 Forum*, American Institute of Aeronautics and Astronautics, VIRTUAL EVENT, 2021. doi:10.2514/6.2021-1187.
- [15] Anderson, J. D., *Fundamentals of aerodynamics*, sixth edition ed., McGraw-Hill series in aeronautical and aerospace engineering, McGraw Hill Education, New York, NY, 2017.
- [16] Horiba, T., Maeshima, T., Matsumura, T., Koseki, M., Arai, J., and Muranaka, Y., "Applications of high power density lithium ion batteries," *Journal of Power Sources*, Vol. 146, No. 1-2, 2005, pp. 107–110. doi:<https://doi.org/10.1016/j.jpowsour.2005.03.205>.
- [17] Withrow, S., Johnson, W., Young, L. A., Cummings, H., Balaram, J., and Tzanatos, T., "An Advanced Mars Helicopter Design," *ASCEND 2020*, American Institute of Aeronautics and Astronautics, Virtual Event, 2020. doi:10.2514/6.2020-4028.
- [18] Koning, W. J., Johnson, W., and Allan, B. G., "Generation of mars helicopter rotor model for comprehensive analyses," Tech. Rep. ARC-E-DAA-TN50660, 2018.

- [19] Coleman, C. P., "A survey of theoretical and experimental coaxial rotor aerodynamic research," Tech. Rep. NASA-TP-3675, 1997.
- [20] "15 - Fibre-polymer composites for aerospace structures and engines," *Introduction to Aerospace Materials*, edited by A. P. Mouritz, Woodhead Publishing, 2012, pp. 338–393. doi:<https://doi.org/10.1533/9780857095152.338>.
- [21] Batrakov, A., Kusyumov, A., Mikhlov, S., and Pakhov, V., "Helicopter Fuselage Drag - Combined CFD and Experimental Studies," *EUCASS Proceedings Series*, Vol. 7, No. 2015, 2015, pp. 21–32. doi:<https://doi.org/10.1051/eucass/201507021>.
- [22] El-Gaaly, T., McMahan, B., and El Qursh, A., "Multi-Segment Zeppelin-Aided Robotic Rover For Ground-Based and Atmospheric Exploration," *Concepts and Approaches for Mars Exploration*, Vol. 4278, 2012.
- [23] Vega, G., Paeres, D., Forteza, E., Claudio, E., Marcial, D., and Araya, G., "Aerodynamic assessment of a drone dirigible-based carrier for search and research purposes," *AIAA SciTech Forum*, 2023. doi:10.2514/6.2023-1735.
- [24] Li, Y., Nahon, M., and Sharf, I., "Airship dynamics modeling: A literature review," *Progress in Aerospace Sciences*, Vol. 47, No. 3, 2011, pp. 217–239. doi:10.1016/j.paerosci.2010.10.001.
- [25] Bardera, R., Sor, S., and García-Magariño, A., *Aerodynamics of Mars 2020 Rover Wind Sensors*, IntechOpen, 2020. doi:10.5772/intechopen.90912.
- [26] Ma, R., Zhong, B., and Liu, P., "Optimization design study of low-Reynolds-number high-lift airfoils for the high-efficiency propeller of low-dynamic vehicles in stratosphere," *Science China Technological Sciences*, Vol. 53, No. 10, 2010, pp. 2792–2807. doi:10.1007/s11431-010-4087-0.
- [27] Group, J. I., *Jane's all the world's aircraft 2021-2022*, 112<sup>th</sup> ed., Jane's, Coulsdon, 2021.
- [28] Haberle, R. M., Clancy, R. T., Forget, F., Smith, M. D., and Zurek, R. W. (eds.), *The Atmosphere and Climate of Mars*, 1<sup>st</sup> ed., Cambridge University Press, 2017. doi:10.1017/9781139060172.
- [29] Koning, W. J., "Airfoil Selection for Mars Rotor Applications," Tech. Rep. ARC-E-DAA-TN70055, 2019.
- [30] Hirshorn, S. R., "NASA Systems Engineering Handbook," Tech. Rep. NASA SP-2016-6105 Rev2, 2016.
- [31] Brundtland, G. H., *Report of the World Commission on environment and development: Our Common Future*, UN, 1987.